ÇUKUROVA UNIVERSITY
INSTITUTE OF NATURAL AND APPLIED SCIENCES

MSc. THESIS

Yunus Emre GÜZELEL

ANALYSIS OF DESICCANT AIR-CONDITIONING SYSTEM WITH DEW-POINT EVAPORATIVE COOLING

DEPARTMENT OF MECHANICAL ENGINEERING

ADANA-2019

ÇUKUROVA UNIVERSITY
INSTITUTE OF NATURAL AND APPLIED SCIENCES

ANALYSIS OF DESICCANT AIR-CONDITIONING SYSTEM WITH DEW-POINT EVAPORATIVE COOLING

Yunus Emre GÜZELEL

MSc. THESIS

DEPARTMENT OF MECHANICAL ENGINEERING

We certified that the thesis titled above was reviewed and approved for the award degree of the master of mechanical engineering by the board of jury on 26/07/2019

……	……	……
Assoc. Prof. Dr. Arif ÖZBEK	Prof. Dr. Orhan BÜYÜKALACA	Assoc. Prof. Dr. Ertaç HÜRDOĞAN
SUPERVISOR	MEMBER	MEMBER

This MSc. thesis is performed in Department of Mechanical Engineering of the Institute of Natural and Applied Sciences of Çukurova University.
Registration No:

Prof. Dr. Mustafa GÖK
Director
Institute of Natural and Applied Science

ABSTRACT

MSc. THESIS

ANALYSIS OF DESICCANT AIR-CONDITIONING SYSTEM WITH DEW-POINT EVAPORATIVE COOLING

Yunus Emre GÜZELEL

ÇUKUROVA UNIVERSITY
INSTITUTE OF NATURAL AND APPLIED SCIENCES
DEPARTMENT OF MECHANICAL ENGINEERING

Supervisor : Assoc. Prof. Dr. Arif ÖZBEK
Year: 2019, Page: 105
Jury : Assoc. Prof. Dr. Arif ÖZBEK
: Prof. Dr. Orhan BÜYÜKALACA
: Assoc. Prof. Dr. Ertaç HÜRDOĞAN

In this thesis, a Maisotsenko cycle based air-conditioning system supported by a desiccant wheel, heat recovery units (recuperators) and a direct evaporative cooler is investigated during a complete cooling season for air-conditioning of a school building located in Adana, Turkey. After modelling the air-conditioning system, hourly analysis for 21st day of each month during cooling season was carried out with a computer program developed. The optimum values of operational parameters, the temperature of the air inside the building and mixing ratio of the exhaust air with supply air are obtained. The effectiveness of desiccant wheel and Maisotsenko cycle, which are the two important components of the system, thermal energy requirement to run the system and cooling performance of the system are investigated in detail. The results show that it is possible to obtain comfort conditions within the building during complete cooling season with the air-conditioning system considered.

Keywords: Dew-point evaporative cooling, Indirect evaporative cooling, Maisotsenko cycle, Desiccant wheel, Air-conditioning, Modelling

ÖZ

YÜKSEK LİSANS TEZİ

ÇİĞ NOKTA NEMLENDİRMELİ DESİSİF İKLİMLENDİRME SİSTEMİNİN ANALİZİ

Yunus Emre GÜZELEL

ÇUKUROVA ÜNİVERSİTESİ
FEN BİLİMLERİ ENSTİTÜSÜ
MAKİNA MÜHENDİSLİĞİ ANABİLİM DALI

Danışman : Doç. Dr. Arif ÖZBEK
Yıl: 2019, Sayfa: 105
Jüri : Doç. Dr. Arif ÖZBEK
: Prof. Dr. Orhan BÜYÜKALACA
: Doç. Dr. Ertaç HÜRDOĞAN

Bu çalışmada, Adana'da bulunan bir okul binasının tüm bir soğutma sezonu boyunca iklimlendirmesi için, desisif bir rotor, ısı geri kazanım üniteleri (reküperatör) ve doğrudan buharlaştırmalı bir soğutucu ile desteklenen Maisotsenko çevrimi esaslı bir iklimlendirme sistemi incelenmiştir. İklimlendirme sisteminin modellenmesinden sonra geliştirilen bir bilgisayar programı ile soğutma sezonu boyunca her ayın 21. günü için saatlik analizler yapılmıştır. İşletme parametrelerinin ideal değerleri, binanın içindeki havanın sıcaklığı ve egzoz havasının besleme havası ile karışım oranı elde edilmiştir. Sistemin iki önemli bileşeni olan desisif rotorun ve Maisotsenko çevriminin etkinlikleri, sistemi çalıştırmak için gereken ısıl enerji ve sistemin soğutma performansı ayrıntılı olarak incelenmiştir. Sonuçlar, ele alınan iklimlendirme sistemi kullanılarak tüm soğutma sezonu boyunca bina içindeki konfor koşullarının sağlanmasının mümkün olduğunu göstermiştir.

Anahtar Kelimeler: Çiğ nokta nemlendirmeli soğutma, Endirekt nemlendirmeli soğutma, Maisotsenko çevrimi, Desisif rotor, İklimlendirme, Modelleme

EXTANDED ABSTRACT

In this thesis, a Maisotsenko cycle based air-conditioning system supported by a desiccant wheel, heat recovery units (recuperators) and a direct evaporative cooling unit is investigated on an hourly basis during a complete cooling season for air-conditioning of a school building located in Adana, Turkey. Flow rate of the air supplied into the building is varied to overcome instantaneous cooling load.

Hourly cooling loads of the sample school building were calculated using hourly outdoor weather data for Adana. The load calculations were performed for the 21st day of each month during a cooling season (between April and October) with 26 °C dry-bulb temperature and 50 % relative humidity indoor conditions. The maximum sensible cooling load of the building is obtained in August, whilst the minimum is in April. Sensible cooling load increases from early morning until noon and later it starts decreasing, while the latent load is constant throughout the day. The minimum and the maximum total cooling loads occur in April and August, respectively. Therefore, the air-conditioning system should be designed using the cooling load obtained in August. The maximum (design) cooling load for the building is 88,4 kW at 13^{00}. At this hour (August, 13^{00} hour), the sensible heat ratio for the building is 0,82. Since the latent load is constant during the day and the sensible cooling load is small at the early hours of the day, the sensible heat ratio can be as small as 0,67 at the early hours.

Air-conditioning system should provide enough fresh air to the people within the building for an acceptable air quality. Fresh air requirement depends on many factors such as type of building, number of people and activity of the people. The minimum fresh air requirement is 9 m^3/h for classrooms for students over 9 years old and total fresh air requirement of the school building is 3606,16 m^3/h.

Equations for predicting the performances (leaving air conditions) of Maisotsenko cycle and desiccant wheel were obtained using the data and equations available in the literature.

Mass balance equations for dry air and the water vapor within air and energy balance equations for dry air were written. Since some of the governing equations are coupled an iterative approach is required for the solution. Various psychometric properties of humid air are required at different locations of the system and an iterative approach is also needed to calculate the desired properties from the known properties. Therefore, the air-conditioning system was modelled with the help of a software so-called EES (Engineering Equation Solver), which eliminates iterations for the solution of governing equations and provides built-in functions for properties of humid air.

In this study, thermophysical properties of humid air were determined by using the property functions available in EES, which require two known (input) properties of the humid air. The mass and balance equations written for each system component were solved simultaneously using the simulation program.

The weather data was needed to simulate outdoor air conditions and they were provided by The State Meteorological Affairs General Directorate (DMİ) of Turkey, include hourly dry-bulb temperature, relative humidity and solar radiation during the years 2009 to 2018. The humidity ratio for these years was also calculated from dry-bulb temperature and relative humidity available.

Analyses were carried out hourly between 7^{00} and 18^{00} for 21^{st} day of each month during the cooling season (from April to October) with the help of the model developed. The runs were performed for building set temperatures ($T_{b,set}$) of 26 °C, 25 °C, 24 °C and 23 °C. For each building set temperature, exhaust air mixing ratio was changed systematically between 0% and 100% with 10% increments. The results showed that it is possible to air-condition the school building during complete cooling season by varying mixing ratio to satisfy ASHRAE comfort conditions. The most economical solution is obtained with the maximum building set temperature (26 °C) and the maximum possible mixing ratio, which vary with time during the cooling season.

Two warm air streams can be directed to the heat exchanger used for preheating regeneration air stream (HX2). Results revealed that regeneration air left desiccant wheel is always warmer than the exhaust air left the first heat exchanger (HX1), which is used to precool supply air upstream of Maisotsenko cycle. Therefore, it is beneficial to utilize the regeneration air left desiccant wheel to the heat exchanger for preheating regeneration air (HX2).

It was found that effectiveness of the desiccant wheel (DW) and Maisotsenko cycle (HMX) do not change significantly during the day. Effectiveness of DW have higher values in cooler months (April and October) and lower in the warmer months (July and August). It varies roughly between 40% and 60% during the cooling season. $\varepsilon_{dp,HMX}$ is minimum around 70% in April and October and maximum around 80% in July and August.

Thermal energy demand profile follows that of total building cooling load and it reaches to a value of as high as 450 kW in July at 14^{00} o'clock. The minimum thermal energy demand is around 100 kW in April and October for most period of the day.

COP changes with both time of the day (hour) and month. The daily change in COP is small for April and October than the other months in cooling season. However, daily change in COP can be as high as 60% in July, which has the smallest COP values. COP changes significantly with the months. It is maximum in October with an average value of 0,77 and minimum in July with an average of 0,21.

COP of the system increases with increasing building set temperature for all mixing ratio values and outdoor air conditions considered. It also increases with the increase of mixing ratio for all building set temperatures and outdoor air conditions considered.

Although COP value is low especially in the summer months of July and August, it should be considered that main energy consumption of the system is

thermal energy and COP is defined in terms of thermal energy as the input. Therefore, it should not be compared directly with a system consuming mainly electricity as input. If the thermal energy is produced from cheap energy source such as waste heat or from solar energy, the system could be an attractive solution.

Another important point that should be considered is that high thermal energy demand for the system coincides with the solar energy available during the summer months. This makes use of solar energy very attractive to produce the thermal energy required for the regeneration of the desiccant wheel of the air-conditioning system.

GENİŞLETİLMİŞ ÖZET

Bu çalışmada, Adana'da bulunan bir okul binasının tüm soğutma sezonu boyunca iklimlendirilmesi için, bir desisif rotor, ısı geri kazanım üniteleri (reküperatör) ve bir doğrudan buharlaştırmalı soğutma ünitesi tarafından desteklenen Maisotsenko çevrimi esaslı bir iklimlendirme sistemi saatlik olarak incelenmiştir. Binaya verilen havanın debisi, anlık soğutma yükünü karışlayacak şekilde değişkendir.

İncelenen okul binasının saatlik soğutma yükleri, Adana için saatlik dış hava iklim verileri kullanılarak hesaplanmıştır. Yük hesapları, soğutma sezonu boyunca (Nisan ve Ekim ayları arasında) her ayın 21. günü için, 26 ^{0}C kuru termometre sıcaklığı ve %50 bağıl nem koşulları için yapılmıştır. Binanın maksimum duyulur soğutma yükü Ağustos ayında, minimum ise Nisan ayında elde edilmiştir. Duyulur soğutma yükü sabahın erken saatlerinden öğlene kadar artmakta ve daha sonra azalmaya başlarken, gizli soğutma yükü gün boyunca sabit kalmaktadır. Minimum ve maksimum toplam soğutma yükleri sırasıyla Nisan ve Ağustos aylarında gerçekleşmiştir. Bu nedenle, iklimlendirme sistemi Ağustos ayında elde edilen soğutma yükü kullanılarak tasarlanmalıdır. Bina için maksimum (tasarım) soğutma yükü saat 13^{00}'de 88.4 kW'tır. Yükün en yüksek olduğu saatte (Ağustos, saat 13^{00}), bina için duyulur ısı oranı ise 0,82'dir. Gizli soğutma yükü gün boyunca sabit olduğundan ve duyulur soğutma yükü günün erken saatlerinde düşük olduğundan, duyulur ısı oranı erken saatlerde 0,67'ye kadar inebilmektedir.

İklimlendirme sistemi, bina içindeki insanlara kabul edilebilir bir hava kalitesi için yeterli temiz hava sağlamalıdır. Taze hava ihtiyacı, bina tipi, insan sayısı ve faaliyeti gibi birçok faktöre bağlıdır. Dersliklerde 9 yaşından büyük öğrenciler için minimum taze hava ihtiyacı 9 m^3/saat, okul binasının toplam taze hava ihtiyacı ise 3606,16 m^3/s' dir.

Maisotsenko çevriminin ve desisif rotorun performansını hesaplayabilmek için gerekli eşitlikler, literatürde mevcut olan veriler ve denklemler kullanılarak elde edilmiştir.

Kuru hava ve hava içindeki su buharı için kütle denge denklemleri ve kuru hava için enerji denge denklemleri yazılmıştır. Bu denklemlerin bazıları birbirine bağlı olduğundan (coupled), çözüm için yinelemeli (iteratif) bir yaklaşım gerekmektedir. Analizler için sistemin farklı noktalarında, nemli havanın çeşitli psikrometrik özelliklerinin bilinmesine ihtiyaç vardır ve bilinen özelliklerden istenilen özellikleri hesaplamak için de yinelemeli bir yaklaşıma ihtiyaç duyulmaktadır.

Bu nedenle iklimlendirme sisteminin analizinde, yazılan denge denklemlerinin çözümü için iterasyonları ortadan kaldıran ve gömülü (built-in) fonksiyonlarla nemli havanın özelliklerini hesaplayabilen, EES adlı bir yazılım ile modelleme yapılmıştır.

Bu çalışmada, nemli havanın özellikleri EES yazılımında mevcut özellik fonksiyonları kullanılarak bulunmuştur. Bu fonksiyonların kullanımı için nemli havanın iki adet özelliğinin bilinmesi yeterlidir. Yazılan modelleme programı kullanılarak sistemi oluşturan her bir eleman için yazılan kütle ve enerji denge denklemleri çözülmüştür.

Çalışmada dış hava koşullarını modellemek için ihtiyaç duyulan iklim verileri, T.C. Devlet Meteoroloji İşleri Genel Müdürlüğü'nden (DMİ) temin edilmiştir. İklim verileri, 2009-2018 yılları saatlik olarak ölçülen kuru termometre sıcaklığı, bağıl nem ve güneş radyasyonunu içermektedir. Ayrıca, DMİ'den alınan kuru termometre sıcaklığı ve bağıl nem kullanılarak özgül nem oranı da hesaplanmıştır.

Geliştirilen model yardımıyla, soğutma mevsimi boyunca (Nisan'dan Ekim'e) her ayın yirmi birinci günü için saat 7^{00} ile 18^{00} arasında saatlik analizler yapılmıştır. Koşturmalar, 26 °C, 25 °C, 24 °C ve 23 °C bina içi hava sıcaklıkları ($T_{b,set}$) için yapılmıştır. Her bir bina içi hava sıcaklığı için egzoz havası karışım

oranı %0 ila %100 arasında %10 artışlarla sistematik olarak değiştirilmiştir. Sonuçlar, egzoz havası karışım oranını değiştirerek, tüm soğutma sezonu boyunca ASHRAE konfor koşullarını yerine getirecek şekilde okul binasını iklimlendirmenin mümkün olduğunu göstermiştir. En ekonomik çözüm, en yüksek bina içi hava sıcaklığı (26 °C) ve mümkün olan en yüksek egzoz havası karışım oranı ile elde edilmiştir. Seçilebilecek en yüksek egzoz havası karışım oranı soğutma sezonu boyunca zamana bağlı olarak değişmektedir.

Rejenerasyon havasını ön ısıtmak için kullanılan ısı değiştiricisine (HX2) iki farklı sıcak hava yönlendirilebilir. Sonuçlar, desisif rotoru terk eden rejenerasyon havasının daima Maisotsenko çevrimi öncesinde ön soğutma yapmak için kullanılan ısı değiştiricisinden (HX1) çıkan egzoz havasından daha sıcak olduğunu ortaya koymuştur. Bu nedenle, rejenerasyon havasını ön ısıtmak için desisif rotoru terk eden rejenerasyon havasını kullanmak her zaman daha faydalıdır.

Desisif rotorun ve Maisotsenko çevriminin etkinliklerinin gün içerisinde önemli ölçüde değişmediği bulunmuştur. Desisif rotorun etkinliği soğuk aylarda (Nisan ve Ekim) yüksek, sıcak aylarda ise (Temmuz ve Ağustos) daha düşüktür. Etkinlik kabaca %40 ila %60 arasında değişmektedir. Maisotsenko çevriminin etkinliği ise en düşük (%70) Nisan ve Ekim aylarında, en yüksek (%80) Temmuz ve Ağustos aylarındadır.

Isıl enerji ihtiyacı profili, bina toplam soğutma yükü profilini izler ve Temmuz ayında saat 14^{00}'de 450 kW gibi yüksek bir değere ulaşır. En düşük ısıl enerji ihtiyacı ise Nisan ve Ekim aylarında günün çoğu döneminde 100 kW civarındadır.

Sistemin performans katsayısı (COP), soğutma sezonu boyunca hem günün saatiyle hem de ay ile değişir. COP'deki günlük değişim, Nisan ve Ekim aylarında soğutma mevsimindeki diğer aylara göre daha küçüktür. Ancak, COP'deki günlük değişim en düşük COP değerlerine sahip olan Temmuz ayında %60 gibi yüksek bir değere kadar çıkabilir. COP aylara göre de önemli ölçüde değişir. En yüksek

ortalama COP değeri Ekim ayında 0,77 ve en düşük değer ise Temmuz ayında 0,21'dir.

Tüm egzoz havası karışım oranları ve dikkate alınan dış hava koşulları için sistem performans katsayısı (COP), artan bina içi hava sıcaklığı ile artar. Benzer şekilde COP, tüm bina içi hava sıcaklıkları ve dikkate alınan dış hava koşulları için egzoz havası karışım oranının artması ile artar.

COP değerleri özellikle yaz aylarından Temmuz ve Ağustosta düşük olmasına rağmen, sistemin ana enerji tüketiminin ısıl enerji olduğu ve bu ısıl enerjinin girdi olarak kullanılarak COP'nin tanımlandığı dikkate alınmalıdır. Isıl enerji, atık ısı gibi ucuz bir enerji kaynağından veya güneş enerjisinden üretilirse, ele alınan iklimlendirme sistem cazip bir çözüm olabilir.

Göz ününde bulundurulması gereken diğer önemli bir husus da, sistemin ısıl enerji ihtiyacının yüksek olduğu yaz aylarında güneş enerjisinin de yüksek olmasıdır. Bu da iklimlendirme sisteminde yer alan kurutucu rotorun rejenerasyonu için gereken ısıl enerjiyi üretmede güneş enerjisi kullanımını çok cazip kılar.

ACKNOWLEDGEMENTS

Firstly, I would like to thank my supervisor Assoc. Prof. Dr. Arif ÖZBEK for providing valuable research advice, continuous support, and his understanding during my thesis.

I would like to express my grate thanks to my dear mother-in-law Prof. Dr. Saadet BÜYÜKALACA, who passed away, for her invaluable support and advices. I will always remember her with her diligence and commitment to life. This thesis dedicated to her.

I am truly grateful to, Prof. Dr. Orhan BÜYÜKALACA, for his invaluable guidance, support and motivation throughout the preparation of this thesis and also as a member of committee.

I would also like to thank to head of the Mechanical Engineering Department Prof. Dr. Hüseyin AKILLI, for his continuous help and advice on my MSc. thesis. I would like to express my special thanks to committee member, Assoc. Prof. Dr. Ertaç HÜRDOĞAN and also Assist. Prof. Dr. Engin PINAR for their devotion of invaluable time throughout my research activities. I would like to thank to Prof. Dr. Azmi AKTACİR for helping and allowing me to use his computer program for cooling load calculations, also thank to The State Meteorological Affairs General Directorate (DMİ) for providing meteorological data.

I am very grateful to my research assistant friend Umutcan OLMUŞ, for his continuous support and motivation. Thank to my course friend Arda YENİÇUN for his support. I want to thank my dear friends Elzem GÜÇLÜ ARSLAN, Fatih Can ARSLAN and Sevil OLMUŞ for their support and motivation.

Another point that should be emphasized here is the continuous moral support, motivation, encouragement and patience of my wife Bilge GÜZELEL, my lovely son Yiğit Emre GÜZELEL, my father Galip GÜZELEL, my mother Havva GÜZELEL and my brothers Osman, Tunahan and Alper throughout my scientific efforts.

CONTENTS **PAGE**

ABSTRACT I
ÖZ II
EXTANDED ABSTRACT III
GENİŞLETİLMİŞ ÖZET VII
ACKNOWLEDGEMENTS XI
CONTENTS XII
LIST OF FIGURES XIV
LIST OF TABLES XVIII
LIST OF SYMBOLS XX
1. INTRODUCTION 1
2. PREVIOUS STUDIES 3
2.1. Dehumidification with Desiccant Wheel 3
2.2. Dew-point Evaporative Cooling with Maisotsenko Cycle 9
2.3. Air-conditioning with Maisotsenko Cycle and Desiccant Wheel 14
3. MATERIAL AND METHOD 19
3.1. Dehumidification with Desiccant Wheel 19
3.2. Evaporative Cooling 20
3.2.1. Direct Evaporative Cooling (DEC) 20
3.2.2. Indirect Evaporative Cooling (IDEC) 22
3.3. Maisotsenko Cycle 23
3.4. Description of the System Investigated 26
3.5. Description of the Building 30
3.5.1. Fresh Air Requirement 33
3.6. Cooling Load of the Building 33
3.7. Weather Data 41
3.8. Modelling of the System Studied 41

3.8.1. Outdoor Air (States 1 and 17) 41
3.8.2. Desiccant Wheel - DW(State 1 to 2) 44
3.8.3. HX1 (State 2 to 3 and 13 to 14) and HX2 (State 17 to 18 and 23 to 24) 49
3.8.4. Maisotsenko Cycle - HMX (State 7 to 8) 52
3.8.5. Supply Air into the Building (States 8 to 9) 54
3.8.6. Direct Evaporative Cooler - DEC (State 10 to 11) 55
3.8.7. Heat Exchanger 3 - HX3 (State 18 to 19) 56
3.8.8. Performance Definition of the System 57
3.8.9. Calculations 57
3.8.10. Thermal Comfort 58
4. RESULTS AND DISCUSSION 63
4.1. Results for a Typical Day with Fixed Mixing Ratio 65
4.1.1. Mass Flow Rate 65
4.1.2. Desiccant Wheel (DW) 68
4.1.3. Heat Exchanger 1 (HX1) 69
4.1.4. Maisotsenko Cycle (HMX) 69
4.1.5. Air Conditions within Building 74
4.1.6. Direct Evaporative Cooler (DEC) 75
4.1.7. Heat Exchanger 2 (HX2) 77
4.1.8. Heat Exchanger 3 (HX3) 77
4.1.9. Coefficient of Performance (COP) of Air-conditioning System 77
4.2. Effect of Building Set Temperature 81
4.3. Effect of Mixing Ratio of Exhaust Air (R) 83
4.4. Results for All the Months 85
5. CONCLUSIONS 91
REFERENCES 95
CURRICULUM VITAE 105

LIST OF FIGURES **PAGE**

Figure 1.1. Working principle of Maisotsenko cycle 2
Figure 2.1. Variation of dew-point effectiveness and outlet air temperature with (a) inlet air temperature and (b) relative humidity of entering air (Anisimov and Pandelidis, 2014)..... 12
Figure 3.1. Schematic representation of desiccant wheel 19
Figure 3.2. Schematic representation (a) and psychometric diagram (b) of a direct evaporative cooler (DEC) 22
Figure 3.3. Schematic representation (a) and psychometric diagram (b) of an indirect evaporative cooler (IDEC)..... 23
Figure 3.4. Maisotsenko (a) and regenerative Maisotsenko (b) cycles (adopted from Mahmood et al., 2016) 24
Figure 3.5. Schematic representation (a) and psychometric diagram (b) of a peforated counter-flow Maisotsenko indirect evaporative cooler (MDEC) (Çalışkan et al., 2012)..... 25
Figure 3.6. Schematic view of the air-conditioned system 28
Figure 3.7. Psychometric chart of the air-conditioning system..... 28
Figure 3.8. Architectural plan of school building 32
Figure 3.9. Schematic of heat transfer for the space (ASHRAE, 2017a)..... 34
Figure 3.10. Calculation procedure for RTS method (ASHRAE, 2017a)..... 38
Figure 3.11. Variation of sensible and latent cooling loads with time for the 21st day of each month during the cooling season 39
Figure 3.12. Variation of total cooling load with time for the 21st day of each month during the cooling season..... 40
Figure 3.13. Variation of sensible heat ratio (SHR) with time for the 21st day of each month during the cooling season..... 40
Figure 3.14. Hourly dry-bulb temperatures measured in Adana during the years 2009 to 2018 for 21st August and average temperature..... 42

Figure 3.15. Hourly relative humidity measured in Adana during the years 2009 to 2018 for 21st August and average relative humidity 42
Figure 3.16. Hourly solar radiation measured in Adana during the years 2009 to 2018 for 21st August and average solar radiation 43
Figure 3.17. Hourly humidity ratio measured in Adana during the years 2009 to 2018 for 21st August and average humidity ratio..... 43
Figure 3.18. The data obtained from the literature and from Eq. 3.12 for process air outlet temperature 47
Figure 3.19. The data obtained from the literature and from Eq. 3.13 for process air outlet humidity..... 47
Figure 3.20. The data obtained from the literature and from Eq. 3.41 for dew-point effectiveness of Maisotsenko cycle 53
Figure 3.21. ASHRAE Comfort zone (adopted from ASHRAE, 2017b) 61
Figure 4.1. A sample output screen from the EES program written 63
Figure 4.2. Psychometric diagram for 21st August at a) 10^{00} o'clock ($T_{b,set}$=26 °C, R=60%) b) 13^{00} ($T_{b,set}$=26 °C, R=70%) and c) 16^{00} ($T_{b,set}$=26 °C, R=60%)..... 66
Figure 4.3. Psychometric diagram for 21st August at 13^{00} o'clock with a) R=50%, b) R=30% and c) R=0% ($T_{b,set}$=26 °C) 67
Figure 4.4. Hourly variation of mass flow rates for 21st August with R=40% ($T_{b,set}$=26 °C) 68
Figure 4.5. Hourly variation of humidity ratio and humidity ratio difference in DW for 21st August ($T_{b,set}$=26 °C, R=40%) 70
Figure 4.6. Hourly variation of temperature and temperature difference in DW for 21st August ($T_{b,set}$=26 °C, R=40%)..... 70
Figure 4.7. Hourly variation of effectiveness of DW for 21st August ($T_{b,set}$=26 °C, R=40%) 71
Figure 4.8. Hourly variation of temperatures and temperature differences in HX1 for 21st August ($T_{b,set}$=26 °C, R=40%)..... 71

Figure 4.9. Hourly variation of sensible precooling of the supply air in HX1 for 21st August ($T_{b,set}$=26 °C, R=40%) 72
Figure 4.10. Hourly variation of temperature, temperature difference and humidity ratio in HMX for 21st August ($T_{b,set}$=26 °C, R=40%)..... 72
Figure 4.11. Hourly variation of cooling of the supply air in HMX for 21st August ($T_{b,set}$=26 °C, R=40%) 73
Figure 4.12. Hourly variation of effectiveness of HMX for 21st August ($T_{b,set}$=26 °C, R=40%) 73
Figure 4.13. Hourly variation of temperature and humidity ratio within the building for 21st August ($T_{b,set}$=26 °C, R=40%) 74
Figure 4.14. Hourly variation of temperatures and temperature difference in DEC for 21st August ($T_{b,set}$=26 °C, R=40%) 75
Figure 4.15. Hourly variation of humidity ratio and humidity ratio difference in DEC for 21st August ($T_{b,set}$=26 °C, R=40%) 76
Figure 4.16. Hourly variation of sensible cooling of the exhaust air in DEC for 21st August ($T_{b,set}$=26 °C, R=40%)..... 76
Figure 4.17. Hourly variation of temperatures at the exit of HX1 (14) and DW (20) for 21st August ($T_{b,set}$=26 °C, R=40%) 78
Figure 4.18. Hourly variation of temperatures and temperature difference in HX2 for 21st August ($T_{b,set}$=26 °C, R=40%) 78
Figure 4.19. Hourly variation of preheating of the regeneration air in HX2 for 21st August ($T_{b,set}$=26 °C, R=40%)..... 79
Figure 4.20. Hourly variation of temperatures and temperature difference in HX3 for 21st August ($T_{b,set}$=26 °C, R=40%)..... 79
Figure 4.21. Hourly variation of heat requirement for heating regeneration air in HX3 for 21st August ($T_{b,set}$=26 °C, R=40%)..... 80
Figure 4.22. Hourly variation of COP of the air-conditioning system for 21st August ($T_{b,set}$=26 °C, R=40%) 80

Figure 4.23. Variation of COP of the air-conditioning system with building set temperature at a)10^{00}, b)13^{00} and c)16^{00} for 21st August 82
Figure 4.24. Variation of COP of the air-conditioning system with mixing ratio of exhaust air at a)10^{00}, b)13^{00} and c)16^{00} for 21st August..... 84
Figure 4.25. Hourly variation of temperature and humidity ratio within the building with the most economic operating conditions ($T_{b,set}$=26 ℃) 87
Figure 4.26. Hourly variation of effectiveness of DW with the most economic operating conditions ($T_{b,set}$=26 ℃) 87
Figure 4.27. Hourly variation of dew-point effectiveness of Maisotsenko cycle with the most economic operating conditions ($T_{b,set}$=26 ℃) 88
Figure 4.28. Hourly variation of thermal energy demand with the most economic operating conditions ($T_{b,set}$=26 ℃) 88
Figure 4.29. Hourly variation of COP of the air-conditioning system with the most economic operating conditions ($T_{b,set}$=26 ℃) 89

LIST OF TABLES **PAGE**

Table 2.1. Parameters to be used in Eqs. 2.16 and 2.17 (Comino et al., 2016)..... 8
Table 2.2. Dew-point effectiveness values reproduced from Riangvilaikul and Kumar (2010)..... 15
Table 2.3. Dew-point effectiveness values from Khalid et al. (2017) 16
Table 2.4. Dew-point effectiveness values from Lin et al. (2018)..... 17
Table 3.1. Suggested maximum overall heat transfer coefficients for the building components for different weather regions of Turkey (TS-825, 2013) 31
Table 3.2. Overall heat transfer coefficients for different building components of the building..... 33
Table 3.3. Heat gain sources for the building 35
Table 3.4. Fresh air requirement of the building..... 36
Table 3.5. The data and the correlations used in the analysis for the performance of the desiccant wheel..... 46
Table 3.6. The data and the correlations used in the analysis for the performance of MC..... 53
Table 4.1. Run plan (codes) for one hour of the day (NS: ASHRAE comfort conditions are not satisfied) 64

LIST OF SYMBOLS

clo : thermal insulation provided by garments and clothing ensembles

c_p : specific heat, [kJ/kg K]

h : enthalpy, [kJ/kg]

$\dot{m}$: mass flow rate, [kg/s]

met : metabolic rate

C : fluid capacitance rate, [W/K]

COP : coefficient of performance

DEC : direct evaporative cooler

DW : desiccant wheel

HMX : heat and mass transfer heat exchanger

HX : heat exchanger

IDEC : indirect evaporative cooler

$\dot{Q}$: heat transfer rate, [W]

T : dry-bulb temperature, [^{o}C]

U : overall heat transfer coefficient, [W/m^{2}K]

V : velocity, [m/s]

Greek Letters

ε : effectiveness, [-]

ρ : density, [kg/m^3]

η : efficiency, [-]

ω : humidity ratio, [kg/kg]

φ : relative humidity, [-]

Subscripts

a : air

b : building

conv : convective
dp : dew-point
e : exhaust
in : inlet
lat : latent
max : maximum
min : minimum
op : operative
out : outlet
p : process
r : regeneration
rad : radiant
sen : sensible
t : total
wb : wet-bulb

1. INTRODUCTION

Final energy use for space cooling in residential and commercial buildings worldwide more than tripled between 1990 and 2016 to 2020 terawatt hours (TWh). The share of cooling in total energy use in buildings rose from about 2.5% to 6% over the same period. For commercial buildings, the share reached 11.5% in 2016 (IEA, 2018).

Energy use for space cooling is expanding rapidly in absolute terms and as a share of overall energy use in buildings. When electricity consumption is considered, cooling accounted for 18.5% of total electricity use in buildings (IEA, 2018).

Only a very small portion of the cooling is produced by absorption refrigeration systems by burning natural gas, the remaining vast majority of the cooling systems are based on vapor compression refrigeration systems, for which energy input is in the form electricity. Vapor compression refrigeration units can impact climate change through two different mechanisms. The first one is that the refrigerants used in vapor-compression refrigeration cycles are greenhouse gases. The second mechanism is related with the electricity generation in which a vast amount of greenhouses gases is emitted to atmosphere.

It is very important to reduce the amount of energy consumption by air-conditioning systems and to investigate new technologies that are less dependent on electricity to run. Many studies have been carried out and still being carried out today to reduce the energy consumption of the air-conditioning systems based on vapor compression refrigeration cycle (Lin et al., 2016) and alternative solutions (Manaf et al., 2018).

One of the newest technologies for air cooling is Maisotsenko cycle that operates with a novel heat and mass exchanger. Maisotsenko cycle is an indirect evaporative cooling-based cycle suggested by Maisotsenko. However, it has a unique heat and mass transfer heat exchanger (HMX) that is different than the

indirect evaporative coolers (Çalışkan et al., 2012).

Maisotsenko cycle based on heat and mass transfer heat exchanger mainly consists of one series of wet and one series of dry channels separated by a thin wall, which does not allow mass transfer from the wet channels to the dry ones. Fig. 1.1 shows working principle of a Maisotsenko cycle.

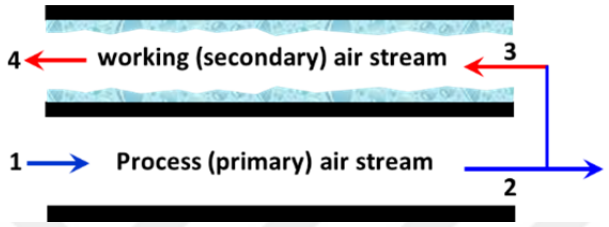

Figure 1.1.Working principle of Maisotsenko cycle

Maisotsenko cycle allows for cooling the air to its dew-point temperature (Gillan, 2008). It is protected by many patents all over the world. Some commercial air-conditioners that are based on Maisotsenko cycle are manufactured by Coolerado Co. today (Mahmood et al., 2016).

The main input for running a Maisotsenko cycle is water rather than electricity, it has potential of reducing electricity consumption up to 90% for dry climates (Rogdakis and Tertipis, 2015).

Maisotsenko cycle allows only sensible cooling of air, which limits its use in hot and humid weather conditions. A desiccant based dehumidifier such as desiccant wheel can be integrated with Maisotsenko cycle under these weather conditions. Maisotsenko cycle provides the sensible cooling, while desiccant wheel removes latent heat.

In this thesis use of Maisotsenko cycle supported by a desiccant wheel for air-conditioning in Adana, Turkey that has a high temperature and humidity during cooling season is investigated.

2. PREVIOUS STUDIES

2.1. Dehumidification with Desiccant Wheel

Hürdoğan et al. (2010) investigated experimentally a novel desiccant cooling system for air-conditioning. Heat recovery heat exchangers that were typically not used were introduced into system to increase the performance. It was concluded that these heat exchangers provided 35% of the total thermal energy requirement for heating regeneration air.

La et al. (2010) presented a review study on the desiccant dehumidification and comfort air-conditioning. Development of new dehumidification materials, the optimisation of system setup and alternative thermal energy sources, such as solar energy, waste heat and bioenergy, that can be used to heat regeneration air were considered. They concluded that, decreasing initial investment cost, minimizing system size, development of routine production procedures and reducing thermal energy requirement are the key points for wider use of these kind of systems.

Heidarinejad and Pasdarshahri (2011) presented a numerical study for a desiccant air-conditioning system with evaporative cooler. The validation of the numerical simulations was confirmed with the experimental measurements. The effects of different ambient conditions on the performance of the system were examined. The results showed that the system studied was more efficient than the conventional evaporative coolers.

Chung and Lee (2011) numerically analyzed effect of different design parameters on the performance of a desiccant cooling system. The performance of the system components and ambient conditions were discussed.

Uçkan et al. (2013) investigated experimentally a configuration of desiccant based evaporative air-conditioning system. Experiments were carried out to investigate the total performance of the system during summer season in a hot and humid climate. The cooling capacity, the energy consumption and the performance coefficient of the system were evaluated. The results showed that, the effectiveness

of the desiccant wheel and evaporative coolers was very high under variable ambient conditions.

Intini et al. (2014) and Comino and Adana (2016) presented a numerical model to investigate the effect of entering air velocity and low regeneration temperatures on optimum working conditions of silica gel desiccant wheels. Rafique et al. (2015), Sultan et al. (2015) and Rambhad et al. (2016) presented review studies for solid desiccant dehumidification and air-conditioning systems. Narayanan (2017) developed a numerical model to investigate the geometry effects of channels of a silica gel desiccant wheel. Güzelel et al. (2017) presented a numerical study for a desiccant seed drying system. Ge et al. (2018) carried out an experimental study on contaminant and moisture removal performance of a silica gel desiccant wheel.

Desiccant wheels are used in many air-conditioning applications to remove moisture of process air. Performance of a desiccant wheel depends on many parameters such as matrix geometry and dimensions; temperature, humidity and flow rates of process (p) and regeneration (r) air streams; rotational speed of the matrix; matrix area designated to supply and regeneration air streams. These parameters are studied analytically, numerically or experimentally in various studies and cross effects are reported.

Beccali et al. (2003) presented two models to evaluate the performance of silica gel desiccant wheel. Relative humidity and enthalpy of outlet process air are calculated through Eqs. 2.1 and 2.2 in one of these models. The correlations presented were based on the data from a silica gel desiccant wheel manufacturer.

$$\varphi_{p,out} = 0{,}9428\ \varphi_{r,in} + 0{,}0572\ \varphi_{p,in} \tag{2.1}$$

$$h_{p,out} = 0{,}1312\ h_{r,in} + 0{,}8688\ h_{p,in} \tag{2.2}$$

In the second model, Beccali et al. (2003) provided correlations to evaluate performance of the silica gel desiccant wheel with the same approach of first model. Although the performance of the second desiccant wheel is similar to the first one, the differences between the two desiccant wheels were not given. In this case, the outlet air relative humidity is also calculated from Eq. 2.1, while the enthalpy of the outlet air is calculated with Eq. 2.3.

$$h_{p,out} = 0{,}1148\, h_{r,in} + 0{,}8852\, h_{p,in} \tag{2.3}$$

Performance of desiccant wheel can also be expressed in terms of combined potentials of the outlet process air ($F_{1,x}$ and $F_{2,x}$) following Jurinak (1982). In this approach, the potentials are calculated with:

$$F_{1,x} = \frac{-2865}{(T_x+273{,}15)^{1{,}49}} + 4{,}344\, {\omega_x}^{0{,}8624} \tag{2.4}$$

$$F_{2,x} = \frac{(T_x+273{,}15)^{1{,}49}}{6360} - 1{,}127\, {\omega_x}^{0{,}07969} \tag{2.5}$$

where, x represents the potentials at the inlet and the outlet of the process air stream ($F_{1,p,in}$, $F_{1,p,out}$ and $F_{2,p,in}$, $F_{2,p,out}$) and at the inlet of the regeneration air stream ($F_{1,r,in}$ and $F_{2,r,in}$). Using the combined potentials $F_{1,x}$ and $F_{2,x}$, characteristic potentials effectiveness can be calculated as:

$$\eta_{F1} = \frac{F_{1,p,out} - F_{1,p,in}}{F_{1,r,in} - F_{1,p,in}} \tag{2.6}$$

$$F_{2,p,out} = \eta_{F2}\left(F_{2,r,in} - F_{2,p,in}\right) + F_{2,p,in} \tag{2.7}$$

Panaras et al. (2010) provided equations (Eqs. 2.8 to 2.10) based on the combined potentials approach explained above. The correlations were obtained from an experimental study carried out with a silica gel desiccant wheel. Three pairs of η_{F1} and η_{F2} were recommended depending on the face velocities of the balanced air streams;

$$\eta_{F1} = 0{,}18 \text{ and } \eta_{F2} = 0{,}72 \text{ (if } V_{p,in} = V_{r,in} = 1{,}1 \text{ m/s)} \tag{2.8}$$

$$\eta_{F1} = 0{,}13 \text{ and } \eta_{F2} = 0{,}66 \text{ (if } V_{p,in} = V_{r,in} = 1{,}8 \text{ m/s)} \tag{2.9}$$

$$\eta_{F1} = 0{,}11 \text{ and } \eta_{F2} = 0{,}67 \text{ (if } V_{p,in} = V_{r,in} = 2{,}2 \text{ m/s)} \tag{2.10}$$

Using the known temperature and humidity ratio of entering process and regeneration air streams, it is possible to calculate at the first step $F_{1,p,in}$, $F_{2,p,in}$, and $F_{1,r,in}$ and $F_{2,r,in}$. In the second step, utilizing the available characteristic potentials effectiveness values $\eta_{F1 \text{ and }} \eta_{F2}$ (Eqs. 2.8, 2.9 and 2.10), $F_{1,p,out}$ and $F_{2,p,out}$ can be obtained from Eqs. 2.6 and 2.7. Once $F_{1,p,out}$ and $F_{2,p,out}$ are determined, $T_{p,out}$ and $\omega_{p,out}$ can be calculated from Eqs. 2.4 and 2.5. As can be seen, this calculation procedure is an implicit method, and thus the solution requires an iterative approach.

Angrisani et al. (2012) also proposed correlations to be used with combined potentials (Eqs. 2.4 and 2.5) and characteristic potentials effectiveness (Eqs. 2.6 and 2.7). The proposed characteristic potentials effectiveness are:

$$\eta_{F1} = 0{,}207 \quad \text{and} \quad \eta_{F2} = 0{,}717 \tag{2.11}$$

Eq. 2.11 was obtained by the researchers from experimental data with a constant airflow of 800 m^3/h.

Ruivo et al. (2012) offered correlations (Eqs. 2.12 and 2.13) to determine the humidity ratio and enthalpy of the outlet air. These equations were obtained from experimental data of Kuma et al. (1998).

$$\varphi_{p,out} = \varphi_{p,in} - 0{,}985\left(\varphi_{p,in} - \varphi_{r,in}\right) \tag{2.12}$$

$$h_{p,out} = h_{p,in} - 0{,}078\left(h_{p,in} - h_{r,in}\right) \tag{2.13}$$

Ruivo and Angrisani (2014) offered the following effectiveness pair to determine the performance of a commercial silica gel desiccant wheel that extrapolated from manufacturer software. The outlet air humidity ratio and the enthalpy are calculated with:

$$\varphi_{p,out} = \varphi_{p,in} - 0{,}921\left(\varphi_{p,in} - \varphi_{r,in}\right) \tag{2.14}$$

$$h_{p,out} = h_{p,in} - 0{,}143\left(h_{p,in} - h_{r,in}\right) \tag{2.15}$$

Comino et al. (2016) suggested the following empirical equations (Eqs. 2.16 and 2.17) to predict the leaving air temperature and humidity ratio as a result of their experimental study with silica gel desiccant wheel, where the terms a_i, b_i, and Y_i are listed in Table 2.1.

$$\omega_{p,out} = \frac{a_0 + \sum_{i=1}^{10}(a_i\, Y_i)}{1000} \tag{2.16}$$

$$T_{p,out} = \frac{b_0 + \sum_{i=1}^{10}(b_i\, Y_i)}{1000} \tag{2.17}$$

Table 2.1.Parameters to be used in Eqs. 2.16 and 2.17 (Comino et al., 2016)

i	a_i	b_i	Y_i
0	6.081,84	−16.707,70	–
1	328,15	144,14	$T_{\mathrm{p,in}}$
2	−400,65	1.786,87	$\omega_{\mathrm{p,in}}$
3	438,02	82,74	$T_{\mathrm{r,in}}$
4	−49,42	505,68	$\omega_{\mathrm{r,in}}$
5	8,64	−19,08	$T_{\mathrm{p,in}}\ \omega_{\mathrm{p,in}}$
6	3,49	3,80	$T_{\mathrm{p,in}}\ T_{\mathrm{r,in}}$
7	−1,91	2,16	$T_{\mathrm{p,in}}\ \omega_{\mathrm{r,in}}$
8	4,62	−6,52	$\omega_{\mathrm{p,in}}\ T_{\mathrm{r,in}}$
9	9,73	−13,22	$\omega_{\mathrm{p,in}}\ \omega_{\mathrm{r,in}}$
10	−6,78	−4,24	$T_{\mathrm{r,in}}\ \omega_{\mathrm{r,in}}$

2.2. Dew-point Evaporative Cooling with Maisotsenko Cycle

Lee and Lee (2013) fabricated an evaporative cooler with counter-flow Maisotsenko cycle and its cooling performance was investigated experimentally. The tests were carried out with an inlet temperature between 28 °C to 32 °C and inlet relative humidity between 40% to 70%. The experimental results showed that the important parameters that affect the cooling performance of the cooler are the water flow rate supplied to the wet channels, temperature and humidity of entering air, working to intake air ratio. The cooling performance was improved if water evaporation rate decreased, while controlling the uniform distribution of the evaporated water. The maximum cooling capacity was obtained with the working to intake air ratio of 0,3. Increasing entering air temperature and humidity resulted in higher dew-point effectiveness values, as expected.

Rogdakis et al. (2014) constructed an experimental installation to identify the effectiveness and consumption. The system was based on Maisotsenko cycle and was able to provide various alternative entering conditions. The conditions that could reach the nominal wet-bulb effectiveness were examined as well as the effect of the outdoor conditions on water consumption. Under different conditions and different optimizations, the water consumption was ranged from 2 kg/kWh to 3 kg/kWh while the wet-bulb effectiveness was changed between 97% and 115%. In addition, a computational simulation of the experimental setup was carried out using ANSYS/FLUENT software and the validation of the model was made with the experimental results. It was also discussed the climate conditions for which the system can operate. The dew-point evaporative cooler was recommended to be used in the Mediterranean regions, because of the low consumption of the electricity and the water. However, it was not recommended for humid climates, for which desirable supply air temperature is high resulting in high consumption.

Jradi and Riffat (2014) presented a numerical study for a cross-flow dew-point evaporative cooler and their numerical results were validated with the data obtained from an experimental setup. The numerical analysis was performed for

air- conditioning applications of buildings with using Matlab software. The system considered achieved 112% wet-bulb effectiveness and 78% dew-point effectiveness with 30 °C and 50% entering air temperature and relative humidity, respectively. In the experimental study, a cross-flow dew-point evaporative cooling system was installed and tested for different operating and ambient conditions. Agreement between the numerical and experimental results are reported to be acceptable. The validated numerical model was used for optimizing the cross-flow dew-point evaporative cooler to achieve the specified comfort conditions. The model was also used to examine the effect on overall performance of dew-point evaporative cooler of various operating parameters such as, inlet air temperature, inlet air velocity, channel height, channel length and working to inlet air ratio.

Anisimov and Pandelidis (2014) investigated cross-flow Maisotsenko cycle numerically. They developed a numerical model based on the modified Ɛ-NTU method to carry out thermal calculations of Maisotsenko cycle evaporative cooling process. The model was validated using the experimental data obtained from the literature. Heat and mass transfer process in working and supply parts were analyzed. They investigated influence of the inlet air temperature and relative humidity on both dew-point and wet-bulb cooling effectiveness. In the study, channel height, channel shape and channel length of the heat exchanger were examined. The influence of inlet air velocity was also discussed on dew-point and wet-bulb effectiveness. The results are given in Fig. 2.1. As can be seen from the figure, dew-point effectiveness increase with the increase of both entering air temperature and relative humidity.

Khalid et al. (2016) analyzed experimentally the performance (dew-point and wet-bulb effectiveness) of a cross-flow dew-point evaporative cooler. Experimental study was carried out with different humidity, temperature and face velocity of entering air stream as well as different water temperatures. They examined variation of dew-point effectiveness with the entering air temperature between 25 ^{o}C and 45 ^{o}C and entering air humidity ratio between 11.2 and 19 g/kg

at a constant entering air velocity of 1.1 m/s. They also investigated the influence of intake air velocity (1.1, 0.62, and 0.49 m/s) at constant humidity ratio (11.2 g/kg). The results showed that wet-bulb effectiveness changed between 92% and 120%, while the dew-point effectiveness ranged between 62% and 85% for different entering conditions. Furthermore, wet-bulb effectiveness of the system studied was found to be 5% bigger in comparison to previous studies.

Cui et al. (2016) developed a performance correlation for the counter-flow Maisotsenko cycle evaporative cooler. Three dimensionless groups were determined to develop a performance correlation based on the dimensionless forms of governing equations. The numerical simulations were performed to specify the empirical constants of the correlation via fitting the simulation results. The numerical results were validated with the results of their experimental study obtained with counter-flow heat and mass heat exchanger and also with the experimental data published in the literature. It was concluded that, the developed correlation predicted the performance of the M-cycle evaporative cooler with a maximum deviation of 12%.

Lin et al. (2017) investigated both experimentally and numerically the cooling potential of a cross-flow dew-point evaporative cooler under various conditions. The experimental part of the study showed that when the ambient humidity ratio exceeds the maximum allowable humidity ratio of 12 g/kg stated in ASHRAE comfort zone, the cooling capacity of the system is not capable of producing design value. To overcome this problem, a dehumidification operation was recommended before the dew-point evaporative cooling process. The dew-point evaporative cooler provided higher cooling effectiveness when suitable inlet conditions were established. In the numerical part of the study, a mathematical model was developed to estimate cooler performance. The outcomes of the study showed that the maximum discrepancy between the simulation and experimental results is 3%. The wet-bulb and the dew-point effectiveness reached to 125% and

85%, respectively. As a conclusion, the dehumidification of the process air resulted in a 70-135% improvement in cooling capacity and energy efficiency.

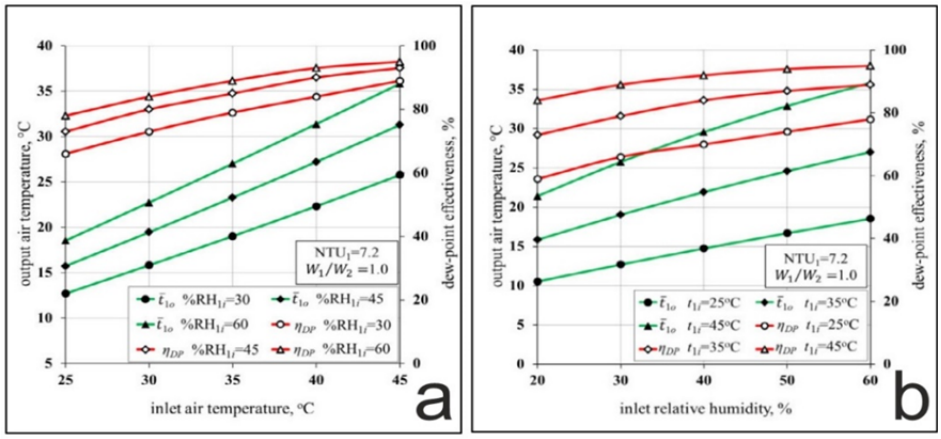

Figure 2.1. Variation of dew-point effectiveness and outlet air temperature with (a) inlet air temperature and (b) relative humidity of entering air (Anisimov and Pandelidis, 2014)

Zhan et al. (2011a) compared cross-flow and counter-flow dew-point evaporative cooling systems. The coolers were investigated both theoretically and experimentally to determine the difference in terms of effectiveness under the same conditions. A parametric study of the performance of the heat exchangers was carried with a computer model developed, and the experimental and theoretical results were compared. According to results; the counter-flow exchanger produced higher (20%) cooling capacity, higher (15%) dew-point effectiveness and also higher (23%) wet-bulb effectiveness under the same physical sizes and the same operation conditions while the cross-flow exchanger resulted higher (10%) COP. In addition, effects of inlet air temperature, inlet air humidity, inlet air flow rate, working to inlet air ratio, channel height and channel length were investigated.

Duan et al. (2016) studied experimentally performance of a counter-flow dew-point evaporative cooler. Temperature, humidity and flow rate of the inlet, outlet and exhaust air streams of the cooler were tested under different operation

conditions. The results of the tests showed that, the wet-bulb effectiveness increased significantly by either increasing wet-bulb depression of inlet air or decreasing the inlet air velocity, also alternatively by increasing the working to inlet air ratio. The cooling capacity and the EER of the cooler increased by increasing the inlet wet-bulb depression, increasing the inlet air velocity or by decreasing the inlet air flow rate. To obtain high efficiency from the exchanger, velocity of inlet air should be low enough, however, cooling requirements of space should be considered. A working to inlet air ratio of 0,4 to 0,5 is suitable for the balance between effectiveness, cooling capacity and energy saving.

Sohani et al. (2018) presented a comparative analysis of various dew-point evaporative coolers for different climates. They performed both a thermodynamic and an economic analysis. Life-cycle cost, annual water consumption and the annual average of the COP were calculated for small-scale residential buildings. According to results, counter-flow was the best configuration in the hot and dry climates while the cross-flow was more suitable for the other climates.

Zhao et al. (2008); Riangvilaikul and Kumar (2010b); Zhan et al. (2011b); Cui et al. (2014); Cui et al. (2015); Heidarinejad and Moshari (2015); Moshari and Heidarinejad (2015); Pandelidis et al. (2015a); Pandelidis et al. (2015b); Lin et al. (2016); Jafarian et al. (2017); Pandelidis et al. (2017a); Wan et al. (2017); Zhu et al. (2017); Liu et al. (2019) performed numerical studies on different Maisotsenko cycles and investigated important variables of the problem.

Bruno (2011); Zube and Gillan (2011); Duan et al. (2017); Xu et al. (2017) studied Maisotsenko cycle experimentally.

Riangvilaikul and Kumar (2010a) reported data for the leaving air temperature and dew-point effectiveness as an outcome of their experimental study with a counter-flow HMX. They presented their effectiveness values in the form of graphs as a function of entering air velocity and temperature for air humidity ratio values of 0,0069; 0,0112; 0,019; 0,02 and 0,0264 kg/kg. The values given in Table 2.2 were reproduced from their graphs.

Khalid et al. (2017) presented the data for the dew-point effectiveness as a result of their experimental study with a counter-flow HMX. They presented their effectiveness values in graphs for air humidity ratio of 0,0127; 0,0144 and 0,018 kg/kg and velocity of 0,88; 1,05 and 1,5 m/s. The results were read from the graphs and listed in Table 2.3.

Lin et al. (2018) presented (Table 2.4) $T_{p,out}$ for fixed value of $V_{p,in}$ (2 m/s) and for $T_{p,in}$ between 27,22 ℃ - 40,32 ℃ and for $\omega_{p,in}$ between 10 - 19,6 g/kg. The data were obtained from their experimental study with a counter-flow HMX and the results were presented in the form of graphs, from which $T_{p,out}$ values were read. The dew-point effectiveness was calculated from Eq. 3.39 utilizing the data given in the table and presented at the last column of Table 2.4.

2.3. Air-conditioning with Maisotsenko Cycle and Desiccant Wheel

Limited research on air-conditioning systems that use Maisotsenko cycle evaporative cooler and the solid desiccant wheel together is available.

Pandelidis et al. (2016) presented a numerical analysis of a desiccant air-conditioning system combined with three different evaporative coolers, namely cross-flow Maisotsenko cycle (System A), counter-flow Maisotsenko cycle (System B) and standard cross-flow evaporative cooler (System C). Dehumidification in these three systems was carried out with a desiccant wheel. The modified Ɛ-NTU model was used in the analysis. The systems were compared under different operational conditions such as, entering air temperature, humidity and regeneration temperature. The results of the numerical study showed that acceptable supply air temperatures were obtained by all three systems even at low regeneration temperatures.

Counter-flow Maisotsenko cycle (System B) was the most complicated and the most expensive system, but it guaranteed the lowest supply air temperature and the highest cooling capacities.

Table 2.2. Dew-point effectiveness values reproduced from Riangvilaikul and Kumar (2010)

$T_{p,in}$ [°C]	$\omega_{p,in}$ [kg/kg]	$V_{p,in}$ [m/s]	ε_{dp}
25,03	0,0069	2,40	0,57
30,02	0,0069	2,40	0,63
35,00	0,0069	2,40	0,67
39,93	0,0069	2,40	0,70
45,05	0,0069	2,40	0,73
24,80	0,0112	2,40	0,60
30,11	0,0112	2,40	0,69
35,03	0,0112	2,40	0,72
40,51	0,0112	2,40	0,75
45,01	0,0112	2,40	0,76
30,02	0,0200	2,40	0,75
35,00	0,0200	2,40	0,79
40,02	0,0200	2,40	0,81
45,05	0,0200	2,40	0,82
32,32	0,0264	2,40	0,78
35,43	0,0264	2,40	0,80
40,31	0,0264	2,40	0,82
45,03	0,0264	2,40	0,84
34,00	0,0190	1,46	0,84
34,00	0,0190	2,36	0,78
34,00	0,0190	3,27	0,69
34,00	0,0190	4,28	0,62
34,00	0,0190	5,13	0,57
34,00	0,0190	6,03	0,53
34,00	0,0112	1,50	0,77
34,00	0,0112	2,39	0,70
34,00	0,0112	3,27	0,64
34,00	0,0112	4,26	0,56
34,00	0,0112	5,17	0,51
34,00	0,0112	5,86	0,49

Table 2.3. Dew-point effectiveness values from Khalid et al. (2017)

$T_{p,in}$ [°C]	$\omega_{p,in}$ [kg/kg]	$V_{p,in}$ [m/s]	ε_{dp}
25,56	0,0127	1,50	0,68
28,09	0,0127	1,50	0,70
35,03	0,0127	1,50	0,75
43,84	0,0127	1,50	0,79
53,01	0,0127	1,50	0,85
25,56	0,0144	1,50	0,70
28,09	0,0144	1,50	0,70
35,09	0,0144	1,50	0,76
38,96	0,0144	1,50	0,79
47,09	0,0144	1,50	0,82
28,77	0,0180	1,50	0,73
33,34	0,0180	1,50	0,76
38,05	0,0180	1,50	0,80
40,05	0,0180	1,50	0,82
48,10	0,0180	1,50	0,86
25,35	0,0144	1,05	0,72
28,05	0,0144	1,05	0,75
35,04	0,0144	1,05	0,80
38,95	0,0144	1,05	0,82
47,03	0,0144	1,05	0,84
24,84	0,0144	0,88	0,74
30,56	0,0144	0,88	0,79
36,04	0,0144	0,88	0,82
40,04	0,0144	0,88	0,83
45,06	0,0144	0,88	0,85

Table 2.4. Dew-point effectiveness values from Lin et al. (2018)

$T_{p,in}$ [°C]	$\omega_{p,in}$ [kg/kg]	$V_{p,in}$ [m/s]	$T_{p,out}$ [°C]	ε_{dp}
27,22	10,00	2,00	17,86	0,71
29,01	10,00	2,00	17,64	0,76
30,71	10,00	2,00	18,14	0,76
32,51	10,00	2,00	18,57	0,76
34,02	10,00	2,00	18,87	0,76
36,23	10,00	2,00	19,64	0,75
38,21	10,00	2,00	20,19	0,75
40,32	10,00	2,00	20,53	0,75
32,50	13,18	2,00	21,71	0,76
32,50	14,01	2,00	22,25	0,77
32,50	15,68	2,00	23,28	0,80
32,50	19,60	2,00	25,82	0,85

Cross-flow Maisotsenko cycle (System A) was slightly cheaper and simple than System B. The most economic and the simplest one was standard cross-flow evaporative cooler (System C). The study concluded that any of these three evaporative coolers can be efficient depending upon the type of operation, energy costs and other operational conditions.

Pandelidis et al. (2018a) presented a numerical study of a multi-stage desiccant air-conditioning system and a typical desiccant air-conditioning system. The numerical simulations were performed for different ambient temperatures and humidities. The multi-stage cooling process consisted two Maisotsenko cycles. One of them was located before dehumidification process, while the second one was located after. Thus, a lower regeneration temperature was also targeted. The authors reported that the system worked efficiently even at low regeneration temperatures (40-50 °C). For this reason, the multi-stage system was gone one step

further in terms of energy consumption. The typical desiccant system included one Maisotsenko cycle located after the dehumidification process. The performances of the systems were compared with each other. The results of the numerical simulations evidently showed that the multi-stage desiccant cooling system supplied process air having lower temperature and humidity under the same ambient conditions.

Shahzad et al. (2018) studied experimentally performance of a system using a desiccant wheel and a cross-flow Maisotsenko cycle evaporative cooler together. They examined performance of the system studied with a wide range of ambient air conditions (temperature and humidity) and with different regeneration temperatures. The system studied was also compared with the classic solid desiccant air-conditioning system. The results of the experiments proved that the desiccant air-conditioning system integrated with Maisotsenko cycle was more efficient (60-65%) than the conventional desiccant air-conditioning system. The researchers also reported that high regeneration temperatures are needed in hot and humid climates, though not as much as the conventional desiccant air-conditioning system.

3. MATERIAL AND METHOD

In this study, air-conditioning of a sample school building located in Adana, Turkey with Maisotsenko cycle supported by desiccant-based dehumidifier, auxiliary direct evaporative cooler and recuperators is investigated during the whole cooling season. Main sensible and latent cooling of the supply air is achieved by Maisotsenko cycle and desiccant wheel, respectively. The proposed system mainly consumes thermal energy, and only air fans and water pump require electricity. Therefore, energy consumption of the fans and pumps are not considered, in the analysis. However, they should also be considered in design project studies of such air-conditioning systems.

3.1. Dehumidification with Desiccant Wheel

Dehumidification of process air (supply air) can be achieved using a desiccant wheel, which consists of a slowly rotating circular matrix coated with a suitable desiccant material (Fig. 3.1).

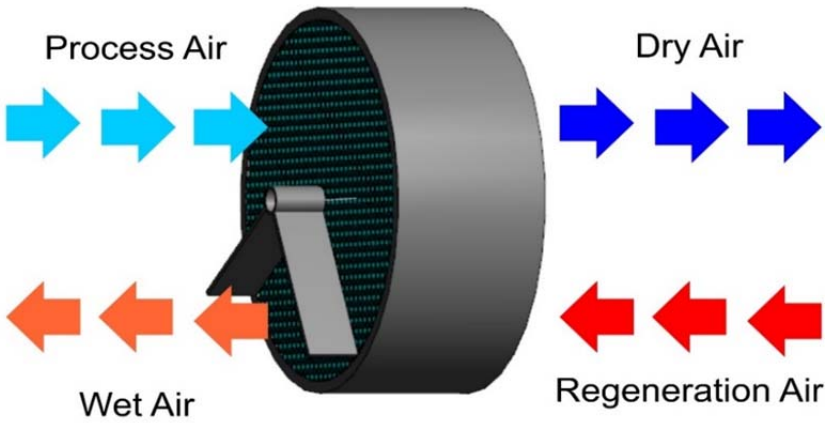

Figure 3.1. Schematic representation of desiccant wheel

The cross-section of desiccant wheel is divided into process air side and regeneration air side (La et al., 2010). Counter-flow is arranged for the flow of process air and regeneration air streams in the desiccant wheel. In most typical application the frontal area of the desiccant wheel is designated equally to the process and regeneration air streams, however area designation could be in favor of process or regeneration air streams depending upon the operating parameters (Antonellis and Joppolo, 2017).

Desiccant wheel rotates through the process air and regeneration air streams, removing moisture from the process air and rejecting it into the regeneration air alternately (Antonellis and Joppolo, 2017). This process results in production of drier but warmer process air and more humid regeneration air at the outlet of the desiccant wheel.

The desiccant material should be able to adsorb moisture easily from the air and desorb at a reasonable regeneration temperature. Different desiccant materials, such as silica gel, molecular sieve (synthetic zeolite), activated alumina, composite materials, liquid and polymer desiccants, biodesiccants and activated carbons and montmorillonite/bentonites clay are available today. New desiccants including composite materials have been developed in recent years. The most commonly used desiccant materials for desiccant wheels is silica gel.

A small electric motors rotates slowly the desiccant wheel typically between 5 rev/h and 90 rev/h (Antonellis and Joppolo, 2017).

3.2. Evaporative Cooling

3.2.1. Direct Evaporative Cooling (DEC)

Evaporative cooling is one of the oldest cooling methods used by human beings. It can be typically classified into two main categories as direct and indirect evaporative cooling.

Dry-bulb temperature of the process air can be lowered using a direct evaporative cooler (Fig. 3.2), in which the added water is evaporated (process air is

humidified directly) and thus humidity increases. Therefore, use of direct evaporative cooling technique is limited to low outdoor air humidity conditions or when high humidity of the supply air can be tolerated for the process such as greenhouses. Various types evaporative media are used for different applications. Fabricated paper, fiberglass or aspen wood fibers are commonly used as the evaporative medium (Kreider and Rabl, 1994) although charcoal, jute material, ceramics, rice husk, clay, recycled high-density polyethylene and wire-mesh pads are also in use.

The minimum outlet temperature of the air (T_2) from a direct evaporative cooler is the wet-bulb temperature of the inlet air ($T_{wb,1}$) and this limits the amount of sensible cooling that can be achieved. Effectiveness of a direct evaporative cooler (ε_{DEC}) is defined as ratio of the dry-bulb temperature depression divided by the difference between the entering dry and wet-bulb temperatures (Kreider and Rabl, 1994):

$$\varepsilon_{DEC} = \frac{T_1 - T_2}{T_1 - T_{wb,1}} \tag{3.1}$$

where;

T_1 : Dry-bulb temperature of entering air

T_2 : Dry-bulb temperature of leaving air

$T_{wb,1}$: Wet-bulb temperature of entering air

It is possible to achieve effectiveness values for the DEC systems higher than 0,9.

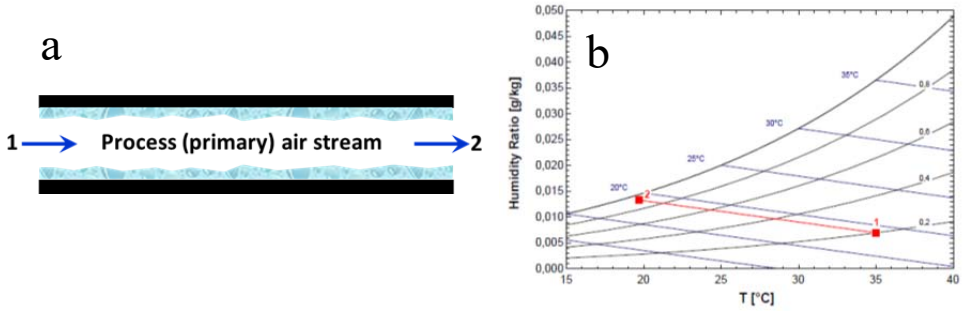

Figure 3.2. Schematic representation (a) and psychometric diagram (b) of a direct evaporative cooler (DEC)

3.2.2. Indirect Evaporative Cooling (IDEC)

It is possible to cool process air sensibly without humidifying it in an indirect evaporative cooler (Fig. 3.3). The process air (primary air) flows through the dry channel of the indirect evaporative cooler, while the working air (secondary air) is evaporatively cooled in wet channel. Sensible heat transfer from the primary air to the secondary air in the heat exchanger decreases the dry-bulb temperature of the process air at constant humidity. Since sensible cooling is achieved without increasing humidity of the process air, indirect evaporative coolers can be used for the weather conditions having higher humidity (Stoitchkov and Dimitrov, 1998).

The minimum outlet temperature of the process air (T_2) from an indirect evaporative cooler is the wet-bulb temperature of the entering secondary air and this limits the amount of sensible cooling that can be achieved. Effectiveness of an indirect evaporative cooler ($\boldsymbol{\varepsilon}_{IDEC}$) is defined as the ratio of the dry-bulb temperature depression divided by the difference between the entering dry and wet-bulb temperatures of the secondary air stream (Kreider and Rabl, 1994):

$$\varepsilon_{IDEC} = \frac{T_1 - T_2}{T_1 - T_{wb,3}} \tag{3.2}$$

where;

T_1 : Dry-bulb temperature of entering process air

T_2 : Dry-bulb temperature of leaving process air

$T_{wb,3}$: Wet-bulb temperature of entering secondary air

Effectiveness of indirect evaporative coolers is lower than that of direct evaporative coolers. Typical effectiveness values range from 0,4 to 0,6 (Maheshwari et al., 2001; Stoitchkov and Dimitrov, 1998). The low effectiveness values for indirect evaporative coolers limit the use of them (Anisimov et al., 2014).

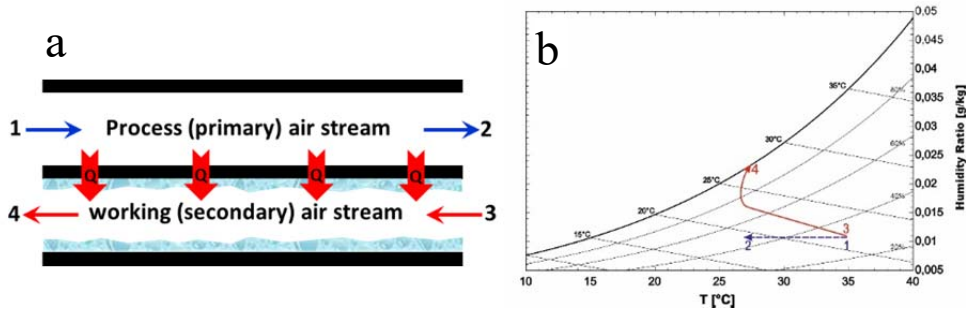

Figure 3.3. Schematic representation (a) and psychometric diagram (b) of an indirect evaporative cooler (IDEC)

Studies available in the open literature revealed that one of the most effective cooling solutions for indirect evaporative air-cooling is the counter-flow cycles (Fig. 3.3) (Pandelidis et al., 2015b).

3.3. Maisotsenko Cycle

The Maisotsenko cycle is an indirect evaporative cooling-based cycle suggested by Maisotsenko (Maisotsenko et al., 2003). However, it has a unique heat and mass transfer heat exchanger (HMX) that is different than the indirect

evaporative coolers (Çalışkan et al., 2012).

Maisotsenko cycle based heat and mass transfer heat exchanger mainly consists of one series of wet and one series of dry channels separated by a thin wall, which does not allow mass transfer from the wet channels to the dry ones.

Different flow arrangements have been offered by researchers (Pandelidis et al., 2017b). Fig. 3.4 shows two configurations so-called the old and the new (regenerative) HMX configurations (Mahmood et al., 2016).

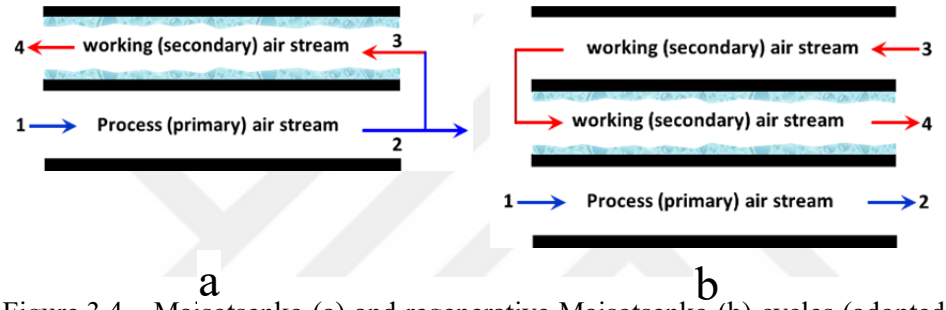

Figure 3.4. Maisotsenko (a) and regenerative Maisotsenko (b) cycles (adopted from Mahmood et al., 2016)

In this study, Maisotsenko cycle with perforated counter-flow heat and mass exchanger (Çalışkan et al., 2012) was considered (Fig. 3.5). In this configuration; supply air stream at the inlet of HMX is split into process and working air streams at different ratios, which is usually 1/3rd of the supply air is utilized as working air, although it is increased up to the half in some studies (Zhan et al., 2011a; Duan et al., 2016).

The working air at first is precooled without an increase in moisture content in the dry channel, and then fractioned into multiple streams and gradually directed into the wet channels, whose surfaces are wetted by water. The holes distributed regularly between the dry and the wet channels designated to the working air stream allow certain amount of the working air to pass from the dry side to the wet side. The precooled working air that is passed to the wet channels flows over the

wet surfaces and is cooled and saturated incrementally in the wet channels, with each stream benefiting from the cooling on the next increment. This cycle is realized many times in a limited volume within the HMX, resulting in progressively lower temperatures. The colder working air stream absorbs heat both from the warmer process air stream and warmer working air stream flowing within the dry channels of the HMX, before it is exhausted. This process allows to produce process air temperature below the wet-bulb temperature of the entering air without an increase its humidity (Çalışkan et al., 2012; Anisimov et al., 2014; Pandelidis et al., 2018b).

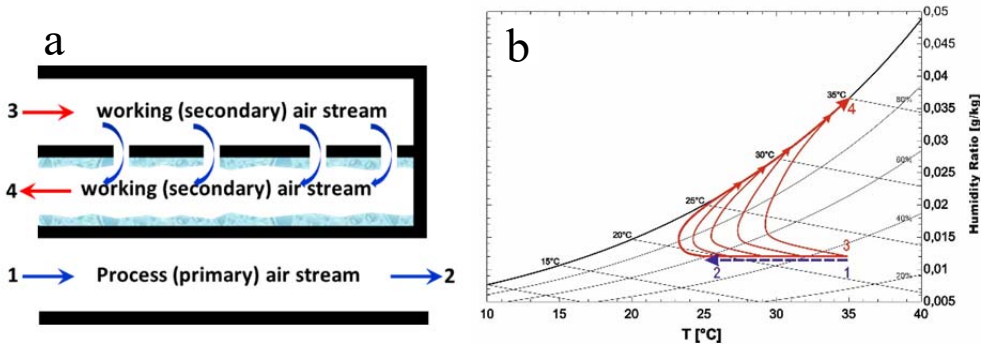

Figure 3.5. Schematic representation (a) and psychometric diagram (b) of a peforated counter-flow Maisotsenko indirect evaporative cooler (MDEC) (Çalışkan et al., 2012)

The minimum outlet temperature of the process air (T_2) from a Maisotsenko cycle is the dew-point temperature of the entering working air. Performance of the Maisotsenko cycle is expressed in terms of dew-point effectiveness (ε_{dp}), which is defined as the ratio of the dry-bulb temperature depression divided by the difference between the entering dry and dew-point temperatures of the working air stream. Since the entering process air and the working air streams are usually split form the same air, the denominator can also be expressed as the difference between the entering dry and dew-point temperatures of the process air:

$$\varepsilon_{dp} = \frac{T_1 - T_2}{T_3 - T_{dp,3}} = \frac{T_1 - T_2}{T_1 - T_{dp,1}} \quad (3.3)$$

where;

T_1 : Dry-bulb temperature of entering process air

T_2 : Dry-bulb temperature of leaving process air

T_3 : Dry-bulb temperature of entering working air

$T_{dp,1}$: Dew-point temperature of entering process air

$T_{dp,3}$: Dew-point temperature of entering working air

If a wet-bulb effectiveness is defined for Maisotsenko cycle similar to indirect evaporative cooling, it can be expressed as (Çalışkan et al., 2012):

$$\varepsilon_{wb} = \frac{T_1 - T_2}{T_3 - T_{wb,3}} = \frac{T_1 - T_2}{T_1 - T_{wb,1}} \quad (3.4)$$

where;

$T_{wb,1}$: Wet-bulb temperature of entering process air

$T_{wb,3}$: Wet-bulb temperature of entering working air

Since dew-point temperature of the entering air ($T_{dp,1}$) is smaller than the wet-bulb temperature ($T_{wb,1}$), wet-bulb effectiveness (ε_{wb}) is higher than dew-point effectiveness (ε_{dp}) and it can be higher than unity.

3.4. Description of the System Investigated

A cost effective air-conditioning can be achieved in dry climates using an air-conditioning system based on Maisotsenko cycle, which does not need energy in the form of electricity except fans for moving air. However, it should be kept in

mind that Maisotsenko cycle cools the air only sensible if it is used alone and it cannot remove the latent part of the building cooling load. This could be an important design issue, especially in humid climates.

Therefore, Maisotsenko cycle is integrated with a desiccant wheel to decrease the humidity of the process air, in this study. Maisotsenko cycle removes the sensible part of the building cooling load whilst desiccant wheel is responsible from the latent part.

The air-conditioning system with Maisotsenko cycle that was studied in this thesis is shown schematically in Fig. 3.6. The Maisotsenko cycle (HMX) and the desiccant wheel (DW) respectively provide the main sensible and latent cooling of the air process air supplied to the air-conditioned space. Sensible heat recovery heat exchangers (HX1 and HX2) and direct evaporative cooling unit (DEC) are utilized for better performance of HMX, better air quality and energy efficiency. Psychometric diagram of the system studied is shown in Fig. 3.7 for a typical outdoor weather condition.

Humidity of the outdoor air is reduced in the desiccant wheel (1-2), whilst its dry-bulb temperature increases. The fresh air leaves the desiccant wheel (DW) drier and warmer. Dehumidifying process takes place approximately at constant wet-bulb temperature, although an increase in wet-bulb temperature is experienced.

A recuperator type heat exchanger (HX1), in which only sensible heat transfer takes from warm fresh air to cooler exhaust air, is used to precool the fresh air (2-3) before it is supplied to Maisotsenko cycle (MC).

Temperature of the exhaust air leaving the direct evaporative cooler (DEC) (state 11) is lower than the fresh air left HX1 (state 3), however more humid. If the temperature and humidity of the exhaust air leaving the direct evaporative cooler (DEC) (state 11) is more advantageous to use, certain amount of it is mixed with the fresh air (state 3) to reduce the temperature of the process air. Monitoring the conditions of the air in the building, automatic control system adjusts the amount of the exhaust air to be mixed so that desired comfort conditions are satisfied.

Process air (state 4) then enters into Maisotsenko cycle, in which it is separated into two streams as process air stream (state 7) and working air stream (state 5). Considering the information given in section 3.3, the ratio of working air mass flow rate to total mass flow rate was taken 0,33 in this study. Temperature of the supply air is reduced sensibly by HMX and provided to the building (at state 8) to be air-conditioned (state 9).

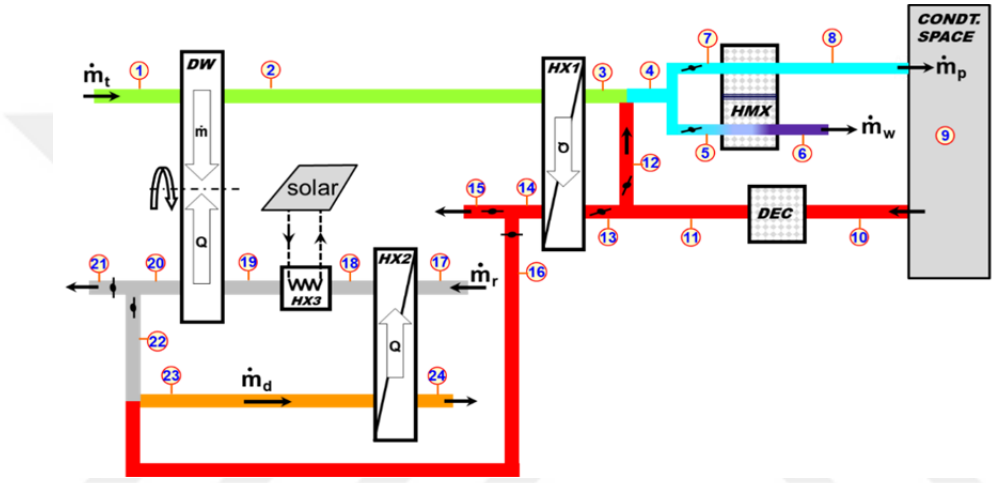

Figure 3.6. Schematic view of the air-conditioned system

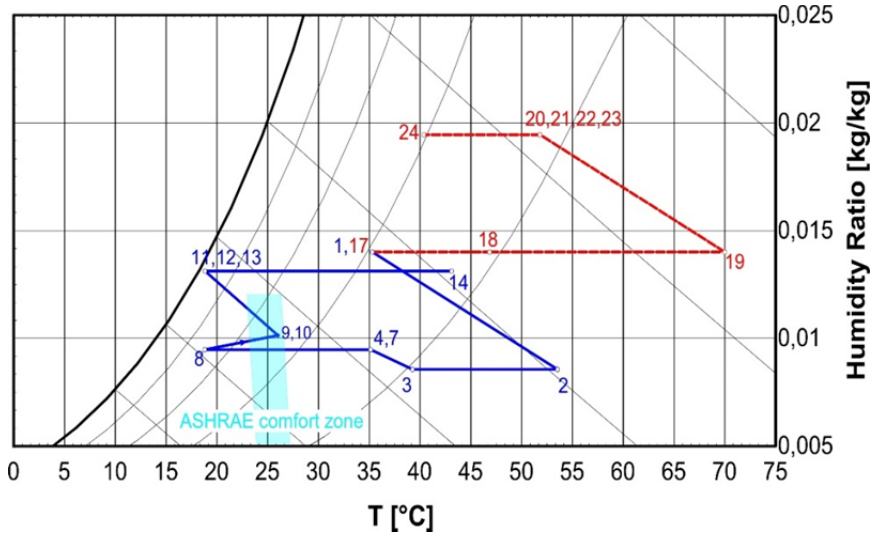

Figure 3.7. Psychometric chart of the air-conditioning system

Exhaust air sucked from the air-conditioned building (state 10) is sent to a direct evaporative cooler (DEC), in which dry-bulb temperature of the exhaust air decreases, whilst its humidity increases (state 11). Humidifying process takes place at almost constant wet-bulb temperature. Certain amount of the exhaust air is mixed (state 12) with fresh air and the remaining part (state 13) is sent to the recuperator (HX1) to precool the fresh air, as explained above. The exhaust air leaving HX1 (state 14) is either directed to HX2 (state 16) or discharged to atmosphere (state 15), for which details are given below.

A cheap thermal energy source for the removal of humidity from the desiccant wheel (regeneration) is of very importance for the performance of the system. In this study, thermal energy for the regeneration is obtained from solar energy or another waste heat at a temperature higher than 70 ^{o}C, which is the minimum temperature required for the regeneration in desiccant wheels.

However, another recuperator (HX2) is utilized to preheat the regeneration air before the main heating process by solar energy to reduce the thermal energy requirement. Either the air leaving HX1 (state 16) or the regeneration air leaving DW (state 20) can be used for preheating regeneration air depending upon their dry-bulb temperature. In this study, use of both warm air streams (states 16 and 20) for preheating regeneration air stream was investigated and automatic control system selects the favorable warm air stream and directs to HX2.

Outdoor air (state 17) is first preheated sensibly in HX2 (state 18) and then heated sensibly to the desired temperature for regeneration of the desiccant wheel in the heat exchanger (HX3) (state 19).

Hot regeneration air (19) removes the humidity of the desiccant material and as a result, humidity of the regeneration air increases and temperature decreases. The regeneration air leaving DW (state 20) is either discharged to the atmosphere (state 21) or directed to HX2 (state 22) for heat recovery. The regeneration air leaving HX2 (state 24) is discharged to atmosphere.

Automatic control system initially sets the desired building temperatures to

26 °C, which is the most economic value, and the mass flow rate of the air that must supplied to the building is calculated accordingly to meet the sensible cooling load of the building. If the conditions within the room do not satisfy the ASHRAE comfort conditions, the building set temperature is reduced gradually from 26 °C until it is in the ASHRAE comfort zone.

Another important parameter that affects the cooling effectiveness of the system is the percentage mixing ratio of the exhaust air to the fresh air:

$$R(\%) = \frac{\dot{m}_{12}}{\dot{m}_{11}} * 100 \quad (3.5)$$

As long as fresh air requirement of the occupants in the building is provided, mixing most of the exhaust air produces the best economic operation. Therefore, automatic control system initially starts with mixing all the exhaust air (*R=100%*) and checks the fresh air requirement and also ASHRAE comfort conditions within the building. If one of the above criteria is not satisfied amount of exhaust air mixed is reduced gradually (*R* reduced).

3.5. Description of the Building

Performance of the air-conditioning system described above was analyzed for a sample school building.

3-storey school building is sited in Adana, Turkey and includes 14 classrooms, 3 laboratories, 5 offices, 1 library, 1 technology laboratory and 3 corridors. The city Adana is located in the south part of Turkey, in the east Mediterranean Region (36.59 latitude, 35.18 longitude and 20 m altitude). The main weather characteristics for the city Adana are mild winters and hot and humid summers. The cooling season typically extents from April 21 to October 21, lasting 184 days.

Architectural plan of the building that has 1628 m^2 gross area is given in Fig. 3.8. Long sides of the building face to the North and the South and the outside surfaces of the walls are light colored.

TS-825, (2013) that is the compulsory Thermal Insulation Regulation for buildings effective in Turkey suggests the maximum overall heat transfer coefficients (U) for the building components given in Table 3.1 for different weather regions (5 regions) of Turkey. Adana is listed in the 1st region.

Table 3.1. Suggested maximum overall heat transfer coefficients for the building components for different weather regions of Turkey (TS-825, 2013)

Region	**U_D [W/m^2K]**	**U_T [W/m^2K]**	**U_t [W/m^2K]**	**U_p [W/m^2K]**
1st	0,66	0,43	0,66	1,8
2nd	0,57	0,38	0,57	1,8
3rd	0,48	0,28	0,43	1,8
4th	0,38	0,23	0,38	1,8
5th	0,36	0,21	0,36	1,8

In this table;

U_D : Overall heat transfer coefficient of outer walls

U_T : Overall heat transfer coefficient of roofs

U_t : Overall heat transfer coefficient of floors that sit on ground

U_P : Overall heat transfer coefficient of windows

The overall heat transfer coefficients of the school building considered are given in Table 3.2. As can be seen from the comparison of Tables 3.1 and 3.2, the building components have always smaller U values than the maximum allowable overall heat transfer coefficients. Building is a thermally insulated building and the glasses are low e-film covered double glazed window.

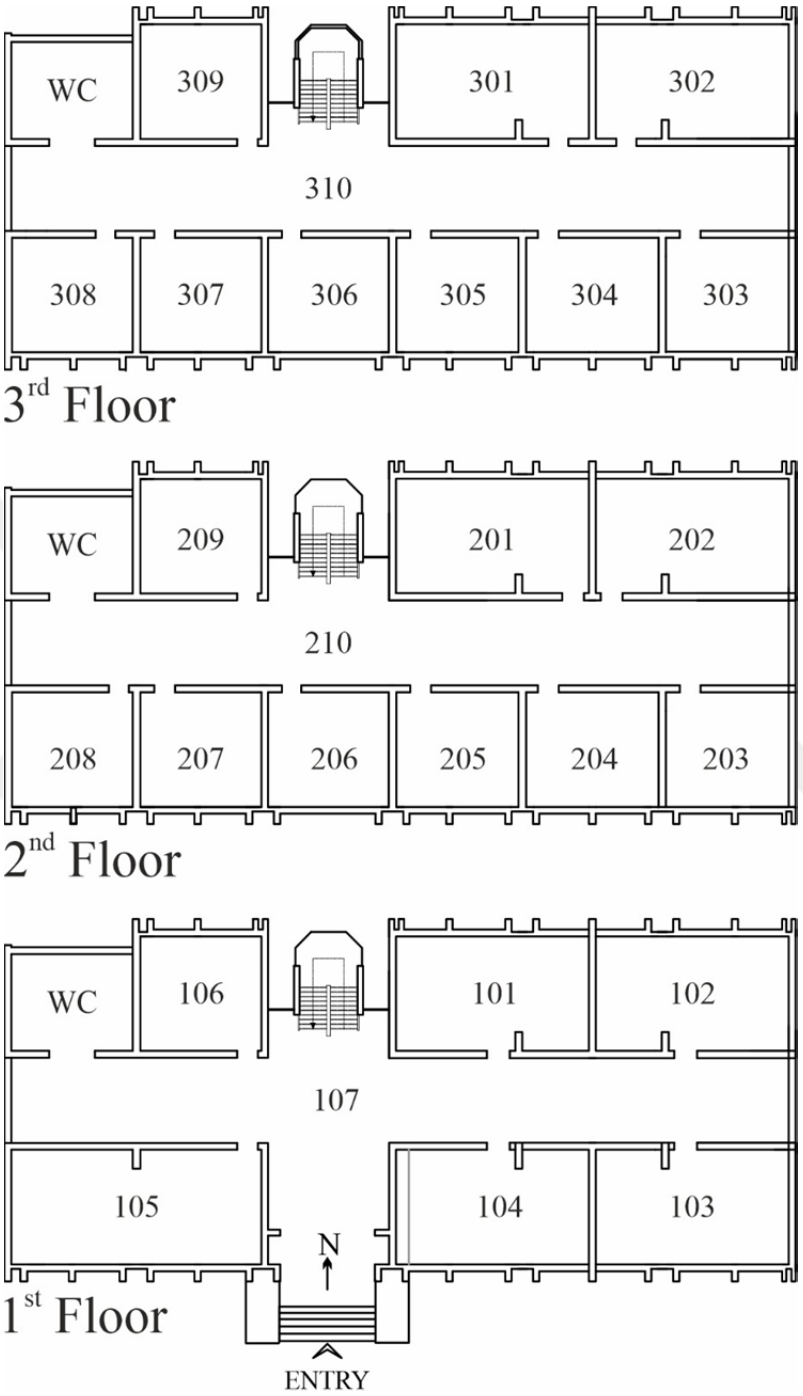

Figure 3.8. Architectural plan of school building

Table 3.2. Overall heat transfer coefficients for different building components of the building

Building component	**U [W/m^{2}K]**
Outer walls	0,436
Roof	0,436
Floor	0,436
Window	1,6

Parameters that affect the internal heat gain of the building namely number of occupants inside the conditioned room, heat gains due to appliances, equipment and lighting and the related diversity factors that were used in the calculation of the cooling load are given Table 3.3.

3.5.1. Fresh Air Requirement

Air-conditioning system should provide enough fresh air to the people within the building for an acceptable air quality. Fresh air requirement depends on many factors such as type of building, number of people and activity of the people. ASHRAE Standard 62.1, (ASHRAE, 2013) specifies minimum fresh air rates for various conditions in the form of tables. The minimum fresh air requirement is 9 m^3/h for classrooms for students over 9 years old and total fresh air requirement of the school building is 3606,16 m^3/h. Table 3.4 lists fresh air requirement of the school building.

3.6. Cooling Load of the Building

Cooling load of a building result from many conduction, convection, and radiation heat transfer processes through the building components (such as walls, windows, roofs, floors) and from internal sources (such as people, lights, devices) and system components (fans and pumps, outside air, leakage and heat gain) in addition to the air infiltration (ASHRAE, 20017a).

Thermal storage of the building components is an important subject that should be considered in detail. Some heat gain components are not converted immediately into cooling load, they are converted with a time lag. Heat transfer mechanics of a space is shown in Fig. 3.9 (ASHRAE, 2017a).

Another point that makes the cooling load estimation complex is heat transfer through building envelopes is a transient process because of the variations in outdoor conditions and heat gains from occupants, lighting, and electrical equipment (Coral et al., 2019).

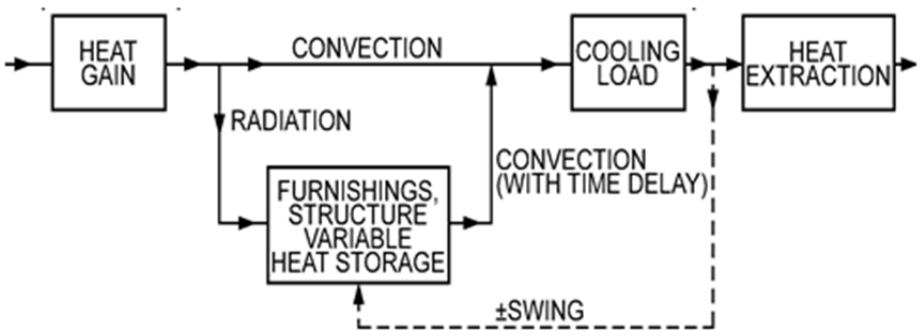

Figure 3.9. Schematic of heat transfer for the space (ASHRAE, 2017a)

Table 3.3. Heat gain sources for the building

Room	Occupants				Appliance and Equipment		Lighting	
	No	Divers. Factor	Sens. Heat Gain [W]	Lat. Heat Gain [W]	Divers. Factor	Sens. Heat Gain [W]	Divers. Factor	Sens. Heat Gain [W]
101	1	0,85	75	55	1	355	1	581,94
102	15	0,3	75	55	1	355	1	850,95
103	15	0,3	75	55	1	355	1	850,95
104	15	0,3	75	55	1	355	1	850,95
105	15	0,5	75	55	1	355	1	1324,1
106	2	0,9	75	55	1	355	0,5	400,68
107	60	0,4	75	55	1	0	0,5	1236,6
201	15	0,3	75	55	1	355	1	603,9
202	25	0,3	75	55	1	355	1	631,35
203	15	0,8	75	55	1	355	1	472,75
204	15	0,8	75	55	1	355	1	489,64
205	15	0,8	75	55	1	355	1	489,64
206	15	0,8	75	55	1	355	1	489,64
207	15	0,8	75	55	1	355	1	489,64
208	10	0,5	75	55	1	355	1	547,43
209	2	0,9	75	55	1	355	0,5	400,68
210	100	0,3	75	55	1	0	0,5	1042,8
301	15	0,8	75	55	1	355	1	735,66
302	15	0,8	75	55	1	355	1	735,66
303	15	0,8	75	55	1	355	1	472,75
304	15	0,8	75	55	1	355	1	489,64
305	15	0,8	75	55	1	355	1	489,64
306	15	0,8	75	55	1	355	1	489,64
307	15	0,8	75	55	1	355	1	489,64
308	15	0,8	75	55	1	355	1	472,75
309	2	0,9	75	55	1	355	0,5	400,68
310	100	0,3	75	55	1	0	0,5	1042,8

Table 3.4. Fresh air requirement of the building

Room	Type	Floor Area (m^2)	People		Outdoor Air Requirement		Total Fresh Air
			NO	Use Factor	m^3/h per person	m^3/h per m^2	m^3/h
101	Manager Office	54,90	1	0,85	9,00	-	7,65
102	Laboratory I	54,90	15	0,30	18,00	-	81,00
103	Laboratory II	54,90	15	0,30	18,00	-	81,00
104	Laboratory III	54,90	15	0,30	18,00	-	81,00
105	Library	71,96	15	0,50	18,00	-	135,00
106	Office	37,80	2	0,90	9,00	-	16,20
107	Corridor	174,17	60	0,40	-	1,08	75,24
201	Art Classroom	54,90	15	0,30	18,00	-	81,00
202	PC Lab	54,90	25	0,30	9,00	-	67,50
203	Classroom	35,28	15	0,80	18,00	-	216,00
204	Classroom	36,54	15	0,80	18,00	-	216,00
205	Classroom	36,54	15	0,80	18,00	-	216,00
206	Classroom	36,54	15	0,80	18,00	-	216,00
207	Classroom	36,54	15	0,80	18,00	-	216,00
208	Teachers Room	41,16	10	0,50	9,00	-	45,00
209	Office	37,80	2	0,90	9,00	-	16,20
210	Corridor	146,87	100	0,30	-	1,08	47,59
301	Classroom	54,90	15	0,80	18,00	-	216,00
302	Classroom	54,90	15	0,80	18,00	-	216,00
303	Classroom	35,28	15	0,80	18,00	-	216,00
304	Classroom	36,54	15	0,80	18,00	-	216,00
305	Classroom	36,54	15	0,80	18,00	-	216,00
306	Classroom	36,54	15	0,80	18,00	-	216,00
307	Classroom	36,54	15	0,80	18,00	-	216,00
308	Classroom	35,28	15	0,80	18,00	-	216,00
309	Office	37,80	2	0,90	9,00	-	16,20
310	Corridor	146,87	100	0,30	-	1,08	47,59
						Total outdoor air requirement=	3606,16

Different cooling load calculation methods are available today. The methods proposed by ASHRAE are Transfer Function Method (TFM), Cooling Load Temperature Differential/Cooling Load Factors (CLTD/SCL/CLF), Total Equivalent Temperature Differential/Time-Averaging (TETD/TA), Heat Balance (HB) and Radiant Time Series (RTS) (Coral et al., 2019). The methods differ from each other in terms of complexity and accuracy of the results.

Radiant Time Series method (RTS) was used for the calculation of the cooling load of the sample building in this study. The details of the RTS calculation procedure is given in ASHRAE (2017a).

RTS method was derived from the most accurate but complex method of the heat balance (HB) method by Spitler et al. (1997). It is a simplified method and effectively replaces all other simplified methods, such as the transfer function method (TFM), the cooling load temperature difference/cooling load factor (CLTD/CLF) method, and the total equivalent temperature difference/time averaging (TETD/TA) method (ASHRAE, 2017a).

The main calculation procedure of the RTS method is presented in Fig. 3.10. Conduction and radiant time delay effects are accounted by multiplying hourly heat gains by 24 h time series. The time series multiplication distributes heat gains over time. Time series coefficients are called radiant time factors and conduction time factors. Radiant time factors reflect the percentage of an earlier radiant heat gain that becomes cooling load during the current hour. Similarly, conduction time factors reflect the percentage of an earlier heat gain at the exterior of a wall or roof that becomes heat gain indoors during the current hour (ASHRAE, 2017a).

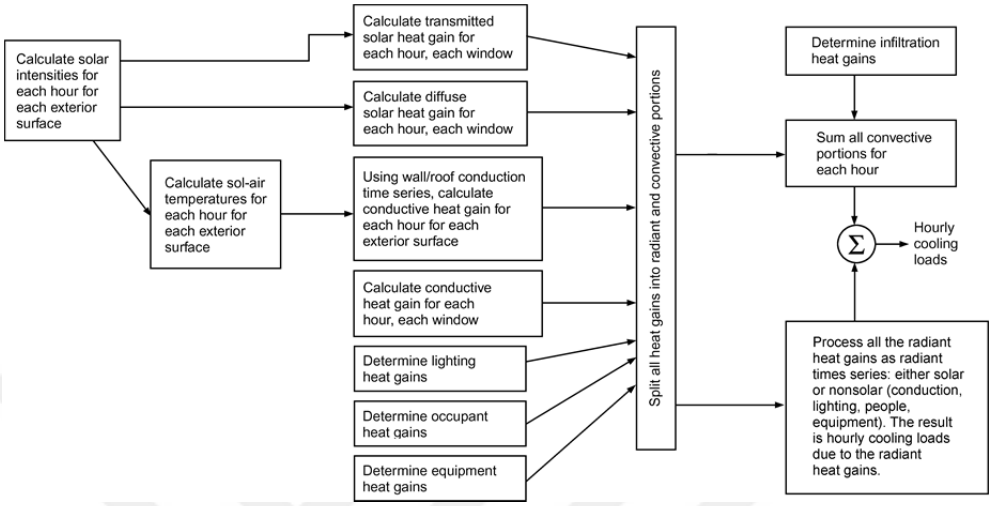

Figure 3.10. Calculation procedure for RTS method (ASHRAE, 2017a)

In this study, hourly cooling loads of the school building were calculated using a computer program developed by Aktacir, (2005), which is based on RTS method. The program was developed to run in MS-EXCEL environment.

Hourly cooling loads of the sample building were calculated using hourly outdoor weather data for Adana. The load calculations were performed for the 21st day of each month during a cooling season (between April and October) with 26 °C dry-bulb temperature and 50 % relative humidity indoor conditions.

Hourly sensible and latent cooling loads of the building are given in Fig. 3.11. It can be seen from the figure that the maximum sensible cooling load of the building is obtained in August, whilst the minimum is in April. Sensible cooling load increases from early morning until noon and later it starts decreasing, while the latent load is constant throughout the day.

Total cooling load (Fig. 3.12) exhibit a similar pattern throughout the day and months. The minimum and the maximum total cooling loads occur in April and August, respectively. Therefore, the cooling system should be designed using the cooling load obtained in August. The maximum (design) cooling load for the

building is 88,4 kW at 13^{00}.

The sharp increase in the cooling load between 7^{00} to 8^{00} and the sharp decrease from 17^{00} to 18^{00} is due to people entering and leaving the building at these hours.

The ratio of sensible to total cooling load is called sensible heat ratio (SHR). At the peak hour (August, 13^{00} hour), the sensible heat ratio for the building is 0,82 (Fig. 3.13). Since the latent heat is constant during the day and the sensible cooling load is small at the early hours of the day, the sensible heat ratio can be as small as 0,67 at the early hours.

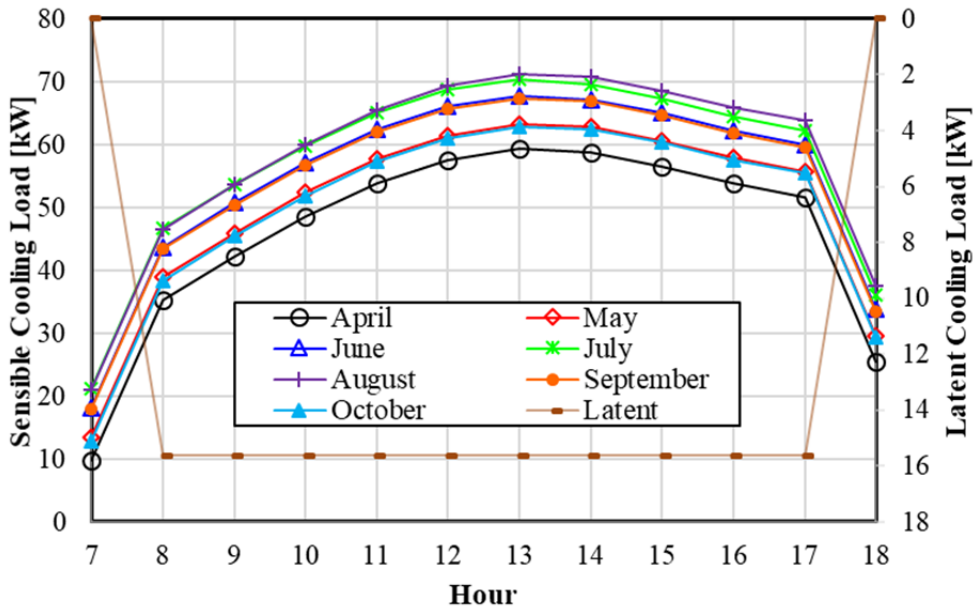

Figure 3.11. Variation of sensible and latent cooling loads with time for the 21st day of each month during the cooling season

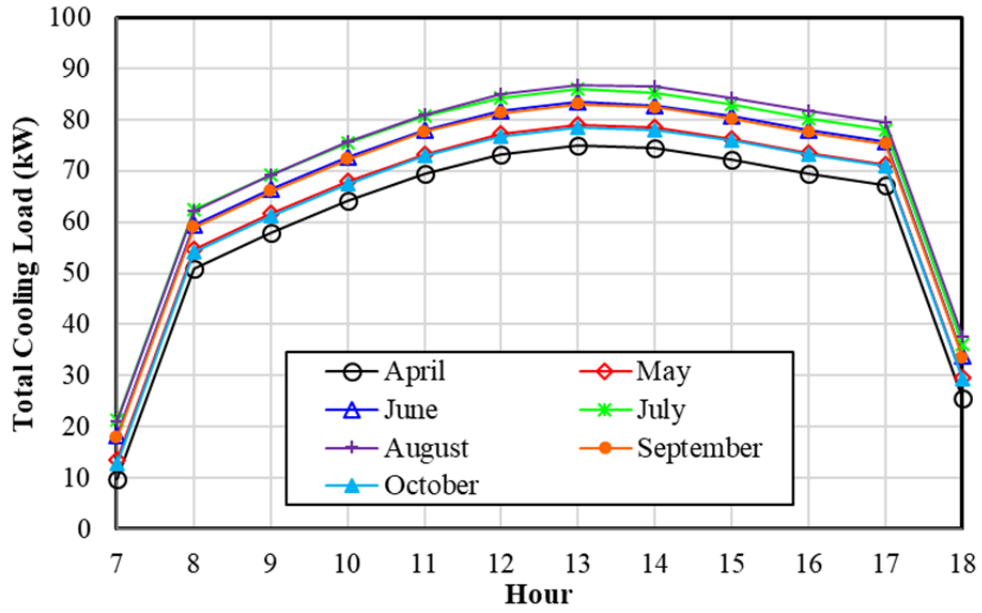

Figure 3.12. Variation of total cooling load with time for the 21st day of each month during the cooling season

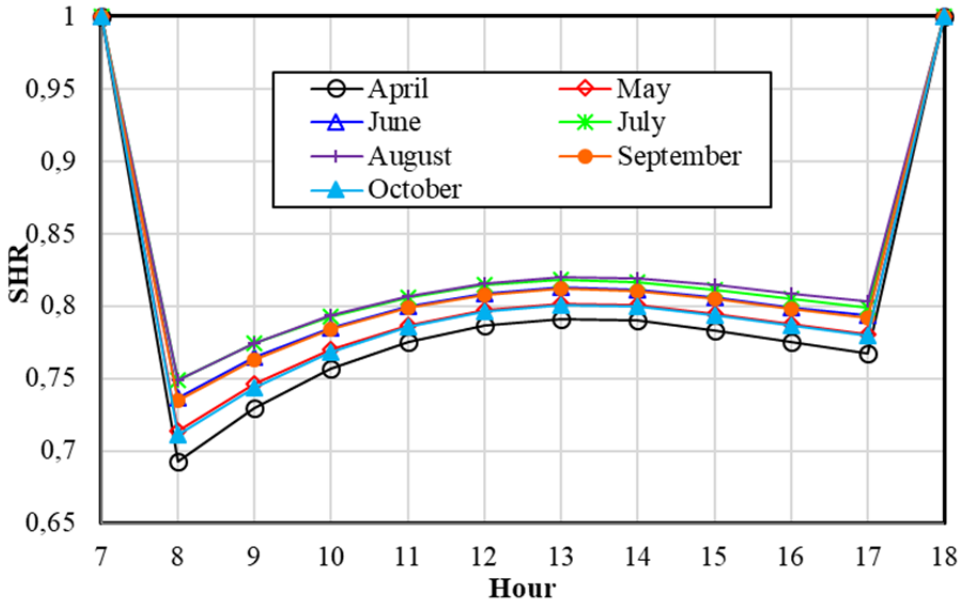

Figure 3.13. Variation of sensible heat ratio (SHR) with time for the 21st day of each month during the cooling season

3.7. Weather Data

Performance of the system studied were calculated hourly at 21st day of each month during the cooling season for Adana. The weather data, which were provided by The State Meteorological Affairs General Directorate (DMİ) of Turkey, include hourly dry-bulb temperature, relative humidity and solar radiation during the years 2009 to 2018.

Hourly average values of the weather parameters for the years 2009 to 2018 were calculated and used in this study. Figs. 3.14 to 3.16 show hourly dry-bulb temperature, relative humidity and solar radiation measured during the years 2009 to 2018 for the 21th August and average values. Using the data obtained, hourly and average humidity ratio were also calculated and presented in Fig. 3.17 for 21st August.

3.8. Modelling of the System Studied

Necessary governing equations for the analysis of the air-conditioning system defined above were described below. The model assumes that the system is under steady state conditions, heat losses from/to all the components and the connecting ducts are negligible (all insulated) and pressure drop in the connecting ducts and the components of the system is neglected.

3.8.1. Outdoor Air (States 1 and 17)

The outdoor air, for which dry-bulb temperature (T) and relative humidity (φ) are known from the metrological data, is taken into the system at states 1 and 17. Other necessary psychometric properties (humidity ratio, enthalpy, wet-bulb temperature, dew-point temperature, density and specific heat) can be calculated using these two known properties. Hourly mean data were used for the calculations as explained in section 3.7., in this thesis.

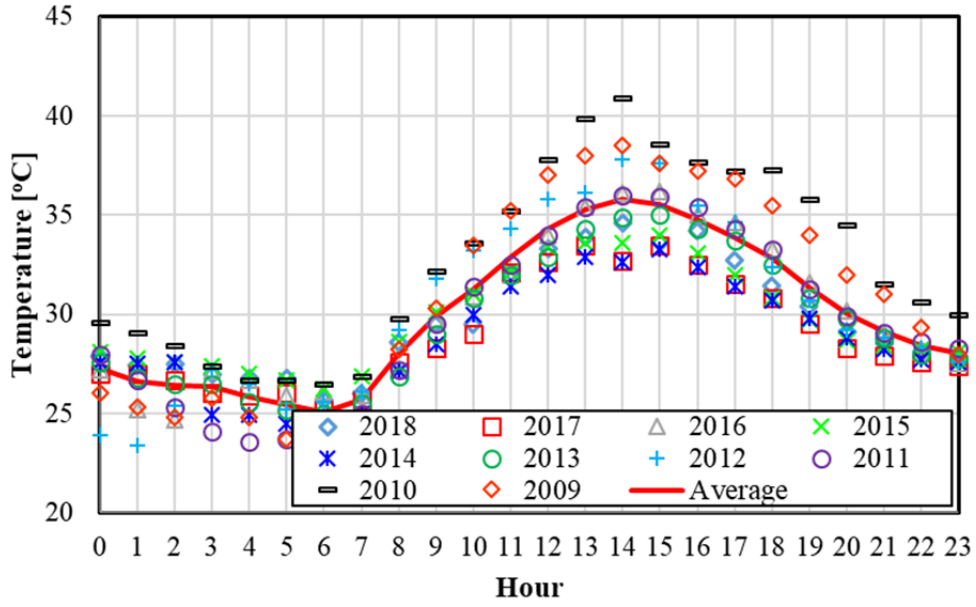

Figure 3.14. Hourly dry-bulb temperatures measured in Adana during the years 2009 to 2018 for 21st August and average temperature

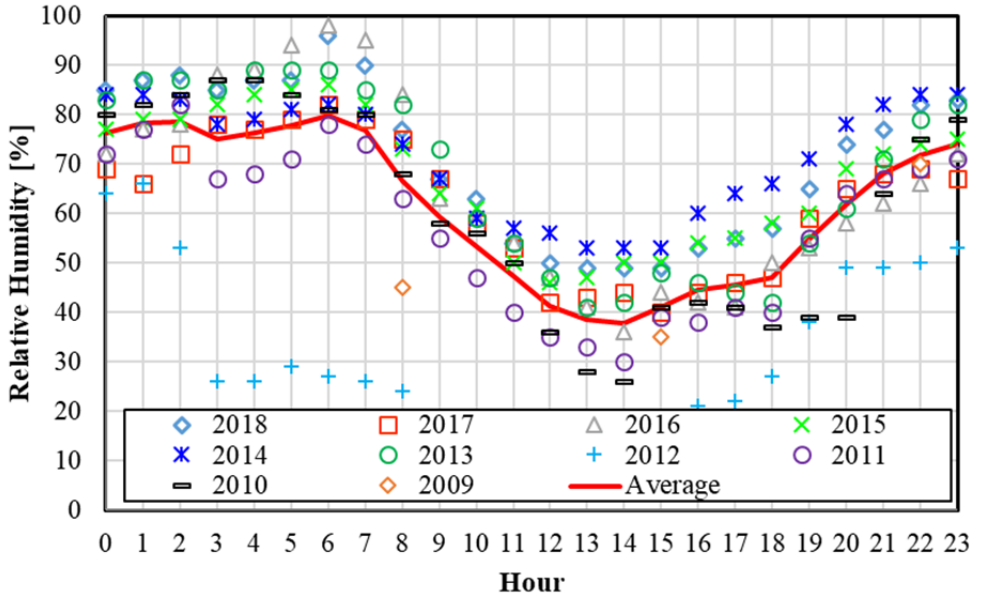

Figure 3.15. Hourly relative humidity measured in Adana during the years 2009 to 2018 for 21st August and average relative humidity

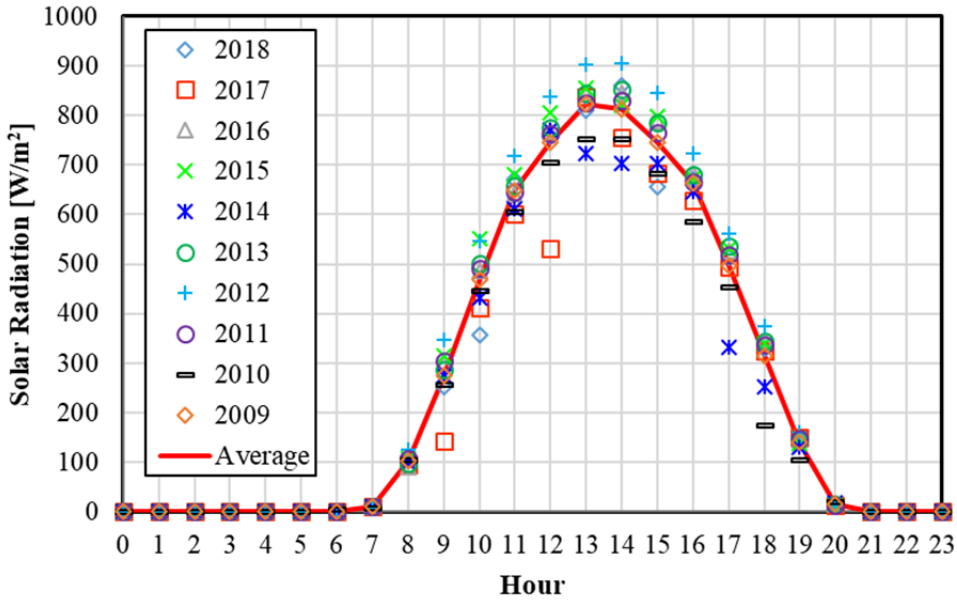

Figure 3.16. Hourly solar radiation measured in Adana during the years 2009 to 2018 for 21st August and average solar radiation

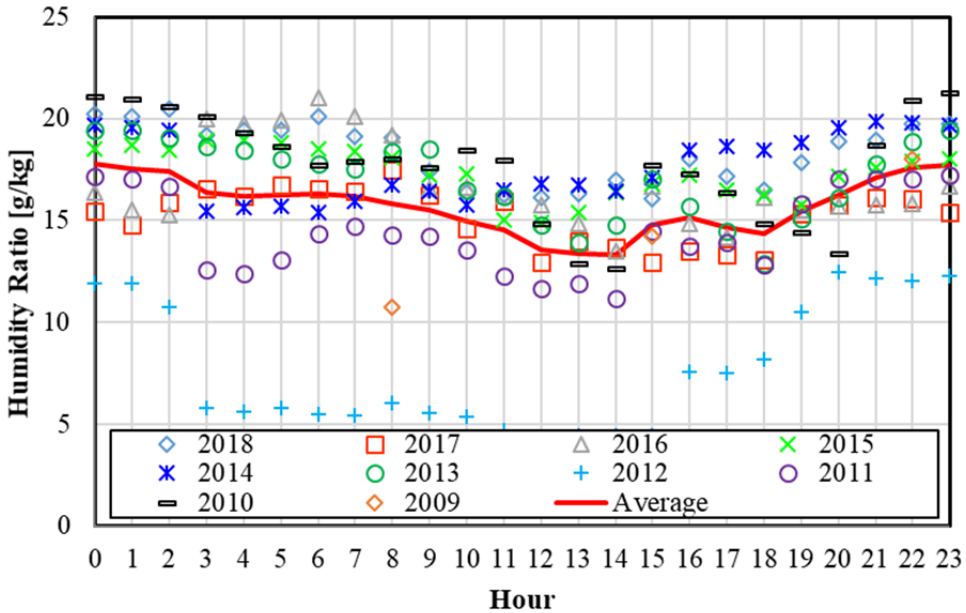

Figure 3.17. Hourly humidity ratio measured in Adana during the years 2009 to 2018 for 21st August and average humidity ratio

3.8.2. Desiccant Wheel - DW(State 1 to 2)

Analysis of desiccant wheel (DW) has a key role for the success of the model studied. Dehumidification of supply air and removal of humidity (regeneration, reactivation) processes within DW are generally accepted to take place approximately at constant enthalpy (approximately at constant wet-bulb temperature) (Jia et al., 2006). However, dehumidification and regeneration processes do not occur at constant wet-bulb temperature according to the data given by the rotary desiccant wheel manufactures. Actual increase in dry-bulb temperature during dehumidification is higher than that of the constant wet-bulb case. This increase can be attributed to the release of chemical thermal energy during dehumidification and also to the heat transfer from warmer regeneration air (T_{19}) to the relatively cooler supply air (T_2) by the DW matrix material (ASHRAE, 2000).

Different performance criteria are proposed to express the performance of desiccant wheels. Moisture Removal Capacity (MRC), effectiveness, latent coefficient of performance, sensible coefficient of performance, total coefficient of performance can be given as the examples to performance criteria (Chung, 2017).

Moisture Removal Capacity (MRC) indicates the amount of moisture removed from the air to be processed as it passes through DW (Chung, 2017).

$$MRC = \dot{m}_t\left(\omega_{p,in} - \omega_{p,out}\right) \tag{3.6}$$

The effectiveness (ε_{DW}) of rotary desiccant dehumidifier is evaluated as the ratio of the change in actual humidity ratio of the air to the maximum possible change in humidity ratio:

$$\varepsilon_{DW} = \frac{\omega_{p,in} - \omega_{p,out}}{\omega_{p,in} - \omega_{p,out,ideal}} \tag{3.7}$$

Air is assumed to be desorbed completely at the outlet under ideal conditions, therefore it can be written:

$$\omega_{p,out,ideal} = 0 \tag{3.8}$$

and inserting the last equation into Eq. 3.7, one gets:

$$\varepsilon_{DW} = \frac{\omega_{p,in} - \omega_{p,out}}{\omega_{p,in}} \tag{3.9}$$

Studies are available in the literature to predict the performance of a DW taking important parameters into account at different levels. Influence of temperature and humidity ratio of process and regeneration air streams are considered in almost all of studies. However, rotational speed of the matrix, flow rates of process and regeneration air streams are not taken into consideration in some studies.

Some of the models provide directly $\omega_{p,out}$ and $T_{p,out}$, whilst some produce $h_{p,out}$ and $\varphi_{p,out}$. The third group of studies calculate the combined potentials of the outlet process air, namely $F_{1,p,out}$ and $F_{2,p,out}$ (Chung, 2017).

In this study, a detailed analysis of the correlations and the data that are in a suitable form to be reused available in the open literature was made. Table 3.5 summarizes the data and the correlations used.

A least square data fit (Figs. 3.18 and 3.19) to the data given in Table 3.5 produced the following equations with R^2=0,94 for $T_{p,out}$ and R^2=0,88 for $\omega_{p,out}$ to predict the outlet conditions of the process air:

$$T_{p,out} = -3{,}6533 + 0{,}7535 * T_{p,in} + 1075{,}1 * \omega_{p,in} + 0{,}3011 * T_{r,in} - 396{,}1 * \omega_{r,in} \tag{3.10}$$

$$\omega_{p,out} = 1{,}3426 + 0{,}0635 * T_{p,in} + 461{,}3 * \omega_{p,in} - 0{,}0756 * T_{r,in} + 271{,}9 * \omega_{r,in} \tag{3.11}$$

Table 3.5. The data and the correlations used in the analysis for the performance of the desiccant wheel

No	Literature	Type (data/corr.)	Input parameters	Range of input parameters	Output parameters
1	Beccali et al. (2003)	Correlation (Eqs. 2.1 and 2.2)	φ h	$20<T_{p,in}<34$ $8<\omega_{p,in}<15$ $40<T_{r,in}<80$ $7<\omega_{r,in}<16$	$\varphi_{p,out}$ $h_{p,out}$
2	Beccali et al. (2003)	Correlation (Eqs. 2.1 and 2.3)	φ h	$20<T_{p,in}<34$ $8<\omega_{p,in}<15$ $40<T_{r,in}<80$ $7<\omega_{r,in}<16$	$\varphi_{p,out}$ $h_{p,out}$
3	Panaras et al. (2010)	Correlation (Eqs. 2.4 to 2.10)	$T_{p,in}$, $\omega_{p,in}$, $T_{r,in}$, $\omega_{r,in}$	$24<T_{p,in}<40$ $4<\omega_{p,in}<14$ $50<T_{r,in}<80$ $3<\omega_{r,in}<15$	$F_{1,p,out}$ $F_{2,p,out}$ $(T_{p,out}$ $\omega_{p,out})$
4	Angrisani et al. (2012)	Correlation (Eqs. 2.4 to 2.7 and Eq. 2.11)	$T_{p,in}$, $\omega_{p,in}$, $T_{r,in}$, $\omega_{r,in}$	$22,2<T_{p,in}<38,8$ $6,4<\omega_{p,in}<15,9$ $49,8<T_{r,in}<68,6$ $6,4<\omega_{r,in}<15,9$	$F_{1,p,out}$ $F_{2,p,out}$ $(T_{p,out}$ $\omega_{p,out})$
5	Ruivo et al. (2012)	Correlation (Eqs. 2.12 and 2.13)	φ h	$5<T_{p,in}<40$ $5<\omega_{p,in}<10$ $60<T_{r,in}<100$ $5<\omega_{r,in}<15$	$\varphi_{p,out}$ $h_{p,out}$
6	Ruivo et al. (2014)	Correlation (Eqs. 2.14 and 2.15)	φ h	$5<T_{p,in}<40$ $5<\omega_{p,in}<10$ $60<T_{r,in}<100$ $5<\omega_{r,in}<15$	$\varphi_{p,out}$ $h_{p,out}$
7	Comino et al. (2016)	Correlation (Eqs. 2.16 and 2.17)	$T_{p,in}$, $\omega_{p,in}$, $T_{r,in}$, $\omega_{r,in}$	$17,5<T_{p,in}<29,5$ $12<\omega_{p,in}<21,5$ $34<T_{r,in}<42,5$ $13<\omega_{r,in}<22,6$	$T_{p,out}$ $\omega_{p,out}$

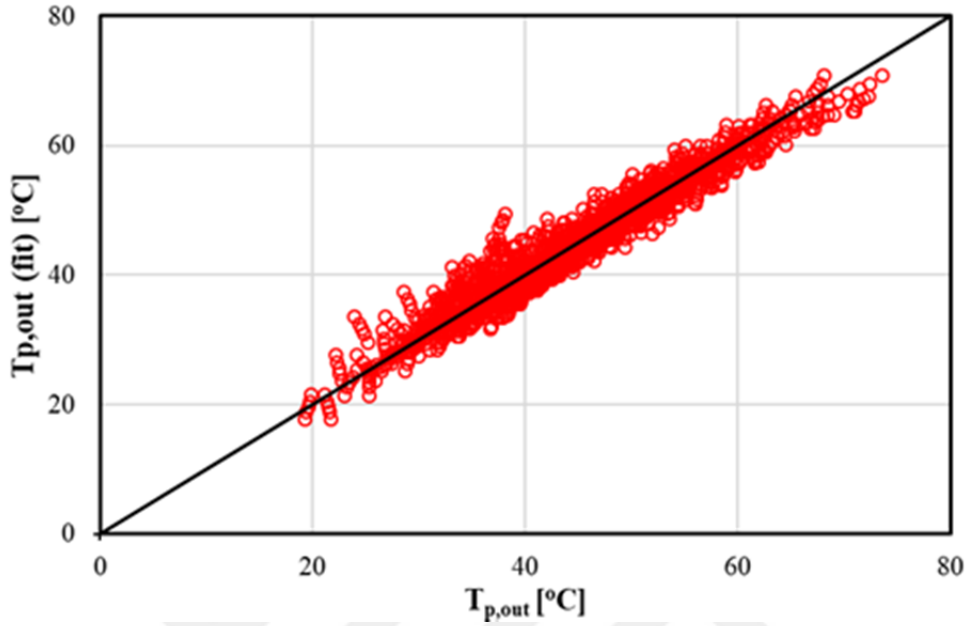

Figure 3.18. The data obtained from the literature and from Eq. 3.12 for process air outlet temperature

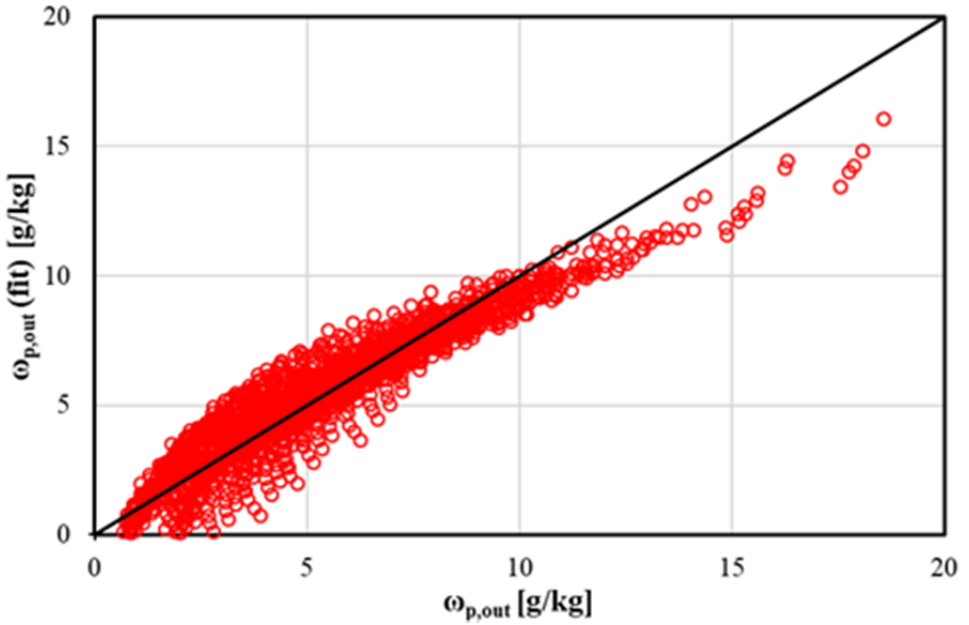

Figure 3.19. The data obtained from the literature and from Eq. 3.13 for process air outlet humidity

These equations can be used within the following ranges:

20 °C < $T_{p,in}$ < 40 °C
0,005 kg/kg < $\omega_{p,in}$ < 0,020 kg/kg
40 °C < $T_{r,in}$ < 100 °C
0,005 kg/kg < $\omega_{r,in}$ < 0,020 kg/kg

Using the equations above, the dry-bulb temperature and the humidity ratio (T_2 and ω_2) can be calculated at the exit of the DW:

$$T_2 = -3{,}6533 + 0{,}7535 * T_1 + 1075{,}1 * \omega_1 + 0{,}3011 * T_{19} - 396{,}1 * \omega_{19} \quad (3.12)$$

$$\omega_2 = 1{,}3426 + 0{,}0635 * T_1 + 461{,}3 * \omega_1 - 0{,}0756 * T_{19} + 271{,}9 * \omega_{19} \quad (3.13)$$

The amount of moisture subtracted from the process air stream will be carried away by the regeneration air stream under steady-state operation conditions:

$$\dot{m}_1(\omega_1 - \omega_2) = \dot{m}_{19}(\omega_{20} - \omega_{19}) \quad (3.14)$$

Using the last equation, humidity ratio of the regeneration air at the exit of the DW can be obtained;

$$\omega_{20} = \omega_{19} + \frac{\dot{m}_1}{\dot{m}_{19}}(\omega_1 - \omega_2) \quad (3.15)$$

The amount of heat released or absorbed during the adsorption and desorption processes will be the same under steady-state operation conditions:

$$\dot{Q} = \dot{m}_p \left(h_{p,out} - h_{p,in}\right) = \dot{m}_r \left(h_{r,in} - h_{r,out}\right) \quad (3.16)$$

The last equation takes the following form for the system studied:

$$\dot{Q} = \dot{m}_t\,(h_2 - h_1) = \dot{m}_r(h_{19} - h_{20}) \tag{3.17}$$

3.8.3. HX1 (State 2 to 3 and 13 to 14) and HX2 (State 17 to 18 and 23 to 24)

Since only sensible heat transfer from a hot fluid to a cold fluid take place in a recuperator, humidity ratio of the hot and the cold fluid streams remain constant:

$$\omega_{hot,out} = \omega_{hot,in} \tag{3.18}$$

$$\omega_{cold,out} = \omega_{cold,in} \tag{3.19}$$

It is possible to calculate dry-bulb temperature of the process air at the exit of a recuperator (HX1 and HX2) if the effectiveness of recuperator (ε_{HX}) is known. (ε_{HX}) is defined as the ratio of actual ($\dot{Q}$) to maximum possible ($\dot{Q}_{max}$) heat transfer rate within the recuperator:

$$\varepsilon_{HX} = \frac{\dot{Q}}{\dot{Q}_{max}} \tag{3.20}$$

Maximum possible heat transfer rate ($\dot{Q}_{max}$) can be calculated from the following equation (Yılmaz and Büyükalaca, 2003):

$$\dot{Q}_{max} = C_{min}\left(T_{hot,in} - T_{cold,in}\right) \tag{3.21}$$

in which C_{min} is the minimum of capacitance rate of hot fluid (C_{hot}) and cold fluid (C_{cold}):

$$C_{hot} = \dot{m}_{hot}\, c_{p,hot} \tag{3.22}$$

$$C_{cold} = \dot{m}_{cold}\, c_{p,cold} \tag{3.23}$$

Actual heat transfer rate ($\dot{Q}$) can be calculated from Eq. 3.24 if $\dot{Q}_{max}$ and ε_{HX} are known:

$$\dot{Q} = \varepsilon_{HX}\, \dot{Q}_{max} \tag{3.24}$$

Once heat transfer rate ($\dot{Q}$) is known, outlet temperatures of hot ($T_{hot,out}$) and cold ($T_{cold,out}$) fluids can be calculated from the energy balance equation:

$$\dot{Q} = \dot{m}_{hot}\left(h_{hot,in} - h_{hot,out}\right) = \dot{m}_{cold}\left(h_{cold,out} - h_{cold,in}\right) \tag{3.25}$$

or in terms of temperature:

$$\dot{Q} = \dot{m}_{hot}\, c_{p,hot}\left(T_{hot,in} - T_{hot,out}\right) = \dot{m}_{cold}\, c_{p,cold}\left(T_{cold,out} - T_{cold,in}\right) \tag{3.26}$$

where;

$c_{p,hot}$: Specific heat of hot fluid, [kJ/kg K]

$c_{p,cold}$: Specific heat of cold fluid, [kJ/kg K]

C_{hot} : Fluid capacitance rate of hot fluid, [W/K]

C_{cold} : Fluid capacitance rate of cold fluid, [W/K]

C_{min} : Minimum fluid capacitance rate of fluids, [W/K]

$h_{hot,in}$: Enthalpy of the hot air at the inlet, [kJ/kg]

$h_{cold,in}$: Enthalpy of the cold air at the inlet, [kJ/kg]

$h_{hot,out}$: Enthalpy of the hot air at the outlet, [kJ/kg]

$h_{cold,out}$: Enthalpy of the cold air at the outlet, [kJ/kg]

$T_{hot,in}$: Dry-bulb temperature of the hot air at the inlet, [°C]

$T_{cold,in}$: Dry-bulb temperature of the cold air at the inlet, [°C]

$T_{hot,out}$: Dry-bulb temperature of the hot air at the outlet, [°C]

$T_{cold,out}$: Dry-bulb temperature of the cold air at the outlet, [°C]

$\dot{m}_{hot}$: Mass flow rate of hot air, [kg/s]

$\dot{m}_{cold}$: Mass flow rate of cold air, [kg/s]

Utilizing the approach given above, the following equations can be written for HX1:

$$\omega_3 = \omega_2 \tag{3.27}$$

$$\omega_{14} = \omega_{13} \tag{3.28}$$

$$\dot{Q}_{max,HX1} = C_{min,HX1}(T_2 - T_{13}) \tag{3.29}$$

$$\dot{Q}_{HX1} = \varepsilon_{HX1}\, \dot{Q}_{max,HX1} \tag{3.30}$$

$$T_3 = T_2 - \frac{\dot{Q}_{HX1}}{\dot{m}_2\, c_{p,2}} \tag{3.31}$$

$$T_{14} = T_{13} + \frac{\dot{Q}_{HX1}}{\dot{m}_{13}\, c_{p,13}} \tag{3.32}$$

Similarly, for HX2 one can write:

$$\omega_{18} = \omega_{17} \tag{3.33}$$

$$\omega_{24} = \omega_{23} \tag{3.34}$$

$$\dot{Q}_{max,HX2} = C_{min,HX2}(T_{23} - T_{17}) \tag{3.35}$$

$$\dot{Q}_{HX2} = \varepsilon_{HX2}\, \dot{Q}_{max,HX2} \tag{3.36}$$

$$T_{18} = T_{17} + \frac{\dot{Q}_{HX2}}{\dot{m}_{17}\, c_{p,17}} \tag{3.37}$$

$$T_{24} = T_{23} - \frac{\dot{Q}_{HX2}}{\dot{m}_{23}\, c_{p,23}} \tag{3.38}$$

3.8.4. Maisotsenko Cycle - HMX (State 7 to 8)

Performance of a HMX is expressed in terms of dew-point effectiveness (Riangvilaikul and Kumar, 2010):

$$\varepsilon_{dp} = \frac{T_{p,in} - T_{p,out}}{T_{p,in} - T_{dp,p,in}} \tag{3.39}$$

Wet-bulb temperature effectiveness is also expressed by some researchers (Zhan et al., 2011a) to be able to compare the performance of MC with that of direct or indirect evaporative cooler:

$$\varepsilon_{wb} = \frac{T_{p,in} - T_{p,out}}{T_{p,in} - T_{wb,p,in}} \tag{3.40}$$

Performance of a HMX depends on temperature, humidity, velocity of the process air and the mass flow ratio of working air to total (process + working) air stream.

In this study, a detailed analysis of the data and the correlations available in the open literature and that are in a suitable form to be reused was made. Table 3.6 summarizes the data and the correlations used.

Table 3.6. The data and the correlations used in the analysis for the performance of MC

No	Literature	Type (data, correlation)	Input parameters	Ranges	Output parameters
1	Riangvilaikul and Kumar (2010)	Data (Table 2.2)	$T_{p,in}$ $\omega_{p,in}$ $V_{p,in}$	$25<T_{p,in}<45$ $6,9<\omega_{p,in}<26,4$ $1,5< V_{p,in} <6$	ε_{dp}
2	Khalid et al. (2017)	Data (Table 2.3)	$T_{p,in}$ $\omega_{p,in}$ $V_{p,in}$	$25<T_{p,in}<53$ $12,7<\omega_{p,in}<18$ $0,88< V_{p,in} <1,5$	ε_{dp}
3	Lin et al. (2018)	Data (Table 2.4)	$T_{p,in}$ $\omega_{p,in}$	$27<T_{p,in}<40$ $10<\omega_{p,in}<19,6$	ε_{dp}

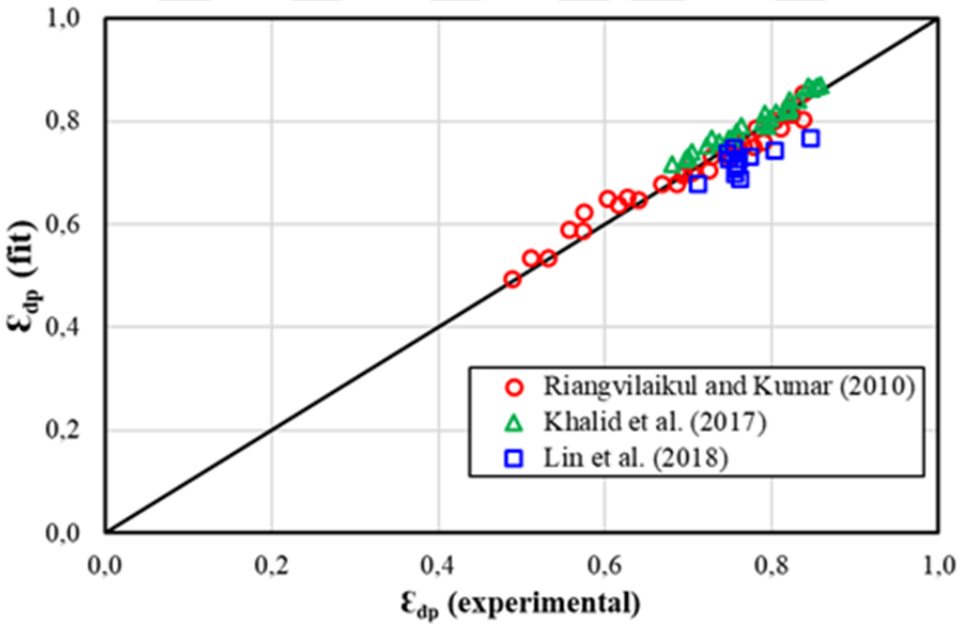

Figure 3.20. The data obtained from the literature and from Eq. 3.41 for dew-point effectiveness of Maisotsenko cycle

A least square data fit (Fig. 3.20) to the data given in Table 6 produced the following equations with R^2=0,89 to predict the dew-point performance of counter-flow Maisotsenko cycle:

$$\varepsilon_{dp} = 0{,}5884 + 0{,}0053T_{in} + 6{,}3\omega_{in} - 0{,}0592V_{in} \quad (3.41)$$

where;

T_{in} : Dry-bulb temperature of air at the inlet, [°C]

ω_{in} : Humidity ratio of air at the inlet, [kg/kg]

V_{in} : Velocity of air at the inlet, [m/s]

Equation 3.41 can be used within the following ranges:

25 ℃ < $T_{p,in}$ < 45 ℃

0,005 kg/kg < $\omega_{p,in}$ < 0,020 kg/kg

0,9 m/s < $V_{p,in}$ < 6 m/s

3.8.5. Supply Air into the Building (States 8 to 9)

The air conditioned in Maisotsenko Cycle is supplied to the building and the following equations can be written:

$$\dot{Q}_{b,t} = \dot{m}_p(h_b - h_{supply}) \quad (3.42)$$

$$\dot{Q}_{b,sen} = \dot{m}_p c_{p,avg}(T_b - T_{supply}) \quad (3.43)$$

$$\dot{Q}_{b,lat} = \dot{m}_p h_{fg}(\omega_b - \omega_{supply}) \quad (3.44)$$

With notation used the last equation can be written as:

$$\dot{Q}_{b,t} = \dot{m}_p(h_9 - h_8) \quad (3.45)$$

$$\dot{Q}_{b,sen} = \dot{m}_p c_{p,avg}(T_9 - T_8) \quad (3.46)$$

$$\dot{Q}_{b,lat} = \dot{m}_p h_{fg}(\omega_9 - \omega_8) \quad (3.47)$$

In this study, desired dry-bulb temperature of the air inside the building was initially set to a value of T_9=26 °C (logic of the automatic control system is given above in section 3.4). Required flow rate of the air to be supplied to the building ($\dot{m}_p$) was calculated from Eq.3.46 and the humidity ratio within the building (ω_9) was obtained from Eq. 3.47, and checking was made with Eq. 3.45.

3.8.6. Direct Evaporative Cooler - DEC (State 10 to 11)

The effectiveness of direct evaporative cooler (ε_{DEC}) is defined as ratio of the dry-bulb temperature depression divided by the difference between the entering dry and wet-bulb temperatures (Kreider and Rabl, 1994):

$$\varepsilon_{DEC} = \frac{T_{in} - T_{out}}{T_{in} - T_{wb,in}} \quad (3.48)$$

where;

T_{in} : Dry-bulb temperature of air at the inlet of DEC, [°C]

T_{out} : Dry-bulb temperature of air at the exit of DEC, [°C]

$T_{wb,\,in}$: Wet-bulb temperature of air at the inlet of DEC, [°C]

It is possible to achieve effectiveness values for the DEC systems higher than 0,9 (Uçkan et al., 2013).

Wet-bulb temperature of the air does not change in the DEC unit, since humidification process take place at almost constant wet-bulb temperature:

$$T_{wb,out} = T_{wb,in} \tag{3.49}$$

For the system studied, using the following equations, it is possible to calculate properties of the exhaust air at the outlet of the DEC unit (11):

$$T_{wb,11} = T_{wb,10} \tag{3.50}$$

$$\varepsilon_{DEC} = \frac{T_{10} - T_{11}}{T_{10} - T_{wb,10}} \tag{3.51}$$

3.8.7. Heat Exchanger 3 - HX3 (State 18 to 19)

A hot air stream is needed for the regeneration of the desiccant wheel. The temperature of the regeneration air is an important parameter for the moisture removal from the DW. Regeneration air temperature should be higher than 60 ^{o}C in general. Amount of moisture removed from the DW will increase with increase of regeneration air temperature.

The thermal energy needed to heat the regeneration air can be obtained from a renewable energy source such as solar energy or from a suitable waste heat source at a suitable temperature. Solar energy is very attractive for this purpose, because solar radiation is high during the summer months for which cooling loads are also high. In this study regeneration air temperature was selected to be 70 ^{0}C in order to minimize the thermal energy requirement.

The amount of thermal energy needed:

$$\dot{Q}_{HX3} = \dot{m}_r(h_{out} - h_{in}) \tag{3.52}$$

Since only sensible heat transfer takes place in the heat exchanger:

$$\omega_{out} = \omega_{in} \tag{3.53}$$

For the system studied:

$$\omega_{19} = \omega_{18} \tag{3.54}$$

$$\dot{Q}_{HX3} = \dot{m}_{18}(h_{19} - h_{18}) \tag{3.55}$$

3.8.8. Performance Definition of the System

The main performance criteria for the air-conditioning system studied is the cooling coefficient of performance (*COP*), which can be defined as the ratio of the total heat extracted from the building ($\dot{Q}_{b,t}$) to the heat input in HX3 ($\dot{Q}_{HX3}$), since the energy requirement for moving the fans and pumps were not considered in this study:

$$COP = \frac{\dot{Q}_{b,t}}{\dot{Q}_{HX3}} \tag{3.56}$$

3.8.9. Calculations

Based on the above given equations, thermodynamic analysis of the proposed HVAC system was carried out using a simulation program, which was developed using EES (Engineering Equation Solver) software (Klein, 2018), which is used for thermodynamic system analysis in the literature.

EES is a general equation-solving program that can numerically solve coupled non-linear algebraic and differential equations. A major feature of EES is the high accuracy thermodynamic and transport property database (built-in functions) that is provided for hundreds of substances in a manner that allows it to be used with the equation solving capability (Klein, 2018).

In this study, thermophysical properties of humid air were determined by using the built-in property functions available in EES, which require two known (input) properties of the humid air. The mass and balance equations written for each system component (desiccant wheel, recuperator, Maisotsenko cooler, direct evaporative cooler) that are given above were solved simultaneously using the simulation program.

3.8.10. Thermal Comfort

Using the model explained above, psychometric properties of the air within the building and at all states of the system were evaluated. In the next step of the analysis, the psychometric properties of the air within the building were checked whether the comfort conditions given by ASHRAE were satisfied.

ASHRAE Standard 55 specifies thermal environmental conditions (temperature, humidity, air speed, and radiant effects) in buildings and other spaces that a significant proportion of the occupants will find acceptable at a certain metabolic rate and clothing level (ASHRAE 2017b).

Thermal comfort of a person depends on many parameters such as air temperature and humidity, metabolic rate (met), clothing insulation (clo), radiant temperature (T_{rad}) and air speed (V_a). Metabolic rate (*met*) is the rate of transformation of chemical energy into heat and mechanical work by metabolic activities of an individual, per unit of skin surface area (expressed in units of met) equal to 58.2 W/m^2, which is the energy produced per unit skin surface area of an average person seated at rest. *clo* is a unit used to express the thermal insulation provided by garments and clothing ensembles (1 clo = 0.155 m^2°C/W).

ASHRAE, (2017b) provides 3 different methods for determining acceptable thermal conditions, namely graphic comfort zone method, analytical comfort zone method and elevated air speed comfort zone method.

In this study, the graphic comfort zone method, which is applicable when;

$V_a < 0{,}2$ m/s

$\omega < 0{,}012$ kg/kg

$1 \leq met < 1{,}3$

$0{,}5 \leq \text{clo} \leq 1$

were used to determine thermal conditions.

Thermal comfort region suggested by (ASHRAE, 2017b) is shown in Fig. 3.21. The temperature on the x axis of the graph is operative temperature (T_{op}), not the air dry-bulb temperature (T_a) of the air-conditioned volume. It is defined as:

$$T_{op} = \frac{h_{conv}T_a + h_{rad}T_{rad}}{h_{conv} + h_{rad}} \tag{3.57}$$

where

h_{conv} = convection heat transfer coefficient

h_{rad} = radiative heat transfer coefficient

T_{rad} = mean radiant temperature

Eq. 3.57 can be simplified according to the procedure given in ASHRAE (2017b):

$$T_{op} = A * T_a + (1 - A)T_{rad} \tag{3.58}$$

and the value of constant A is 0,5 for V_{air} < 0,2 m/s. In this case Eq. 3.58 becomes:

$$T_{op} = 0{,}5 * T_a + 0{,}5 * T_{rad} \tag{3.59}$$

Mean radiant temperature (T_{rad}) can be calculated with the following equation (ASHRAE, 2017a):

$$T_{rad}^4 = T_1^4 F_{p-1} + T_1^4 F_{p-2} + \cdots . + T_N^4 F_{p-N} \tag{3.60}$$

where

T_N = surface temperature of surface N

$F_{p\text{-}N}$ = angle factor between a person and surface N

If relatively small temperature differences exist between the surfaces of the

enclosure, Eq. 3.60 can be simplified to a linear form:

$$T_{rad} = T_1 \ F_{p-1} + T_2 \ F_{p-2} + \cdots . + T_N \ F_{p-N} \tag{3.61}$$

Angle factor between a person and a surface *N* (F_{p-N}), which depends on the position and orientation of the person, was estimated using the charts given in ASHRAE, (2017a) which were originally published by Fanger 1982. Calculations for the school building considered in this thesis showed that mean radiant temperature is approximately 26,6 ^{0}C at maximum for all the rooms of the building. T_{rad} was taken 27 ^{0}C to be on the safe side.

The relation between the operative temperature and the air temperature can be rewritten from Eq. 3.59 as:

$$T_{op} = T_a + 0{,}5 \tag{3.62}$$

The ASHRAE comfort region was modified to consider the difference between the air temperature and operative temperature, which resulted a narrower comfort region in terms of air temperature.

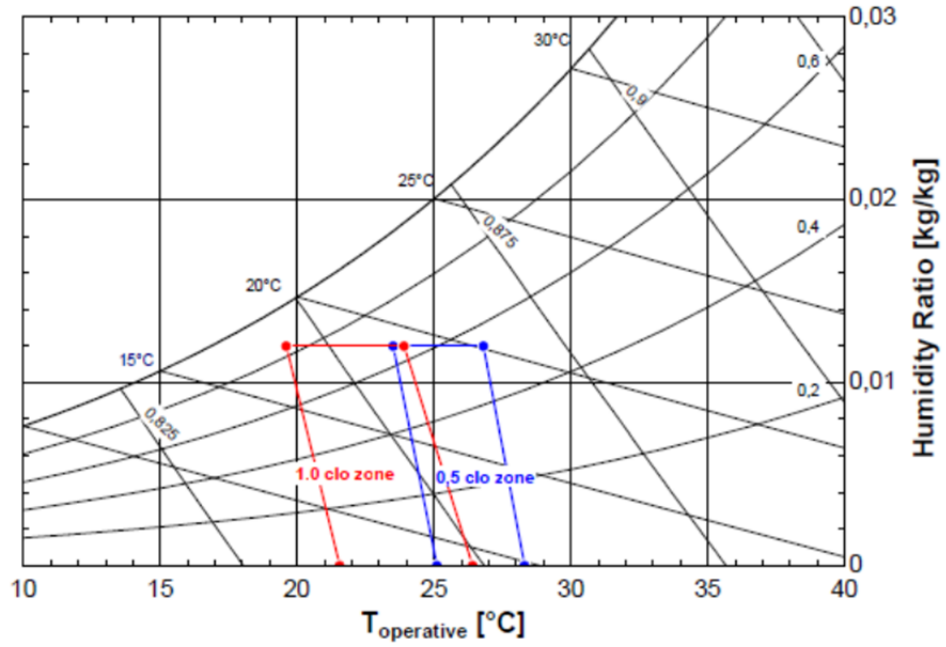

Figure 3.21. ASHRAE Comfort zone (adopted from ASHRAE, 2017b)

Mixing exhaust air with fresh supply air reduces energy consumption of the system (increases COP) considering the amount of fresh air needed required within the building. However, when the cooling load is high (approximately coincides with high outdoor temperature and humidity), the thermal comfort conditions (dry-bulb temperature and humidity ratio) are not satisfied according to ASHRAE, (2017b). In this case, the amount of exhaust air mixed with the fresh air is reduced (R is reduced) first, and if it is not enough, dry-bulb set temperature of the air inside the building is reduced gradually.

4. RESULTS AND DISCUSSION

Using the model developed in EES, a detailed analysis of the air-conditioning system was carried out. Fig. 4.1 shows a typical output screen (diagram window) from the EES program developed.

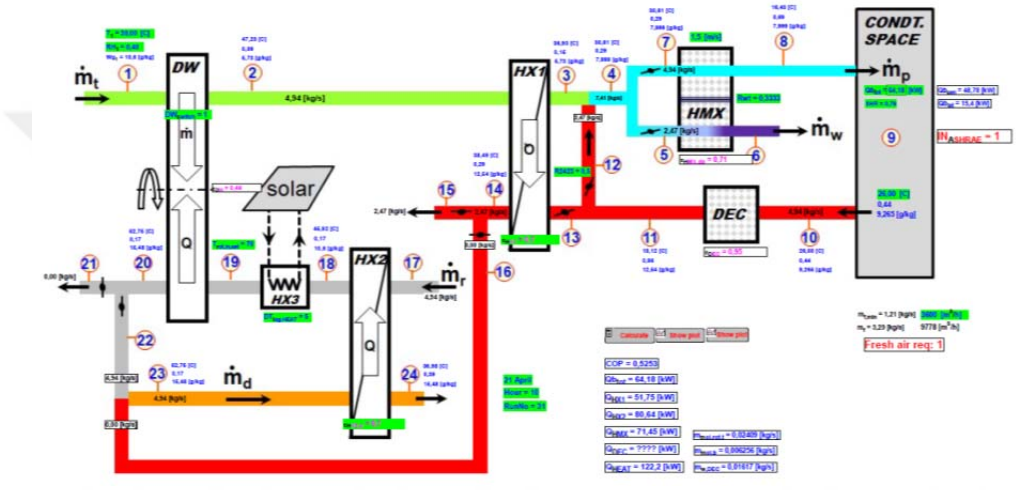

Figure 4.1. A sample output screen from the EES program written

Effectiveness were taken to be 70% for the recuperators (HX1 and HX2) and 95% for the direct evaporative cooler unit (DEC). Effectiveness of the desiccant wheel (DW) and Maisotsenko cycle (HMX) were calculated depending upon the entering air stream conditions using the equations given in Materials and Methods section (Eqs. 3.9 and 3.39).

Analyses were carried out hourly between 7^{00} o'clock and 18^{00} for 21^{st} day of each month during the cooling season (from April to October). The runs were performed for building set temperatures ($T_{b,set}$) of 26 °C, 25 °C, 24 °C and 23 °C. For each building set temperature, exhaust air mixing ratio (R) was changed systematically between 0% and 100%. In total, 11 different R value (0%, 10%, 20%, 30%, 40%, 50%, 60%, 70%, 80%, 90% and 100%) were tested. Number of

the runs sums to 44 for one hour and to 484 for one day (Table 4.1). As can be seen from the table that desired thermal conditions within the building cannot be obtained at high mixing ratio values, especially with high building set temperature. Air conditions are out of ASHRAE comfort conditions at 8 runs out of 44 for 21st August, at 13^{00} hour, for this sample case.

Table 4.1. Run plan (codes) for one hour of the day (NS: ASHRAE comfort conditions are not satisfied)

Date: 21st August **Time:**13^{00}				
Exhaust air mixing ratio (*R*%) ↓	**Building set temperature**			
	26 °C	25 °C	24 °C	23 °C
100	21Aug13R1^{NS}	21Aug13R2^{NS}	21Aug13R3^{NS}	21Aug13R4^{NS}
90	21Aug13R5^{NS}	21Aug13R6^{NS}	21Aug13R7^{NS}	21Aug13R8
80	21Aug13R9 ^{NS}	21Aug13R10	21Aug13R11	21Aug13R12
70	21Aug13R13	21Aug13R14	21Aug13R15	21Aug13R16
60	21Aug13R17	21Aug13R18	21Aug13R19	21Aug13R20
50	21Aug13R21	21Aug13R22	21Aug13R23	21Aug13R24
40	21Aug13R25	21Aug13R26	21Aug13R27	21Aug13R28
30	21Aug13R29	21Aug13R30	21Aug13R31	21Aug13R32
20	21Aug13R33	21Aug13R34	21Aug13R35	21Aug13R37
10	21Aug13R37	21Aug13R38	21Aug13R39	21Aug13R40
0	21Aug13R41	21Aug13R42	21Aug13R43	21Aug13R44

Typical results obtained for 21st August are presented in Figs. 4.2 to 4.22 as an example to the runs. Fig. 4.2 shows the psychometric diagram for 10^{00}, 13^{00} and 16^{00} hours, respectively. As can be seen the figure, the air conditions within the building is just within the ASHRAE comfort zone, since these diagrams show the

results of the runs of most efficient set conditions, namely at maximum building set temperature (26 °C) and at maximum possible exhaust air mixing percentage (*R*). When the psychometric diagrams (Fig. 4.3) for the same day and the hour with the same building set temperature (26 °C), but with smaller mixing ratio values (50%, 30% and 0%) are considered, the humidity ratio obtained within the building move towards smaller humidity ratio values.

4.1. Results for a Typical Day with Fixed Mixing Ratio

Results obtained for a typical day are given and discussed in this section of the thesis. 21st August was chosen as the typical day since maximum cooling load was obtained for this month (Fig. 3.12). Hourly variations of various parameters (temperature, humidity ratio, flow rate, effectiveness, heat transfer and COP) during the day are given and discussed below for a fixed mixing ratio of *R*=40%.

4.1.1. Mass Flow Rate

Since capacity control of the air-conditioning system is based on variable flow rate, flow rates change during the day (Fig. 4.4). Fig. 4.4. also shows variation of the total building cooling load during the day. The mass flow rate profiles exhibit a similar trend with the building cooling load. Maximum flow rates are observed at 16^{00} o'clock. 11,73 kg/s supply air is taken into system and it is mixed with 4,27 kg/s exhaust air before it is split into process air (10,67 kg/s) and working air (5,33 kg/s) at the inlet of the Maisotsenko cycle. 10,67 kg/s conditioned air is supplied into the building and the same amount of exhaust air (10,67 kg/s) is taken out from the building ($\dot{m}_p=\dot{m}_e$). The same amount of air flows (11,73 kg/s) from the both sides of the desiccant wheel ($\dot{m}_t=\dot{m}_r$).

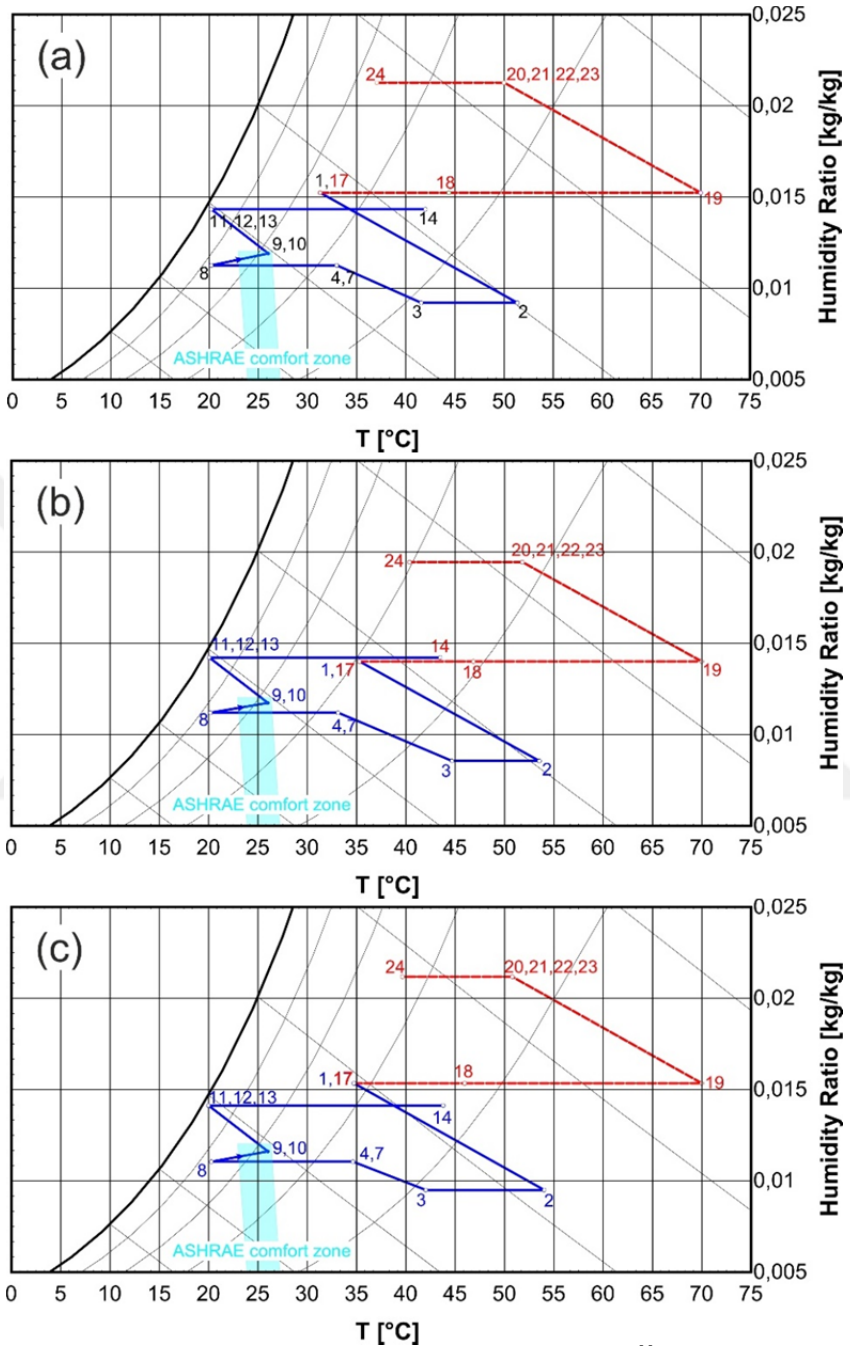

Figure 4.2. Psychometric diagram for 21st August at a) 10^{00} o'clock ($T_{b,set}$=26 °C, R=60%) b) 13^{00} ($T_{b,set}$=26 °C, R=70%) and c) 16^{00} ($T_{b,set}$=26 °C, R=60%)

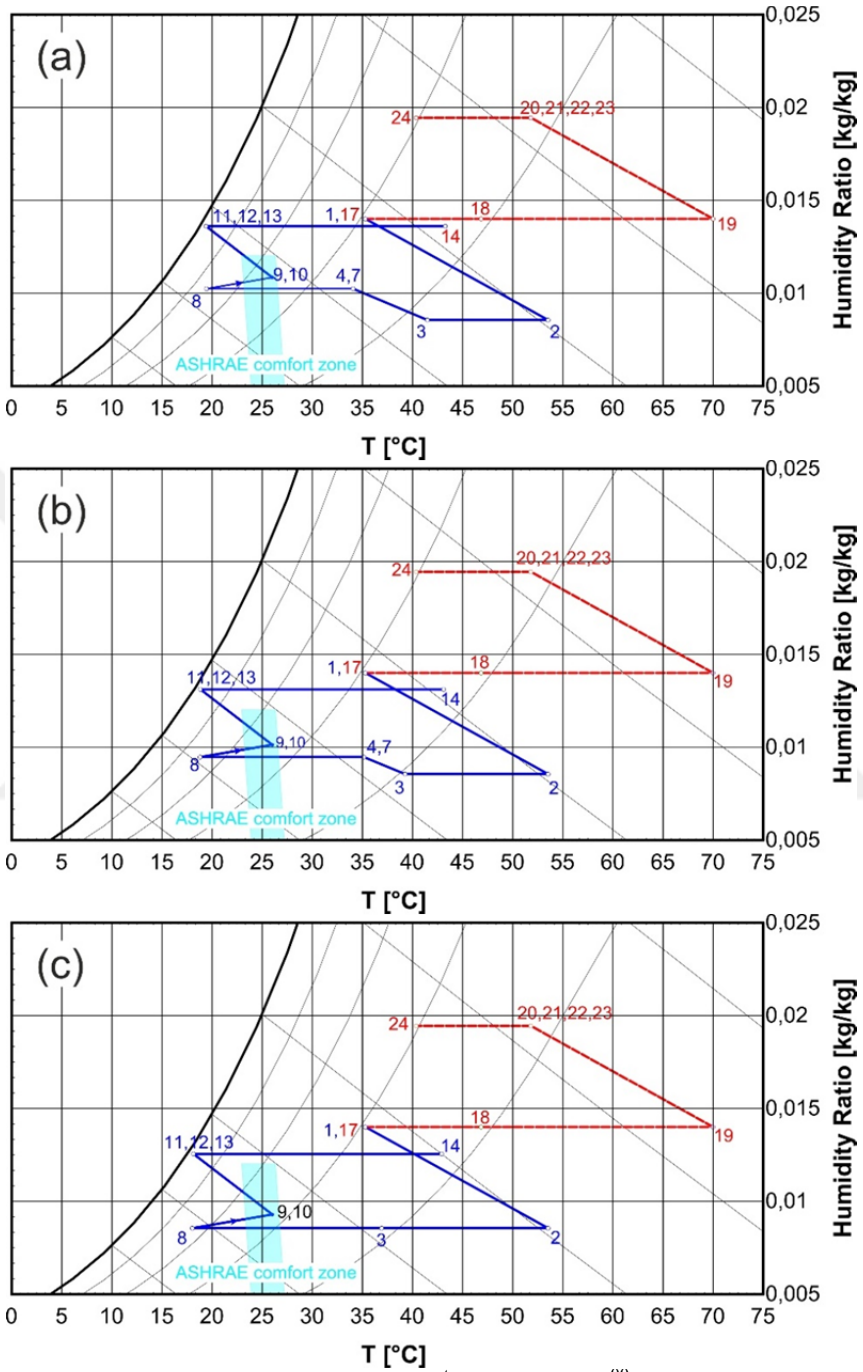

Figure 4.3. Psychometric diagram for 21st August at 13^{00} o'clock with a) R=50%, b) R=30% and c) R=0% ($T_{b,set}$=26 °C)

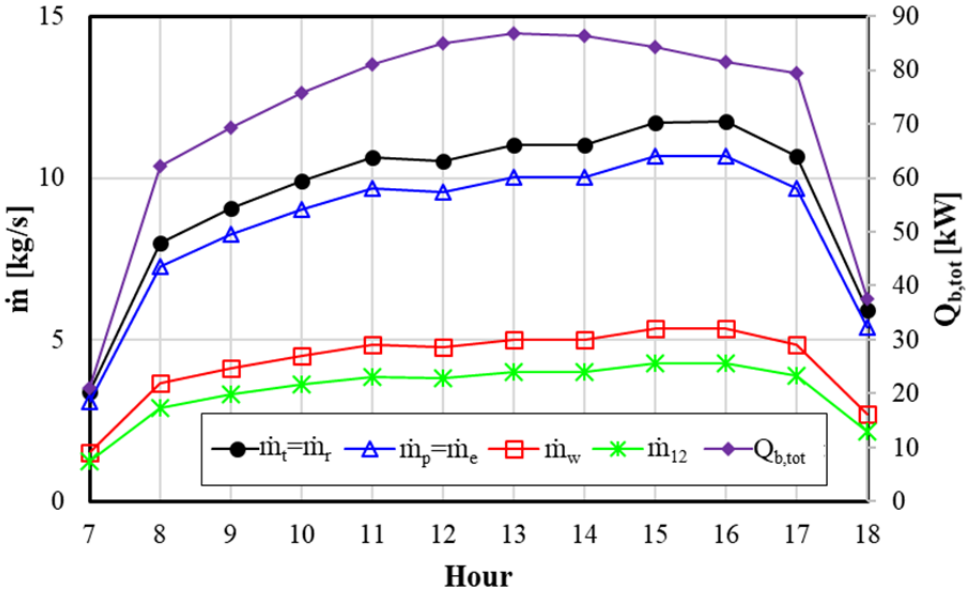

Figure 4.4. Hourly variation of mass flow rates for 21st August with R=40% ($T_{b,set}$=26 °C)

4.1.2. Desiccant Wheel (DW)

Figs. 4.5 to 4.7 show hourly variation of humidity ratio, temperature and effectiveness of DW. Desiccant wheel (DW) removes approximately 6 g/kg moisture from the supply air (1 to 2) and transfers it to regeneration air (19 to 20) with an approximately 20 °C increase in the temperature (Figs. 4.5 and 4.6). Humidity and temperature profiles of the leaving air follow that of the entering outdoor air. Humidity of the entering outdoor air decreases slightly from morning to noon and then it increases, while the outdoor air temperature exhibits an opposite profile.

The same amount of moisture removed from the supply air is transferred to the regeneration air under steady-state conditions. Since mass flow rates of the supply air ($\dot{m}_t$) and regeneration air ($\dot{m}_r$) are the same, both humidity and temperature changes for the supply air stream are equal to that for the regeneration air stream.

Effectiveness of the desiccant wheel does not change considerably during the day and is approximately 40%, as can be seen from Fig. 4.7.

4.1.3. Heat Exchanger 1 (HX1)

HX1 is used to precool sensibly the supply air before it is directed to Maisotsenko cycle. Fig. 4.8 shows the variation with time of the supply and exhaust air stream temperatures and temperature differences took place in HX1. Temperature of the supply air (2) is decreased approximately 12 ℃ by the cooler exhaust air (13), which is almost constant at approximately 20 ℃ during the day. Sensible heat transfer from the supply air to the exhaust air causes approximately 23 ℃ increase in the temperature of the exhaust air compared with the 12 ℃ decrease in the supply air temperature. This is due to difference in the mass flow rates of the hot and the cold air streams.

The amount of sensible precooling achieved in HX1 is shown in Fig. 4.9. As can be seen from the figure that, it is approximately 40 kW at the beginning of the day and increases gradually to a maximum of 160 kW around 15^{00} o'clock before decreasing.

4.1.4. Maisotsenko Cycle (HMX)

Sensible cooling of the supply air achieved mainly with Maisotsenko cycle in the air-conditioning system considered. Inlet (T_7) and outlet (T_8) temperatures, the difference between them and the heat transfer rate experienced are given in Figs. 4.10 and 4.11, respectively. Temperature of the supply air is decreased approximately 15 ℃ in HMX, whilst heat transfer rate changes between 40 kW and 170 kW.

Effectiveness of the Maisotsenko cycle (HMX) is almost constant during the day at a value of approximately 74% (Fig. 4.12). This is due to stable air temperature (T_7 in Fig. 4.10) and humidity ratio (ω_7 in Fig. 4.10) at the inlet of HMX.

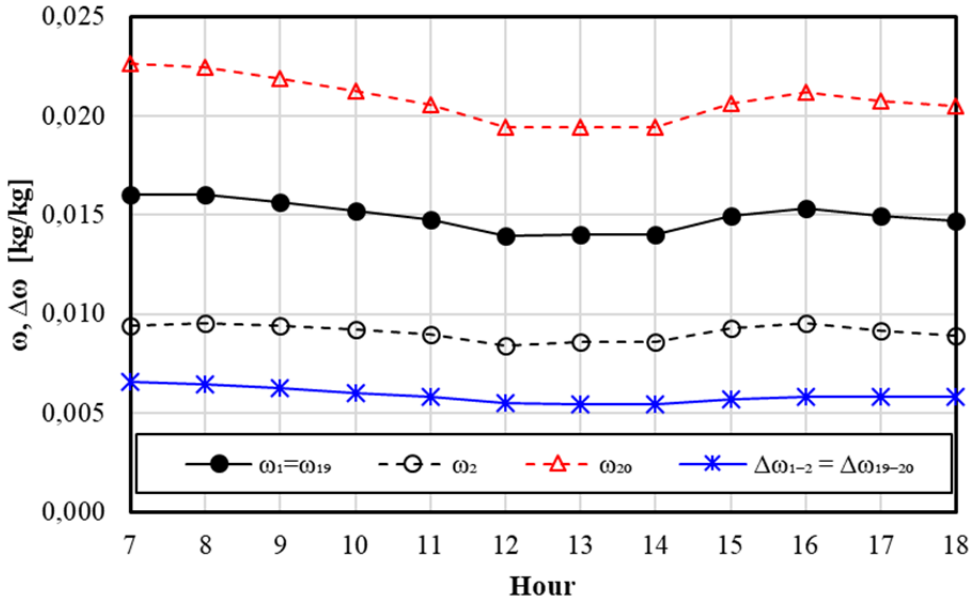

Figure 4.5. Hourly variation of humidity ratio and humidity ratio difference in DW for 21st August ($T_{b,set}$=26 °C, R=40%)

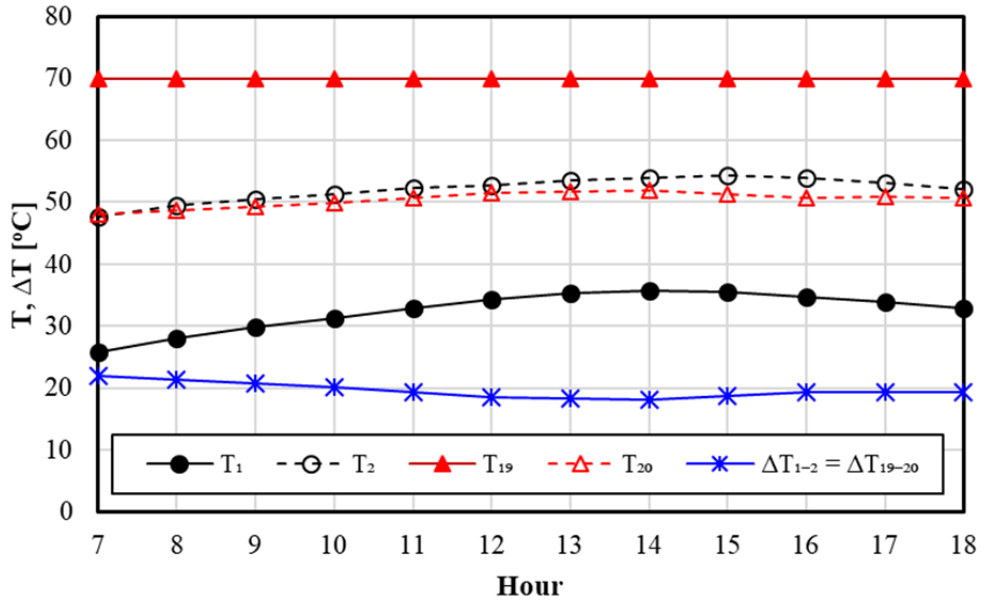

Figure 4.6. Hourly variation of temperature and temperature difference in DW for 21st August ($T_{b,set}$=26 °C, R=40%)

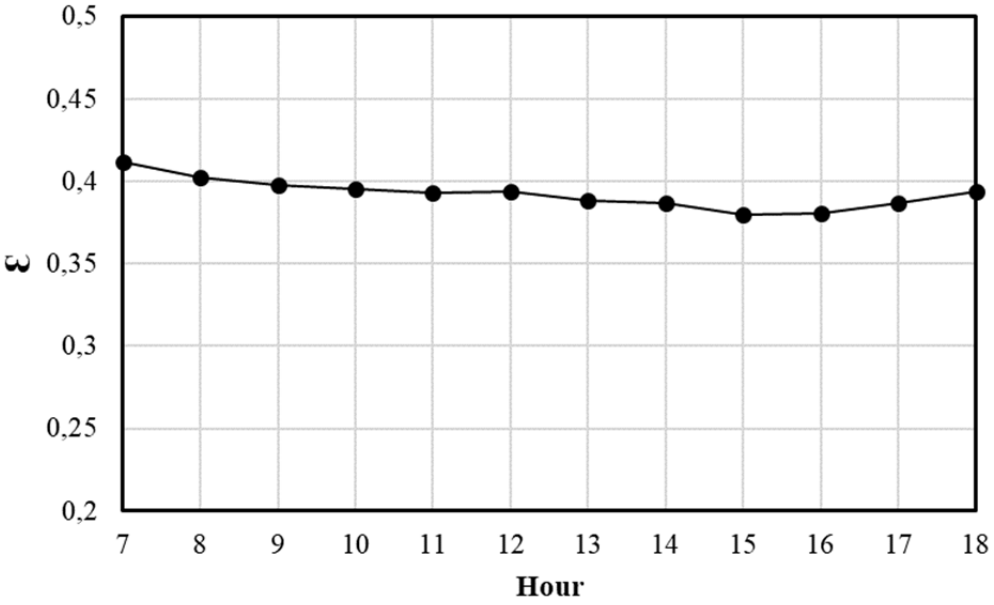

Figure 4.7. Hourly variation of effectiveness of DW for 21st August ($T_{b,set}$=26 °C, R=40%)

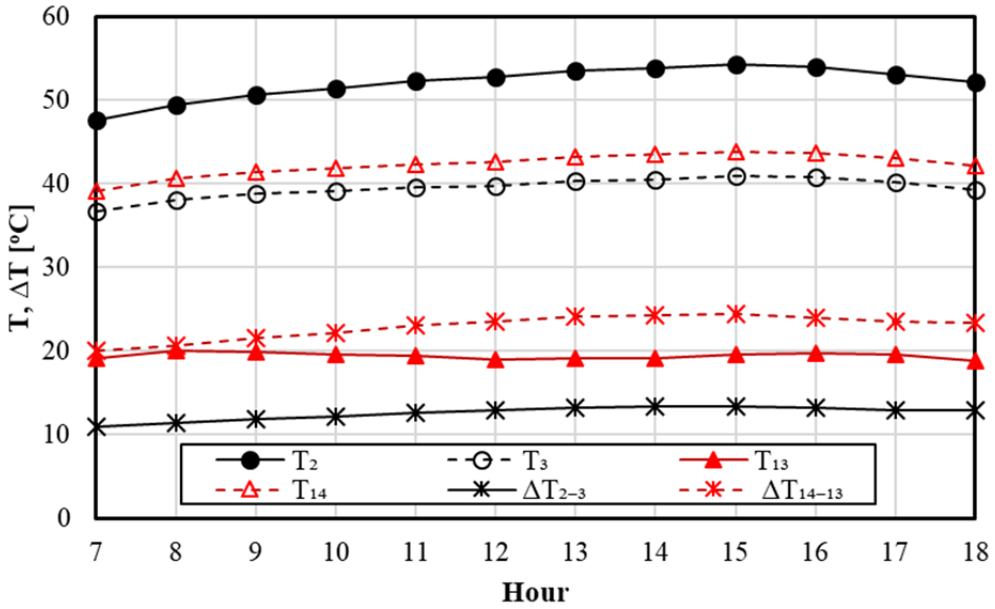

Figure 4.8. Hourly variation of temperatures and temperature differences in HX1 for 21st August ($T_{b,set}$=26 °C, R=40%)

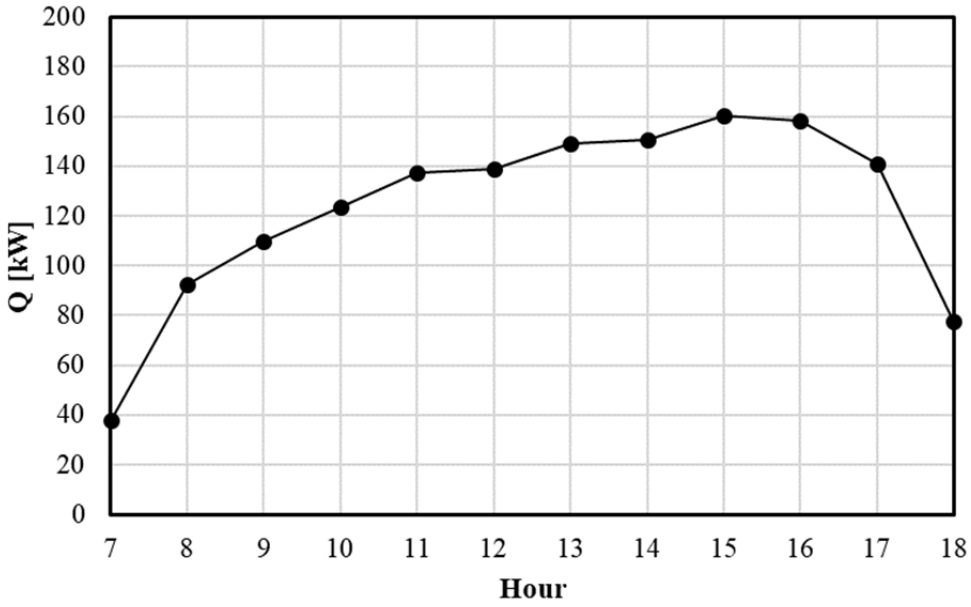

Figure 4.9. Hourly variation of sensible precooling of the supply air in HX1 for 21st August ($T_{b,set}$=26 °C, R=40%)

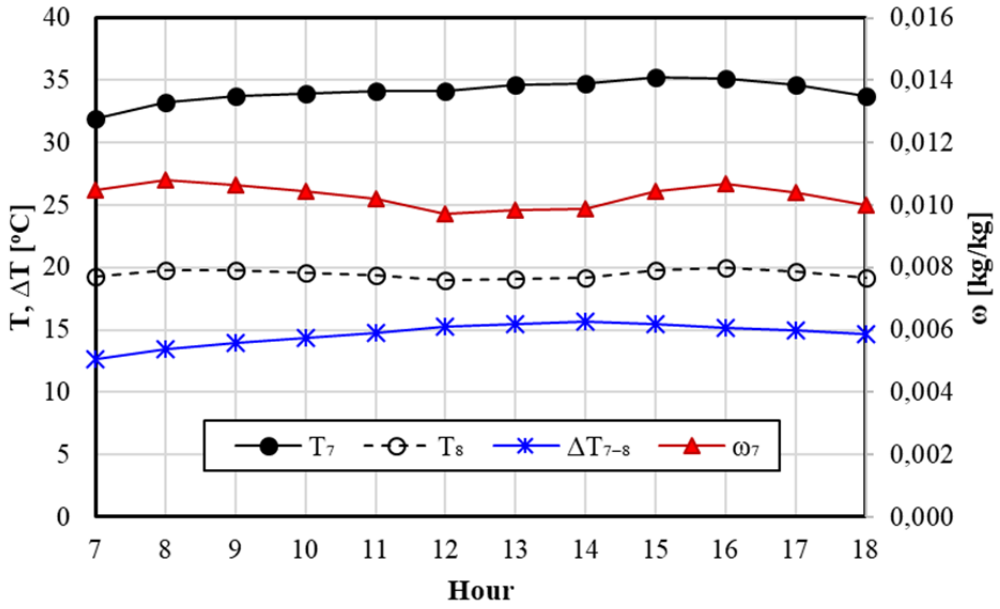

Figure 4.10. Hourly variation of temperature, temperature difference and humidity ratio in HMX for 21st August ($T_{b,set}$=26 °C, R=40%)

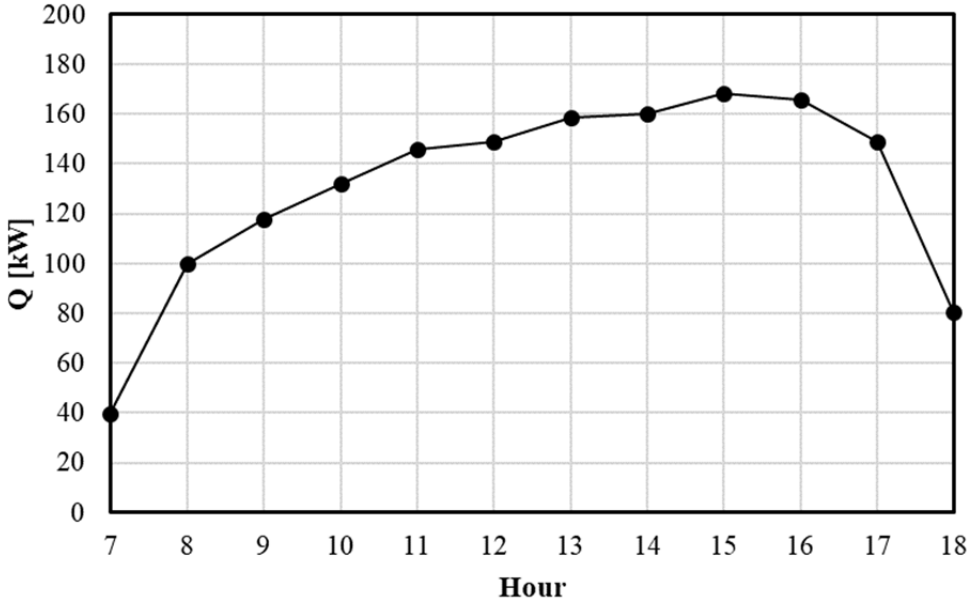

Figure 4.11. Hourly variation of cooling of the supply air in HMX for 21st August ($T_{b,set}$=26 °C, R=40%)

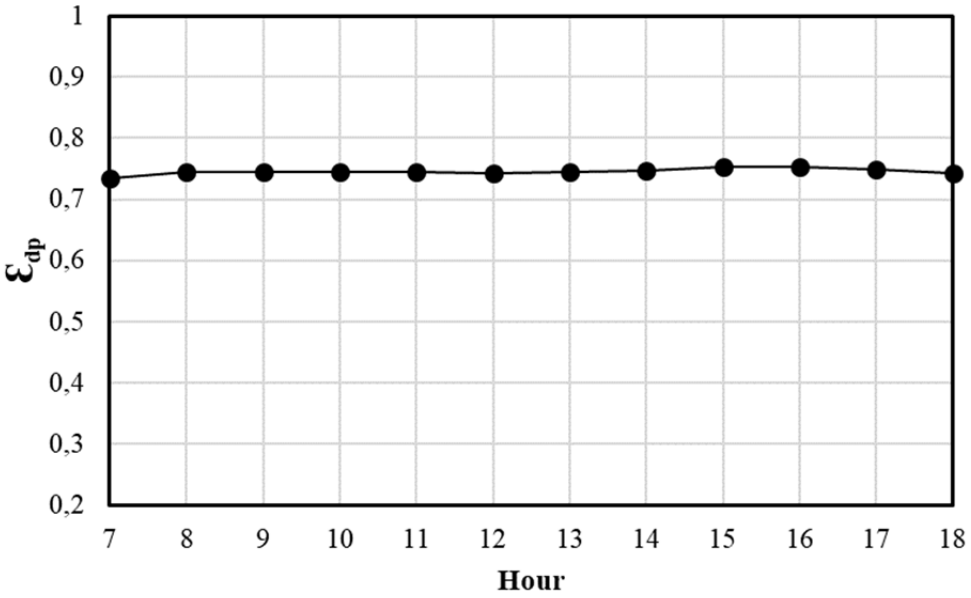

Figure 4.12. Hourly variation of effectiveness of HMX for 21st August ($T_{b,set}$=26 °C, R=40%)

4.1.5. Air Conditions within Building

Temperature and humidity ratio within the building is depicted in Fig. 4.13. As can be seen from the figure, temperature within the building is always at the set temperature of 26 ℃ for this case and humidity ratio changes roughly between 10,4 and 11,7 g/kg, which is less than the maximum allowable humidity ratio of 12 g/kg according to ASHRAE comfort zone. It is possible to obtain slightly lower humidity ratio values at early hours, around noon and at late hours of the day.

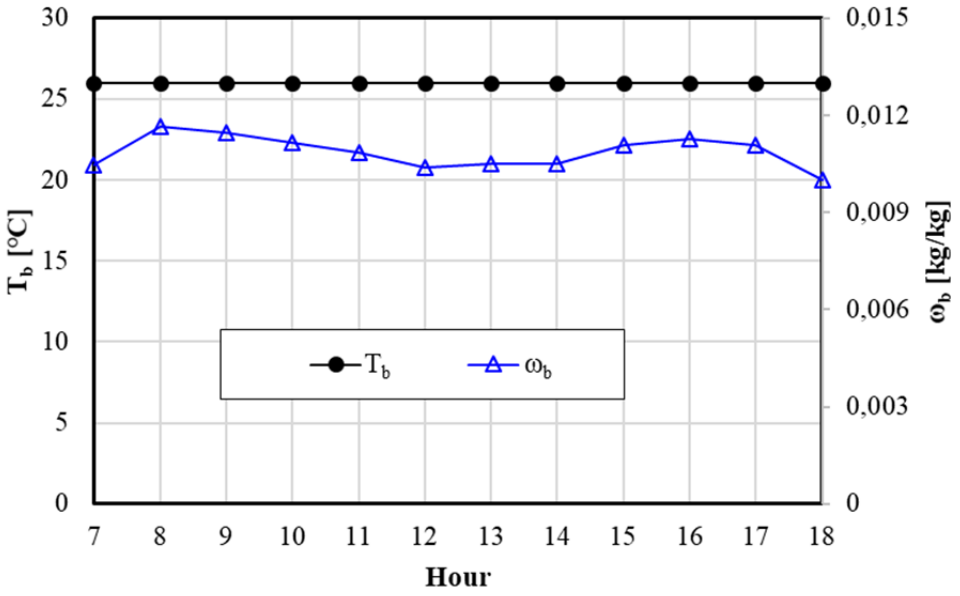

Figure 4.13. Hourly variation of temperature and humidity ratio within the building for 21st August ($T_{b,set}$=26 ℃, R=40%)

4.1.6. Direct Evaporative Cooler (DEC)

The exhaust air is cooled approximately 6,7 ℃ in the direct evaporative cooler, whilst its humidity ratio increases approximately 2,8 g/kg during the process (Figs. 4.14 and 4.15). Sensible cooling of air is achieved at a rate of between about 20 and 70 kW (Fig. 4.16).

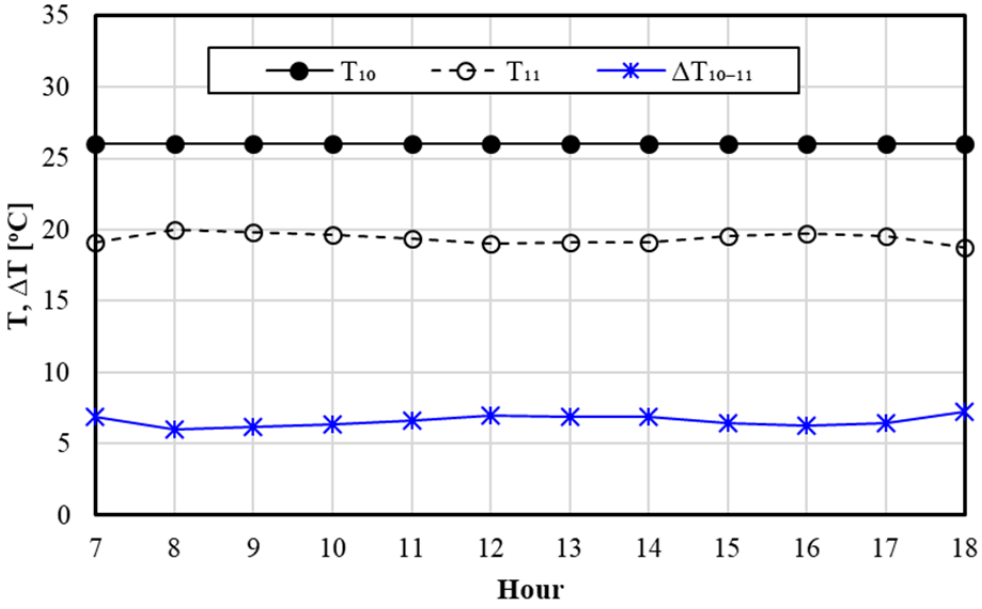

Figure 4.14. Hourly variation of temperatures and temperature difference in DEC for 21st August ($T_{b,set}$=26 ℃, R=40%)

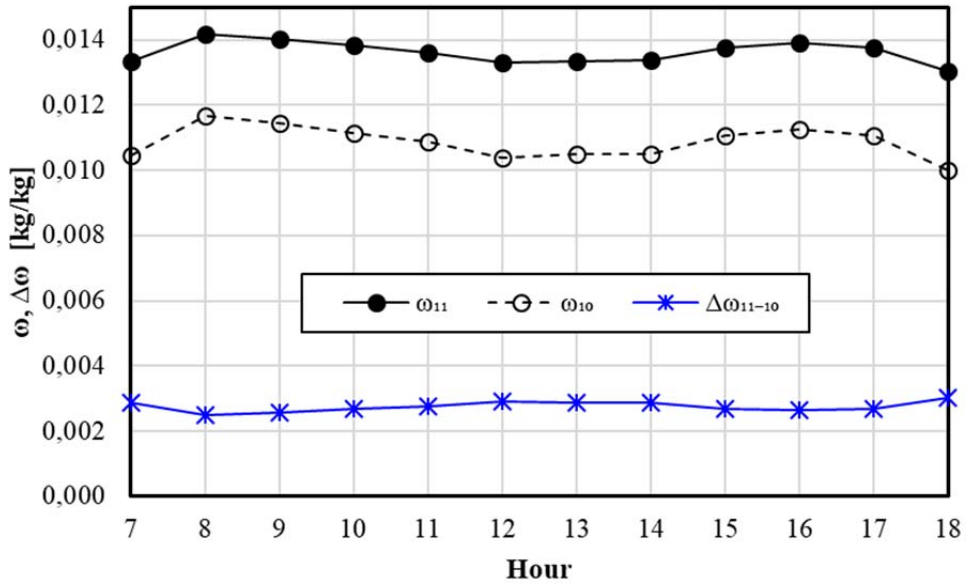

Figure 4.15. Hourly variation of humidity ratio and humidity ratio difference in DEC for 21st August ($T_{b,set}$=26 °C, R=40%)

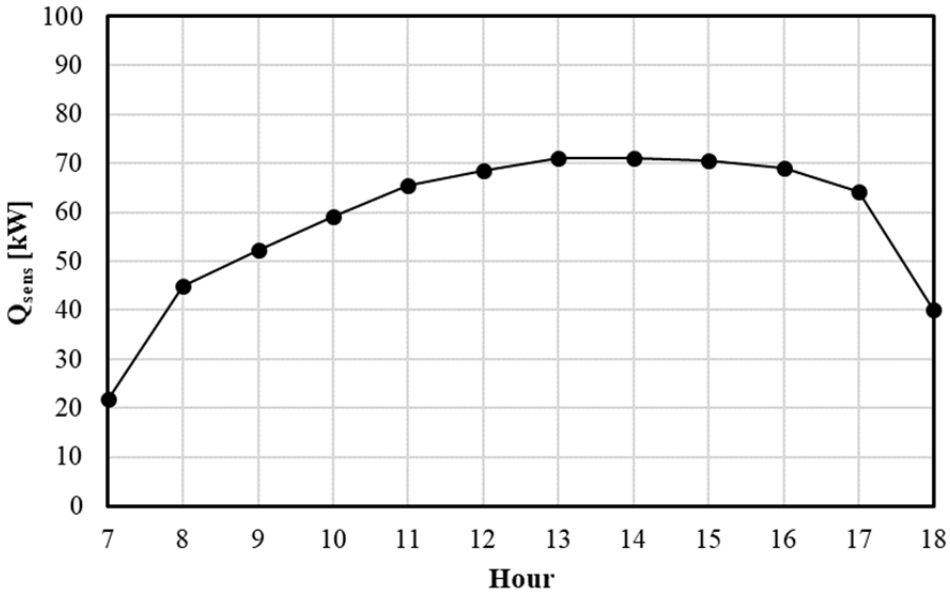

Figure 4.16. Hourly variation of sensible cooling of the exhaust air in DEC for 21st August ($T_{b,set}$=26 °C, R=40%)

4.1.7. Heat Exchanger 2 (HX2)

Warm exhaust air left HX1 (state 14) or warm regeneration air left desiccant wheel (state 20) can be used for preheating regeneration air. The air-conditioning system and the analyses were designed to investigate the favorable source for preheating. The automatic control system selects the suitable source (14 or 20) having the higher temperature. Fig. 4.17 shows the variation of temperature at states 14 and 20. It is seen that the regeneration air left DW (20) is always 8 ℃ warmer than the exhaust air left HX1 (14). Therefore, the automatic control system directs the air left DW to HX2 for preheating regeneration air before it enters HX3.

Temperature of the regeneration air is increased approximately 12 ℃ in HX2 (Fig. 4.18) resulting a heat transfer rate of about 130 kW (Fig. 4.19). The heat transfer rate is around 55 kW at 7^{00} o'clock and reaches to a level of 130 kW at 9^{00} o'clock and swings slightly around this value till 17^{00} o'clock before starts decreasing.

4.1.8. Heat Exchanger 3 (HX3)

A cheap thermal energy source for regeneration of desiccant wheel (DW) such as solar energy or waste heat is very important for the economic operation of the air-conditioning system. It should also be considered that the temperature of the regeneration air should be increased at least up to 70 ℃, which is the minimum suggested temperature by the manufacturers. As can be seen from Fig. 4.20, the temperature increases in HX3 between 22 and 30 ℃ during the day, which corresponds to a thermal energy requirement of between 100 kW and 290 kW (Fig. 4.21).

4.1.9. Coefficient of Performance (COP) of Air-conditioning System

Cooling performance of the air-conditioning system (COP) is shown in Fig. 4.22 for the day considered. As can be seen from the figure that, COP varies between 0,21 and 0,33 during the day.

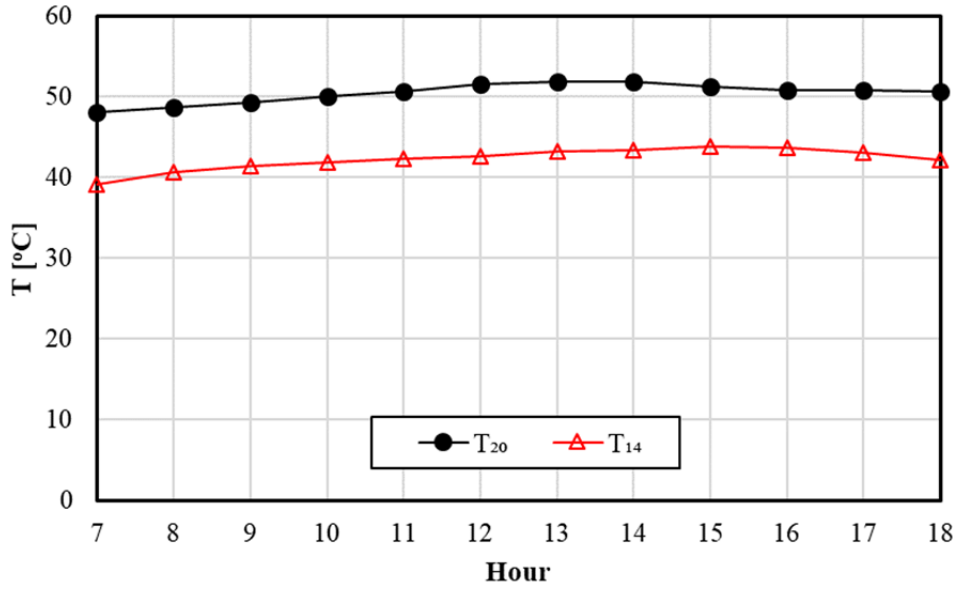

Figure 4.17. Hourly variation of temperatures at the exit of HX1 (14) and DW (20) for 21st August ($T_{b,set}$=26 °C, R=40%)

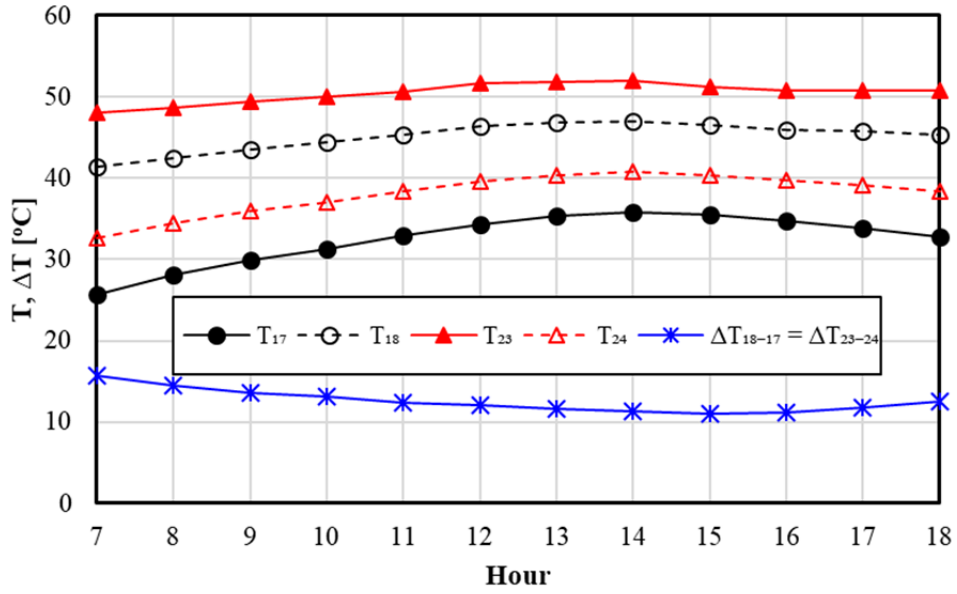

Figure 4.18. Hourly variation of temperatures and temperature difference in HX2 for 21st August ($T_{b,set}$=26 °C, R=40%)

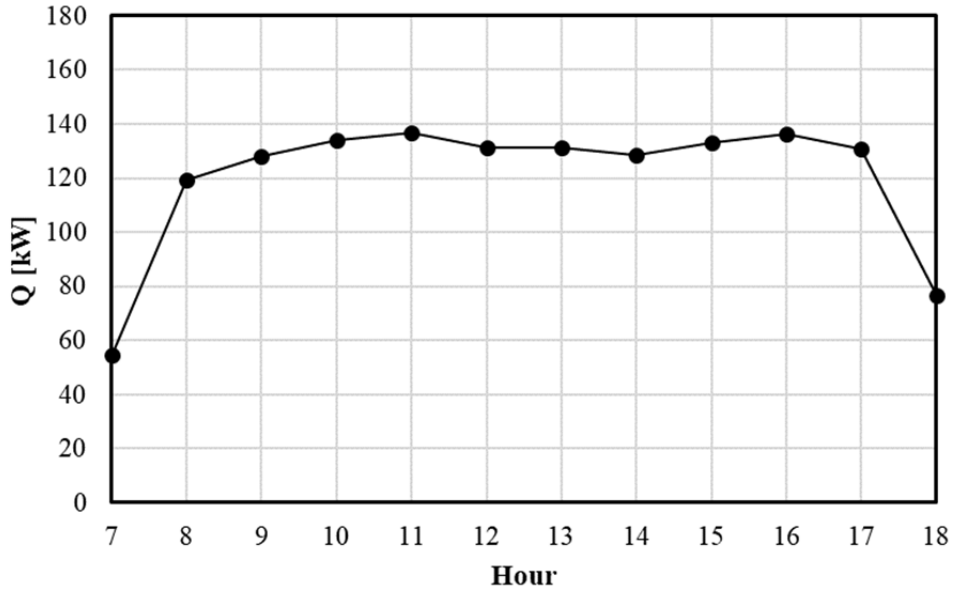

Figure 4.19. Hourly variation of preheating of the regeneration air in HX2 for 21st August ($T_{b,set}$=26 °C, R=40%)

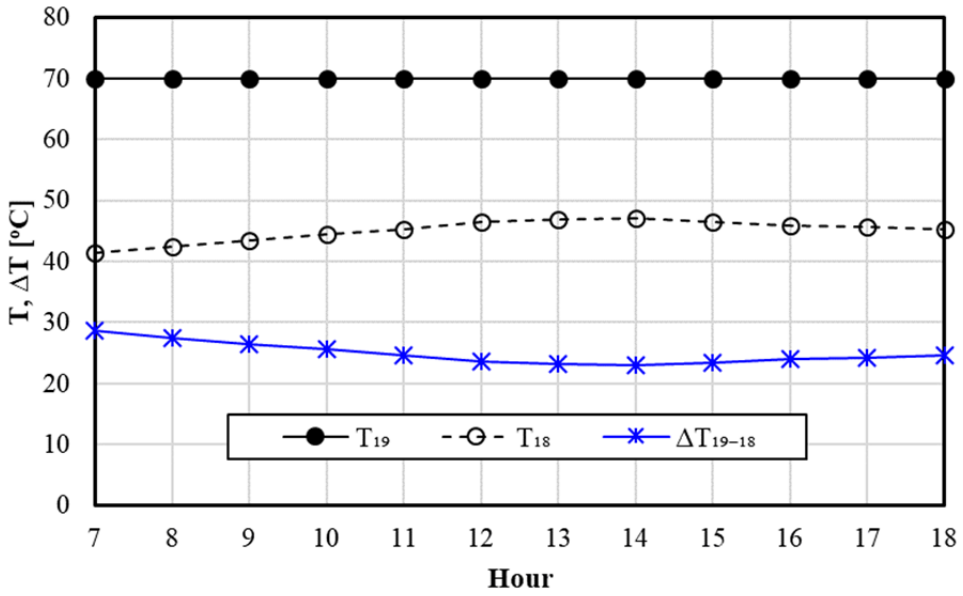

Figure 4.20. Hourly variation of temperatures and temperature difference in HX3 for 21st August ($T_{b,set}$=26 °C, R=40%)

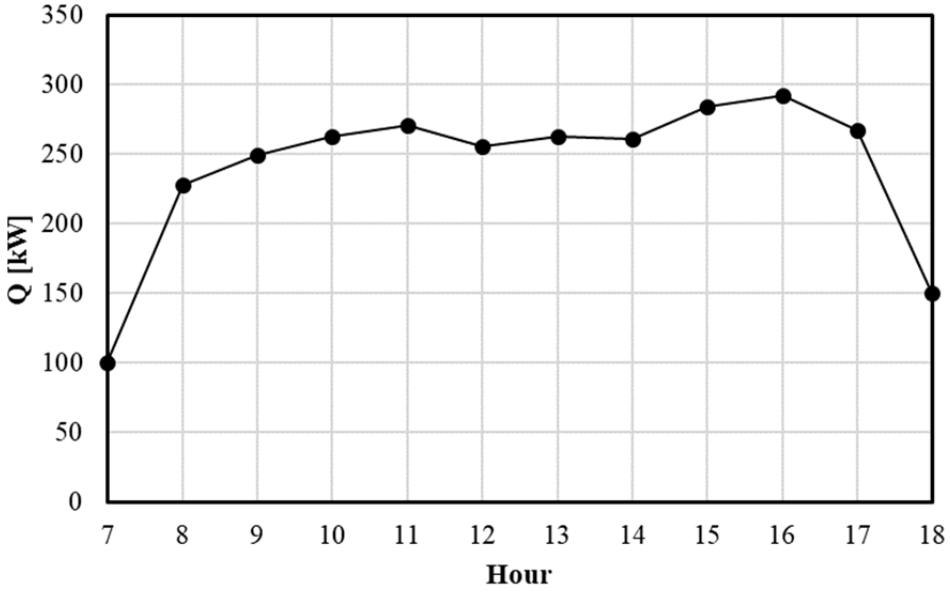

Figure 4.21. Hourly variation of heat requirement for heating regeneration air in HX3 for 21st August ($T_{b,set}$=26 °C, R=40%)

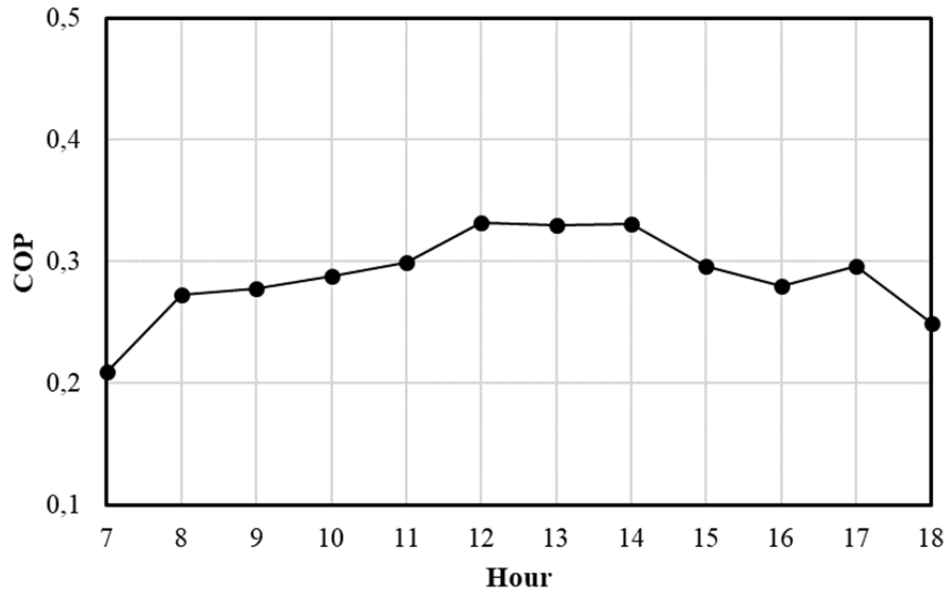

Figure 4.22. Hourly variation of COP of the air-conditioning system for 21st August ($T_{b,set}$=26 °C, R=40%)

4.2. Effect of Building Set Temperature

In this study, analyses of the air-conditioning system considered was made for 4 different building set temperatures, namely 26 ℃, 25 ℃, 24 ℃ and 23 ℃. Exhaust air mixing ratio was varied between 0% to 100%. The results are given below again for the month having the maximum building cooling load, namely 21st August.

Effect of building set temperature on the cooling performance of the system (COP) can be seen from Fig. 4.23, which show variation of COP with building set temperature at 10^{00}, 13^{00} and 16^{00} hours for different exhaust air mixing ratio values (R) for which ASHRAE comfort conditions are satisfied.

It is clear from the figures that COP of the system increases with increasing building set temperature for all R values and outdoor air conditions (hours) considered. COP increases from 0,19 for 23 ℃ to 0,32 for 26 ℃, which corresponds to 68% increase for R=60% at 10^{00}. The increase in COP is very similar for other R values for this data set at 10^{00}.

The increase in COP is approximately 60% and 75% at 13^{00} and 16^{00}, respectively.

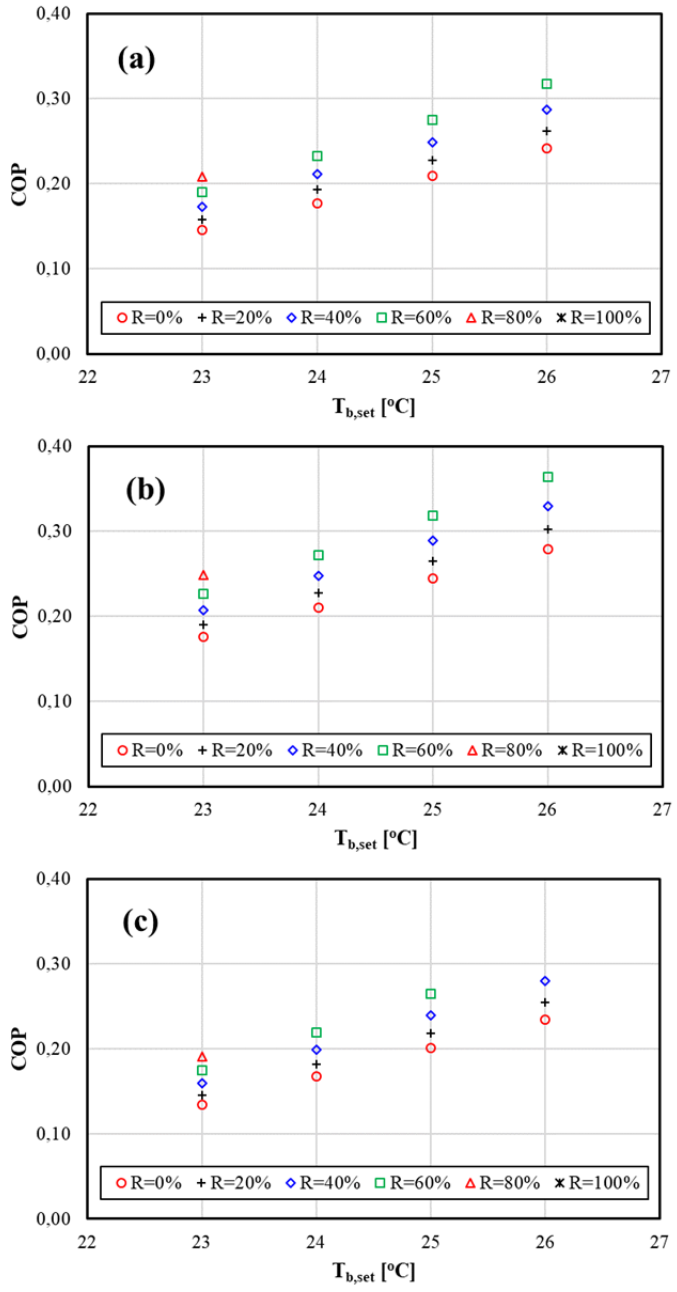

Figure 4.23. Variation of COP of the air-conditioning system with building set temperature at a)10^{00}, b)13^{00} and c)16^{00} for 21st August

4.3. Effect of Mixing Ratio of Exhaust Air (R)

In this study, hourly system performance was calculated for different exhaust air mixing ratio values (between 0% to 100%) satisfying ASHRAE comfort conditions for 4 different building set temperatures (26 ℃, 25 ℃, 24 ℃ and 23 ℃). The results are given below again for August that has the maximum building cooling load.

Effect of R on the cooling performance of the system (COP) can be seen from Fig. 4.24, which show variation of COP with R at 10^{00}, 13^{00} and 16^{00} hours for different building set temperatures.

Analysis of the figures reveal that COP of the air-conditioning system increases with increase of R for all building set temperatures and outdoor air conditions (hours) considered. COP increases from 0,24 for R=0% to 0,32 for R=60%, which corresponds to 32% increase for $T_{b,set}$=26 ℃ at 10^{00}. The increase in COP is very similar for other $T_{b,set}$ values for this data set at 10^{00}. Similar increases are obtained for the other hours of the day.

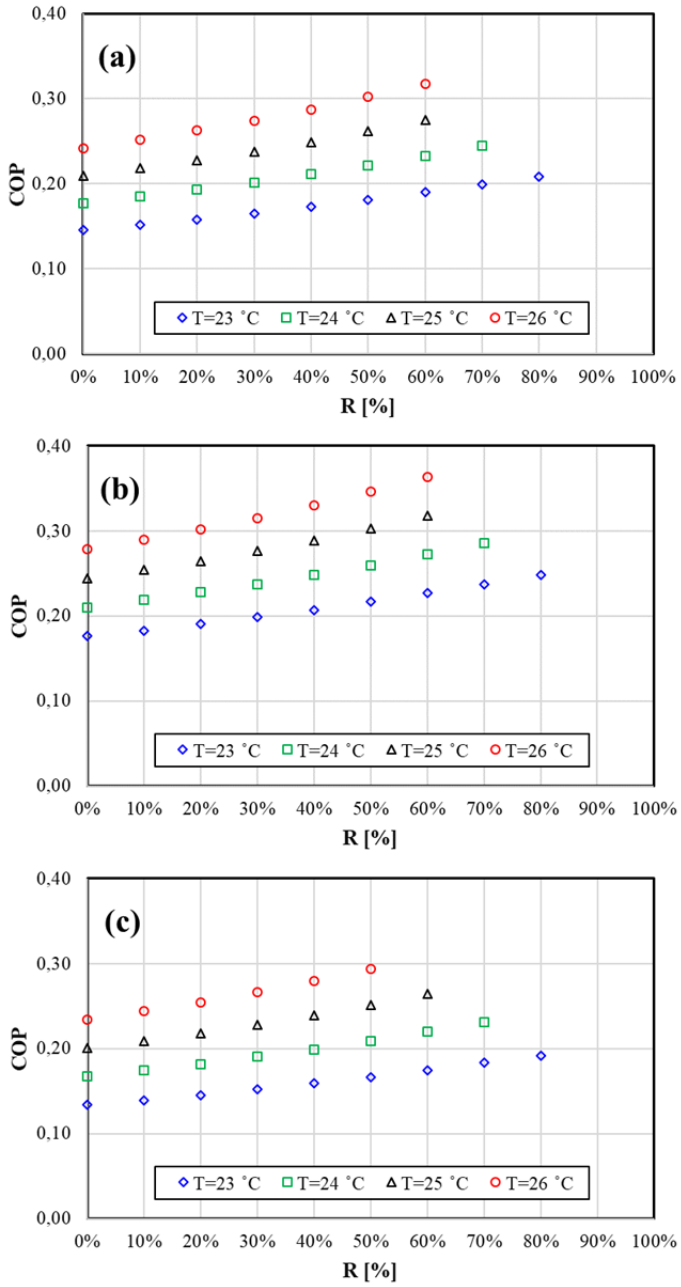

Figure 4.24. Variation of COP of the air-conditioning system with mixing ratio of exhaust air at a)10^{00}, b)13^{00} and c)16^{00} for 21st August

4.4. Results for All the Months

Cooling season in Adana starts in April and lasts in October. Results of the all runs, for which ASHRAE comfort conditions are satisfied, at 21th day of each month are presented in this section of the thesis. Only the results with the most economic operating conditions ($T_{b,set}$=26 °C and maximum possible exhaust air mixing ratio, R) are shown in the following figures.

The temperature and humidity ratio obtained within the building are shown in Fig. 4.25. As can be seen from the figure that air temperature within the building is always 26 °C, since automatic control system initially sets the building temperature to this value and the set value is always obtained. When the humidity ratio of the air within the building is considered, it changes between 0,011 and the maximum allowed humidity ratio of 0,012 kg/kg, except very early (7^{00} o'clock) and late (18^{00} o'clock) hours in April and October.

Figs. 4.26 and 4.27 show hourly variations of effectiveness of DW (ε_{DW}) and HMX ($\varepsilon_{dp,HMX}$), respectively. Effectiveness of DW is almost constant during a day and it has higher values in cooler months (April and October), and lower in warmer months (July and August). ε_{DW} changes roughly between 40% and 60% during cooling season. Variations in dew-point effectiveness of Maisotsenko cycle are much less during a day (Fig. 4.27). Effect of month is also very limited and it is reverse of effectiveness of DW. $\varepsilon_{dp,HMX}$ is minimum around 70% in April and October and maximum around 80% in July and August.

Thermal energy demand profile follows that of total building cooling load and it reaches to a value of as high as 450 kW in July at 14^{00} o'clock (Fig. 4.28). The minimum thermal energy demand is around 100 kW in April and October for most period of the day.

COP changes with both time of the day (hour) and month (Fig. 4.29). The change in COP during day is small for April and October, which have the lower building cooling loads and lower outdoor air temperatures than the other months in

cooling season. However, change in COP can be as high as 60% in July, which has the smallest COP values.

COP changes significantly with the months (Fig. 4.29). It is maximum in October with an average value of 0,77 and minimum in July with an average of 0,21. Although maximum building cooling load is in August (Fig. 3.12), the minimum COP is not in August (it is the second lowest with an average of 0,32), it is in July. This is due to fact that humidity of the outdoor is higher in July than in August. COP in the other months lies between October and July in accordance with the building cooling load (Fig. 3.12). September and June have very close COP values, changing between roughly 0,3 and 0,5 with an average of 0,41. The results of May (average 0,59) are between that of June-September and April.

Although COP value is low especially in the summer months of July and August, it should be considered that main energy consumption of the system is thermal energy (not electricity) and COP is defined in terms of thermal energy as the input. Therefore, it should not be compared directly with a system consuming mainly electricity as input. If the thermal energy is produced from cheap energy source such as waste heat or from solar energy, the system could be an attractive solution.

Another point that should be considered is that high thermal energy demand for the system coincides with the solar energy available during the summer months (Fig. 3.16). This makes use of solar energy very attractive to produce the thermal energy required for the regeneration of the desiccant wheel of the air-conditioning system.

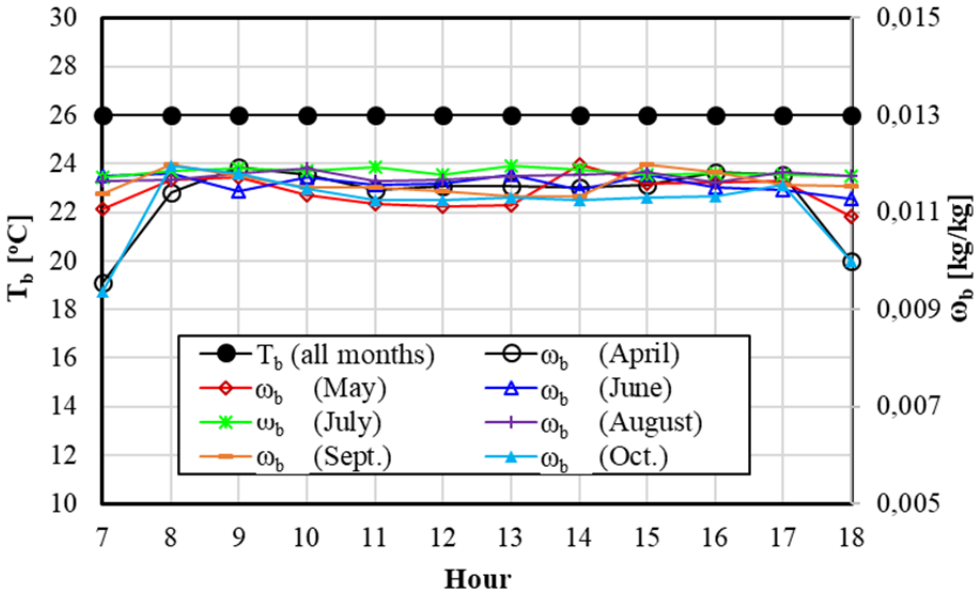

Figure 4.25. Hourly variation of temperature and humidity ratio within the building with the most economic operating conditions ($T_{b,set}$=26 °C)

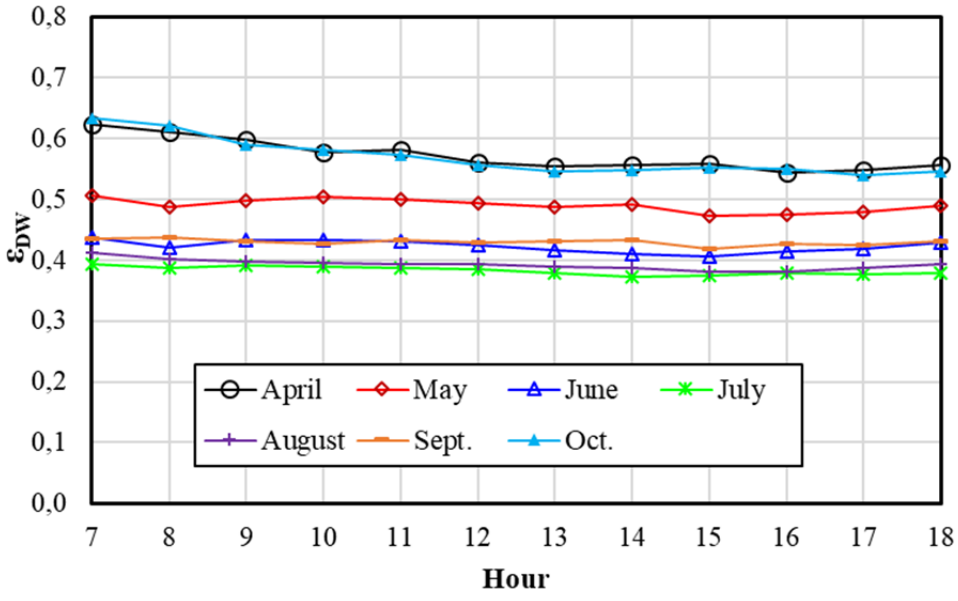

Figure 4.26. Hourly variation of effectiveness of DW with the most economic operating conditions ($T_{b,set}$=26 °C)

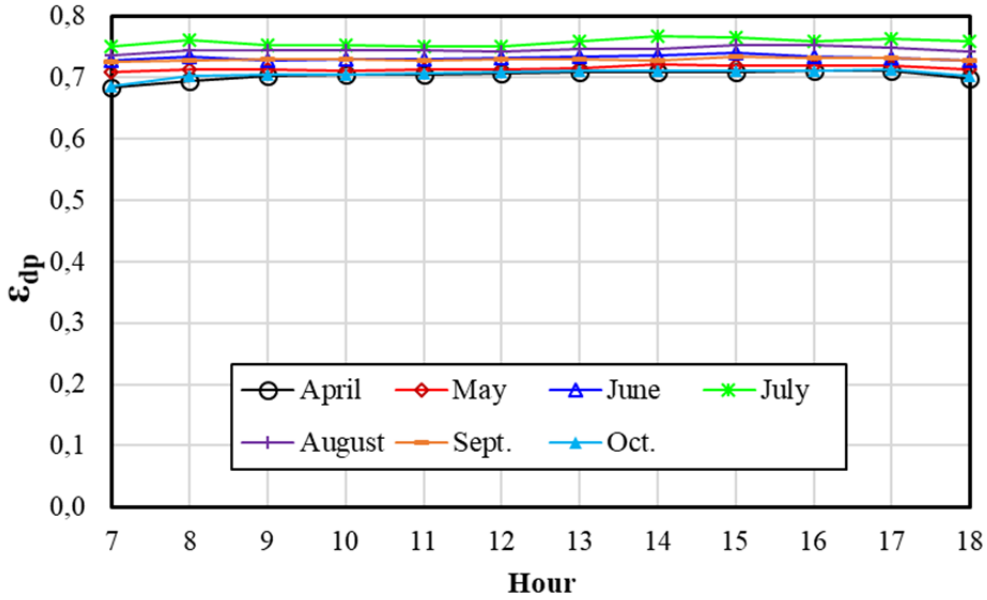

Figure 4.27. Hourly variation of dew-point effectiveness of Maisotsenko cycle with the most economic operating conditions ($T_{b,set}$=26 °C)

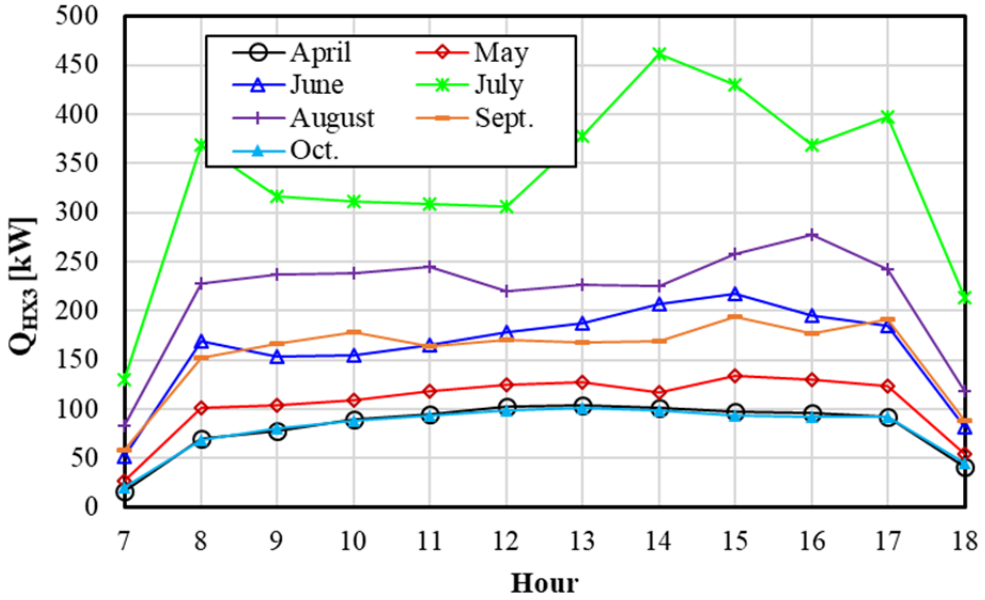

Figure 4.28. Hourly variation of thermal energy demand with the most economic operating conditions ($T_{b,set}$=26 °C)

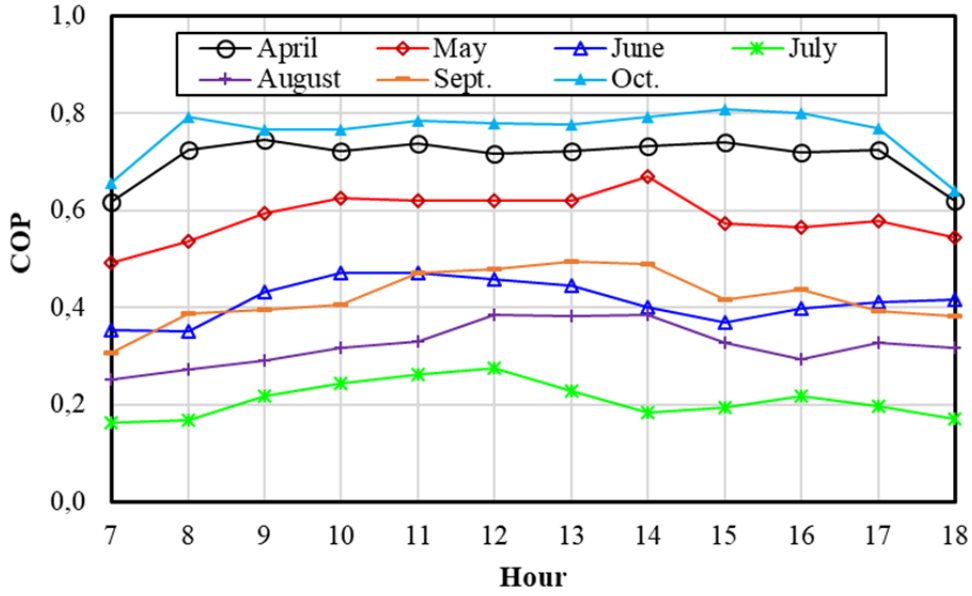

Figure 4.29. Hourly variation of COP of the air-conditioning system with the most economic operating conditions ($T_{b,set}$=26 °C)

5. CONCLUSIONS

In this thesis, a Maisotsenko-based air-conditioning system supported by a desiccant wheel, heat recovery units (recuperators) and a direct evaporative cooling unit is investigated on an hourly basis during a complete cooling season for air-conditioning of a school building located in Adana, Turkey.

Hourly cooling load of the building was calculated using Radiant Time Series (RTS) method and it was found that the maximum total cooling load is in August with a value of 88,44 Kw.

Equations for predicting the performances (leaving air conditions) of Maisotsenko cycle (Eq. 3.41) and desiccant wheel (Eqs. 3.12 and 3.13) were obtained using the data and equations available in the literature by curve fitting. Constant effectiveness values for the recuperators (HX1 and HX2) and direct evaporative cooling unit (DEC) were utilized.

Mass balance equations for dry air and the water vapor within air and energy balance equations for dry air were written. Since some of the governing equations are coupled an iterative approach is required for the solution. Various properties (dry, wet and dew-point temperatures, humidity ratio, relative humidity, specific heat and volume) of humid air are required at different locations of the system and an iterative approach is also needed to calculate the desired properties from the known properties. Therefore, modelling of the air-conditioning system was made on a software so-called EES (Energy Equation Solver), which eliminates iterations for the solution of governing equations and provides properties of humid air with built-in functions.

Analyses were carried out hourly between 7^{00} and 18^{00} for 21^{st} day of each month during the cooling season (from April to October) with the help of model developed. The runs were performed for building set temperatures ($T_{b,set}$) of 26 °C, 25 °C, 24 °C and 23 °C. For each building set temperature, exhaust air mixing ratio was changed systematically between 0% and 100% with 10% increments.

The analysis showed that ASHRAE thermal comfort conditions cannot be obtained at high mixing ratio values (R) especially at high building set temperatures. For example, the air conditions are out of ASHRAE comfort conditions at 8 runs out of 44 for 21st August, at 13^{00} hour. However, it was possible to obtain ASHRAE comfort conditions during complete cooling season by setting R to lower values. The temperature and the humidity ratio within the building are always less than or equal to 26 ℃ and 0,012 kg/kg, respectively.

Results revealed that regeneration air left DW is always warmer than the exhaust air left HX1. Therefore, it is beneficial to direct the regeneration air left DW to HX2 for preheating regeneration air before it enters HX3.

It was found that air mass flow rates ($\dot{m}_t$, $\dot{m}_p$, $\dot{m}_w$, $\dot{m}_e$ and $\dot{m}_r$) all increase from early morning to noon and then decrease during the day for all months. The profiles are very similar to each other.

Effectiveness of the desiccant wheel and Maisotsenko cycle do not change significantly during the day. Effectiveness of DW have higher values in cooler months (April and October) and lower in the warmer months (July and August). It varies roughly between 40% and 60 % during cooling season. $\varepsilon_{dp,HMX}$ is minimum around 70% in April and October and maximum around 80% in July and August.

Thermal energy demand profile follows that of total building cooling load and it reaches to a value of as high as 450 kW in July at 14^{00} o'clock. The minimum thermal energy demand is around 100 kW in April and October for most period of the day.

COP changes with both time of the day (hour) and month. The daily change in COP is small for April and October than the other months in cooling season. However, change in COP in a day can be as high as 60% in July, which has the smallest COP values. COP changes significantly with the months. It is maximum in October with an average value of 0,77 and minimum in July with an average of 0,21. Although maximum building cooling load is in August, the minimum COP

occurs in July. This is due to fact that humidity of the outdoor is higher in July than in August. COP in the other months lies between October and July in accordance with the building cooling load.

Although COP value is low especially in the summer months of July and August, it should be considered that main energy consumption of the system is thermal energy and COP is defined in terms of thermal energy as the input. Therefore, it should not be compared directly with a system consuming mainly electricity as input. If the thermal energy is produced from cheap energy source such as waste heat or from solar energy, the system could be an attractive solution.

Another point that should be considered is that high thermal energy demand for the system coincides with the solar energy available during the summer months. This makes use of solar energy very attractive to produce the thermal energy required for the regeneration of the desiccant wheel of the air-conditioning system.

More detailed studies should be carried out taking pressure drops and fan and pump power requirements into account. Effectiveness of the heat recovery units and direct evaporative cooler were taken constant in this study. They can also be calculated considering the operational conditions in a more accurate model. Although it was shown in this study that air-conditioning with the considered system is possible in a hot and humid climate, a thermoeconomic analysis that contains both initial and operational costs should also be carried out.

REFERENCES

Aktacir, M.A., 2005. Influence of Outdoor Air Conditions on Operating Capacity of Air Conditioning Systems. PhD Thesis. Çukurova University-Adana.

Angrisani, G., Roselli, C., Sasso, M., 2012. Experimental validation of constant efficiency models for the subsystems of an unconventional desiccant-based Air Handling Unit and investigation of its performance. Applied Thermal Engineering, 33-34:100-108.

Anisimov, S., Pandelidis, D., Jedlikowski, A., Polushkin, V., 2014. Performance investigation of a M (Maisotsenko)-cycle cross-flow heat exchanger used for indirect evaporative cooling. Energy, 76:593-606.

Anisimov, S., Pandelidis, D., 2014. Numerical study of the Maisotsenko cycle and mass exchanger. International Journal of Heat and Mass Transfer, 75:75 96.

Antonellis, S.D., Joppolo, C.M., 2017. Ch.3 Simplified Models for the Evaluation of Desiccant Wheels Performance (Editors: N. Enteria, H. Awbi, H. Yoshino). Desiccant Heating, Ventilating, and Air Conditioning Systems. Springer Nature, Singapore, p.63-85.

ASHRAE, 2000. ASHRAE Handbook-2000 Systems and Equipment, American Society of Heating, Refrigerating and Air-Conditioning Engineers, Atlanta.

ASHRAE, 2013. ASHRAE Standard-62.1. Ventilation for Acceptable Indoor Air Quality, American Society of Heating, Refrigerating and Air-Conditioning Engineers, Atlanta.

ASHRAE, 2017a. ASHRAE Handbook-2017 Fundamentals, American Society of Heating, Refrigerating and Air-Conditioning Engineers, Atlanta.

ASHRAE, 2017b. ASHRAE Standard-55, 2017, Thermal Environmental Conditions for Human Occupancy, American Society of Heating Refrigerating, and Air-Conditioning Engineers, Atlanta.

Beccali, M., Butera, F., Guanella, R., Adhikari, R.S., 2003. Simplified models for the performance evaluation of desiccant wheel dehumidification. International Journal of Energy Research, 27:17-29.

Bruno, F., 2011. On-site experimental testing of a novel dew point evaporative cooler. Energy and Buildings, 43:3475-3483.

Chung, J.D., Lee, D.Y., 2011. Contributions of system components and operating conditions to the performance of desiccant cooling systems. International Journal of Refrigeration, 34:922-927.

Chung, J.D., 2017. Ch.2 Modelling and Analysis of Desiccant Wheel. (Editors: N. Enteria, H. Awbi, H. Yoshino). Desiccant Heating, Ventilating and Air Conditioning Systems. Springer Nature, Singapore, p.11-62.

Comino, F., Adana, M.R., Peci, F., 2016. First and second order simplified models for the performance evaluation of low temperature activated desiccant wheels. Energy and Buildings, 116:574-582.

Comino, F., Adana, M.R., 2016. Experimental and numerical analysis of desiccant wheels activated at low temperatures. Energy and Buildings, 133:529-540.

Coral, E.C.V., Solorio, C.I.R., Rivera, M.G., Puebla, H.F.Z., 2019. Theoretical and experimental development of cooling load temperature difference factors to calculate cooling loads for buildings in warm climates. Applied Thermal Engineering, 150:576-590.

Cui, X., Chua, K.J., Yang, W.M., Ng, K.C., Thu, K., Nguyen, V.T., 2014. Studying the performance of an improved dew-point evaporative design for cooling application. Applied Thermal Energy, 63:624-633.

Cui X., Chua, K.J., Islam, M.R., Ng, K.C., 2015. Performance evaluation of an indirect pre-cooling evaporative heat exchanger operating in hot and humid climate. Energy Conversion and Management, 102:140-150.

Cui, X., Islam, M.R., Mohan, B., Chua, K.J., 2016. Developing a performance correlation for counter-flow regenerative indirect evaporative heat exchangers with experimental validation. Applied Thermal Energy, 108:774-784.

Çalışkan, H., Dinçer, İ., Hepbaşlı, A., 2012. Exergoeconomic, enviroeconomic and sustainability analyses of a novel air cooler. Energy and Buildings, 55:747 -756

Duan, Z., Zhan, C., Zhao, X., Dong, X., 2016. Experimental study of a counter-flow regenerative evaporative cooler. Building and Environment, 104:47-58.

Duan, Z., Zhao, X., Zhan, C., Dong, X., Chen, H., 2017. Energy saving potential of a counter-flow regenerative evaporative cooler for various climates of China: Experiment-based evaluation. Energy and Buildings, 148:199-210.

Fanger, P.O., 1982. Thermal comfort. Robert E. Krieger, Malabar, FL.

Ge, T.S., Qi, D., Dai Y.J., Wang, R.Z, 2018. Experimental testing on contaminant and moisture removal performance of silica gel desiccant wheel. Energy and Buildings, 176:71-77.

Gillan, L., 2008. Maisotsenko cycle for cooling processes. Clean Air, 9:47-64.

Güzelel, Y.E., Akıllı, H., Hürdoğan, E., Büyükalaca, O., 2017. Parametric Analysis of a Desiccant Seed Drying System. International Advanced Researches & Engineering Congress.

Heidarinejad, G., Pasdarshahri H., 2011. Potential of a desiccant-evaporative cooling system performance in a multi-climate country. International Journal of Refrigeration, 34:1251-1261.

Heidarinejad, G., Moshari, S., 2015. Novel modeling of an indirect evaporative cooling system withcross-flow configuration. Energy and Buildings, 92:351-362.

Hürdoğan, E., Büyükalaca, O., Yılmaz, T., Hepbaşlı, A., 2010. Experimental investigation of a novel desiccant cooling system. Energy and Buildings, 42: 2049-2060.

IEA Report, 2018. The Future of Cooling: Opportunities for energy efficient air conditioning, International Energy Agency, Paris. IEA,2018.

Intini, M., Antonellis, S.D., Joppolo, C.M., 2014. The effect of inlet velocity and unbalanced flows on optimal working conditions of silica gel desiccant wheels. Energy Procedia, 48:858-864.

Jafarian, H., Sayyaadi, H., Torabi, F., 2017. A numerical model for a dew-point counter-flow indirect evaporative cooler using a modified boundary condition and considering effects of entrance regions. International Journal of Refrigeration, 84:36-51.

Jia, C.X., Dai, Y.J., Wu, J.Y., Wang, R.Z., 2006. Analysis on a hybrid desiccant air -conditioning system. Applied Thermal Engineering, 26:2393-2400.

Jradi, M., Riffat, S., 2014. Experimental and numerical investigation of a dew-point cooling system for thermal comfort in buildings. Applied Energy, 132:524-535.

Jurinak, J.J., 1982. Open cycle desiccant cooling: component models and system simulations. PhD Thesis. University of Wisconsin-Madison.

Khalid, O., Ali, M., Sheikh, N.A., Ali, H.M., Shehryar, M., 2016. Experimental analysis of an improved Maisotsenko cycle design under low velocity conditions. Applied Thermal Energy, 95:288-295.

Khalid, O., Butt, Z., Tanveer, W., Rao, H.I., 2017. Design and experimental analysis of counter-flow heat and mass exchanger incorporating (M-cycle) for evaporative cooling. Heat Mass Transfer, 53:1391-1403.

Klein, S. A. (2018). Engineering Equation Solver (EES) Academic Commercial v.10.493-3D, F-Chart Software LLC.

Kreider, J. F., Rabl, A., 1994, Heating and Cooling of Buildings, McGraw-Hill.

Kuma, T., Hirose, T., Goto, M., Kodama, A., 1998. Thermally regenerative monolithic rotor dehumidifier for adsorption cooling system. Journal of Solar Energy Engineering, 120:45-50.

La, D., Dai, Y.J., Li, Y., Wang, R.Z., Ge, T.S., 2010. Technical development of rotary desiccant dehumidification and air conditioning: A review. Renewable and Sustainable Energy Reviews,14:130–147.

Lee, J., Lee, D.Y., 2013. Experimental study of counter-flow regenerative evaporative cooler with finned channels. International Journal of Heat and Mass Transfer, 65:173-179.

Lin, J., Thu, K., Bui, T.D., Wang, R.Z., Ng, K.C., Chua, K.J., 2016. Study on dew point evaporative cooling system with counter-flow configuration. Energy Conversion and Management, 109:153–165.

Lin, J., Wang, R.Z., Kumja, M., Bui, T.D., Chua, K.J., 2017. Modelling and experimental investigation of the cross-flow dew point evaporative cooler with and without dehumidification. Applied Thermal Engineering, 121:1-13.

Lin, J., Bui, D.T., Wang, R., Chua, K.J., 2018. On the fundamental heat and mass transfer analysis of the counter-flow dew point evaporative cooler. Applied Energy, 217:126-142.

Liu, Y., Li, J.M., Yang, X., Zhao, X., 2019. Two-dimensional numerical study of a heat and mass exchanger for a dew-point evaporative cooler. Energy, 168:975-988.

Maheshwari, G.P., Al-Ragom, F., Suri, R.K., 2001. Energy-saving potential of an indirect evaporative cooler. Applied Energy, 69:69-76.

Mahmood, M.H., Sultan, M., Miyazaki, T., Koyama, S., Maisotsenko, S., 2016. Overview of the Maisotsenko cycle-A way towards dew-point evaporative cooling. Renewable and Sustainable Energy Reviews, 66:537-555.

Maisotsenko V., Gillan, L.E., Heaton, T.L., Gillan, A.D., 2003. Method and plate apparatus for dew point evaporative cooler. United State Patent, 6,581,402.

Manaf, I.A., Durrani, F., Eftekhari, M., 2018. A review of desiccant evaporative cooling systems in hot and humid climates. Advances in Building Energy Research

Moshari, S., Heidarinejad, G., 2015. Numerical study of regenerative evaporative coolers for sub-wet-bulb cooling with cross- and counter-flow configuration. Applied Thermal Engineering, 89:669-683.

Narayanan, R., 2017. Investigation of geometry effects of channels of a silica-gel desiccant wheel. Energy Procedia, 110:20-25.

Panaras, G., Mathioulakis, E., Belessiotis, V., Kyriakis, N., 2010. Experimental validation of a simplified approach for a desiccant wheel model. Energy and Buildings, 42:1719-1725.

Pandelidis, D., Anisimov, S., Worek, W.M., 2015a. Performance study of the Maisotsenko Cycle heat exchangers in different air-conditioning applications. International Journal of Heat and Mass Transfer, 81:207-211.

Pandelidis, D., Anisimov, S., Worek, W.M., 2015b. Performance study of counter-flow indirect evaporative air coolers. Energy and Buildings, 109:53-64.

Pandelidis, D., Anisimov, S., Worek, W.M., Drag, P., 2016. Comparison of desiccant air conditioning systems with different indirect evaporative air coolers. Energy Conversion and Management, 117:375-392.

Pandelidis, D., Anisimov, S., Worek, W.M., Drag, P., 2017a. Analysis of different applications of Maisotsenko cycle heat exchanger in the desiccant air conditioning systems. Energy and Buildings, 140:154-170.

Pandelidis, D., Anisimov, S., Rajski, K., Brychcy, E., Sidorczy, M., 2017b. Performance comparison of the advanced indirect evaporative air coolers. Energy, 135:138-152.

Pandelidis, D., Pacak, A., Cichon, A., Anisimov, S., Drag, P., Vager, B., Vasilijev, V., 2018a. Multi-stage desiccant cooling system for moderate climate. Energy Conversion and Management, 177:77-90.

Pandelidis, D., Anisimov, S., Drag, P., Sidorczyk, M., Pacak, A., 2018b. Analysis of application of the M-Cycle heat and mass exchanger to the typical air conditioning systems in Poland. Energy and Buildings, 158:873-883.

Rafique, M.M., Gandhidasan, P., Rehman, S., Al-Hadhrami, L.M., 2015. A review on desiccant based evaporative cooling systems. Renewable and Sustainable Energy Reviews, 45:145-159.

Rambhad, K.S., Walke, P.V., Tidke, D.J., 2016. Solid desiccant dehumidification and regeneration methods-A review. Renewable and Sustainable Energy Reviews, 59:73-83.

Riangvilaikul, B., and Kumar, S., 2010a. An experimental study of a novel dew point evaporative cooling system. Energy and Buildings, 42:637–644.

Riangvilaikul, B., and Kumar, S., 2010b. Numerical study of a novel dew point evaporative cooling system. Energy and Buildings, 42:2241-2250.

Rogdakis, E.D., Koronaki, I.P., Tertipis, D.N., 2014. Experimental and computational evaluation of Maisotsenko evaporative cooler at Greek climate. Energy and Buildings, 70:497-506.

Rogdakis, E.D., Tertipis, D.N., 2015. Maisotsenko cycle: technology overview and energy-saving potential in cooling systems. Energy and Emission Control Technologies, 3:15-22.

Ruivo, C.R., Costa, J.J., Figueiredo, A.R., Kodama, A., 2012. Effectiveness parameters for the prediction of the global performance of desiccant wheels An assessment based on experimental data. Renewable Energy, 38:181-187.

Ruivo, C.R., Angrisani, G., 2014. The effectiveness method to predict the behavior of a desiccant wheel: An attempt of experimental validation. Applied Thermal Engineering, 71:643-651.

Shahzad, M.K., Chaudhary, G.Q., Ali, M., Sheikh, N.A., Khalil, M.S., Rashid, T.U., 2018. Experimental evaluation of a solid desiccant system integrated with cross flow Maisotsenko cycle evaporative cooler. Applied Thermal Energy, 128:1476-1478.

Sohani, A., Sayyaadi, H., Mohammadhosseini, N., 2018. Comparative study of the conventional types of heat and mass exchangers to achieve the best design of dew point evaporative coolers at diverse climatic conditions. Energy Conversion and Management, 158:327-345.

Spitler, J.D., D.E. Fisher, and C.O. Pedersen. 1997. The radiant time series cooling load calculation procedure. ASHRAE Transactions 103:503–15.

Stoitchkov, N.J., Dimitrov, G.I., 1998. Effectiveness of crossflow plate heat exchanger for indirect evaporative cooling. International Journal of Refrigeration, 21:463-471.

Sultan, M., El-Sharkawy, I.I., Miyazaki, T., Saha, B.B., Koyama, S., 2015. An overview of solid desiccant dehumidification and air conditioning systems. Renewable and Sustainable Energy Reviews, 46:16-29.

TS-825, 2013, Turkish Standard 825. Thermal insulation in buildings. Ankara: Official gazette, 18 December 2013.

Uçkan, İ., Yılmaz, T., Hürdoğan, E., Büyükalaca, O., 2013. Experimental investigation of a novel configuration of desiccant based evaporative air conditioning system. Energy Conversion and Management, 65:606-615.

Wan, Y., Ren, C., Wang, Z., Yang, Y., Yu, L., 2017. Numerical study and performance correlation development on counter-flow indirect evaporative air coolers. International Journal of Heat and Mass Transfer, 115:826-830.

Xu, P., Ma, X., Zhao, X., Fencey, K., 2017. Experimental investigation of a super performance dew point air cooler. Applied Energy, 203:761-777.

Yılmaz, T., Büyükalaca, O., 2003. Design of regenerative heat exchangers. Heat Transfer Engineering, 24:32-38.

Zhao, X., Li, JM., Riffat, S.B., 2008. Numerical study of a novel counter-flow heat and mass exchanger for dew point evaporative cooling. Applied Thermal Engineering, 28:1942-1951.

Zhan, C., Duan, Z., Zhao, X., Smith, S., Jin, H., Riffat, S., 2011a. Comparative study of the performance of the M-cycle counter-flow and cross-flow heat exchangers for indirect evaporative cooling e Paving the path toward sustainable cooling of buildings. Energy, 36:6790-6805.

Zhan, C., Zhao, X., Smith, S., Riffat, S.B., 2011b. Numerical study of a M-cycle cross-flow heat exchanger for indirect evaporative cooling. Building and Environment, 46: 657-668.

Zhu, G., Chow, T.T., Lee, C.K., 2017. Performance analysis of counter-flow regenerative heat and mass exchanger for indirect evaporative cooling based on data-driven model. Energy and Buildings, 155:503-512.

Zube, D., Gillan, L., 2011. Evaluating Coolerado Corportion's Heat-Mass Exchanger Performance Through Experimental Analysis. International Journal of Energy for a Clean Enviroment, 12:101-116.

CURRICULUM VITAE

Yunus Emre GÜZELEL was born in 1991. He graduated from Adana Anatolian High School and enrolled in Mechanical Engineering Department of Çukurova University. He graduated from Çukurova University as a Mechanical Engineer in June 2015. He started his Master of Science education in Mechanical Engineering Department of Çukurova University in January 2016. He has been working as a Research Assistant at the same department since June 2018.